Simulation of High-Speed Interconnects

RAMACHANDRA ACHAR, MEMBER, IEEE AND MICHEL S. NAKHLA, FELLOW, IEEE

Invited Paper

With the rapid developments in very large-scale integration (VLSI) technology, design and computer-aided design (CAD) techniques, at both the chip and package level, the operating frequencies are fast reaching the vicinity of gigahertz and switching times are getting to the subnanosecond levels. The ever increasing quest for high-speed applications is placing higher demands on interconnect performance and highlighted the previously negligible effects of interconnects, such as ringing, signal delay, distortion, reflections, and crosstalk. In this review paper, various high-speed interconnect effects are briefly discussed. In addition, recent advances in transmission line macromodeling techniques are presented. Also, simulation of high-speed interconnects using model-reduction-based algorithms is discussed in detail.

Keywords*—Asymptotic waveform evaluation, AWE, CFH, circuit simulation, complex frequency hopping, distributed networks, high-speed interconnects, Krylov-subspace methods, macromodeling, model-order reduction, moment-matching techniques, multiconductor transmission lines.*

I. INTRODUCTION

The recent trend in the VLSI industry toward miniature designs, low power consumption, and increased integration of analog circuits with digital blocks has made the signal integrity analysis a challenging task. The quest for high-speed applications has highlighted the previously negligible effects of interconnects (Fig. 1), such as ringing, signal delay, distortion, reflections, and crosstalk. Interconnects can exist at various levels of design hierarchy (Fig. 2) such as on-chip, packaging structures, multichip modules, printed circuit boards, and backplanes. It is predicted that interconnects will be responsible for majority of signal degradation in high-speed systems [1]–[22].

Manuscript received July 31, 2000; revised February 16, 2001. This work was supported in part by the Natural Sciences and Engineering Research Council of Canada (NSERC), by Micronet, a Canadian Network of Centers of Excellence on Microelectronics, Communication and Information Technology Ontario (CITO), by Canadian Microelectronics Corporation (CMC), by Nortel Networks, Ottawa, and by Gennum Corporation, Toronto.

The authors are with the Department of Electronics, Carleton University, Ottawa, ON K1S 5B6, Canada (e-mail: msn@doe.carleton.ca; achar@doe.carleton.ca).

Publisher Item Identifier S 0018-9219(01)03967-6.

High-speed interconnect problems are not always handled appropriately by conventional circuit simulators, such as SPICE [23]. If not considered during the design stage, these interconnect effects can cause logic glitches that render a fabricated digital circuit inoperable or they can distort an analog signal such that it fails to meet specifications. Since extra iterations in the design cycle are costly, accurate prediction of these effects is a necessity in high-speed designs. Hence, it becomes extremely important for designers to simulate the entire design along with interconnect subcircuits as efficiently as possible while retaining the accuracy of simulation [23]–[139].

A. What is High-Speed?

Speaking on a broader perspective, a "high-speed interconnect" is the one in which the time taken by the propagating signal to travel between its end points cannot be neglected. An obvious factor that influences this definition is the physical extent of the interconnect; the longer the interconnect, the more time the signal takes to travel between its end points. Smoothness of signal propagation suffers once the line becomes long enough for the signal's rise/fall times to roughly match its propagation time through the line. Then the interconnect electrically isolates the driver from the receivers, which no longer function directly as loads to the driver. Instead, within the time of the signal's transition between its high and low voltage levels, the impedance of interconnect becomes the load for the driver and also the input impedance to the receivers [1]–[12]. This leads to various transmission line effects, such as reflections, overshoot, undershoot, crosstalk, and modeling of these needs the blending of EM and circuit theory.

Alternatively, the term "high-speed" can be defined in terms of the frequency content of the signal. At low frequencies an ordinary wire, in other words, an interconnect, will effectively short two connected circuits. However, this is not the case at higher frequencies. The same wire, which is so effective at lower frequencies for connection purposes, has too much inductive/capacitive effects to function as a short at higher frequencies. Faster clock speeds and sharper slew rates tend to add more and more high-frequency contents.

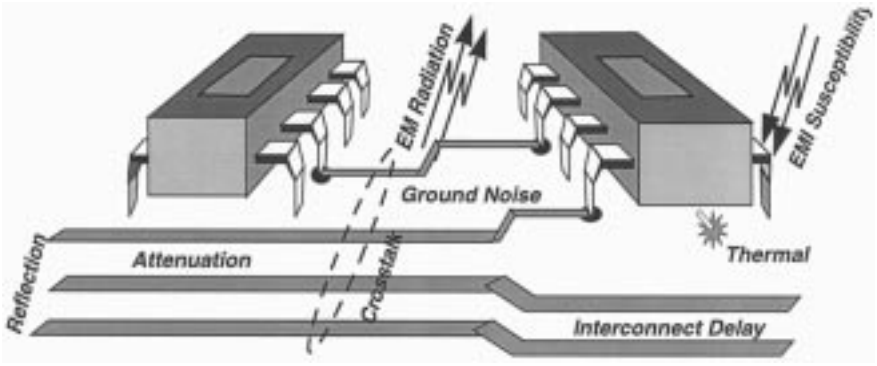

Fig. 1. High-speed interconnect effects.

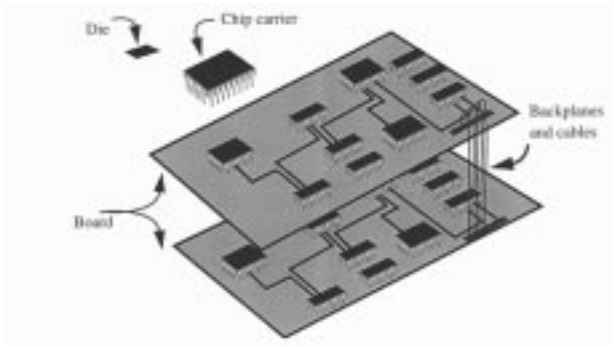

Fig. 2. Interconnect hierarchy.

An important criterion used for classifying interconnects is the *electrical length* of an interconnect. An interconnect is considered to be "*electrically short*" if, at the highest operating frequency of interest, the interconnect length is physically shorter than approximately one-tenth of the wavelength (i.e., *length of the interconnect*/$\lambda \approx 0.1$, $\lambda = v/f$). Otherwise, the interconnect is referred to as "*electrically long*" [1], [12]. In most digital applications, the desired highest operating frequency (which corresponds to the minimum wavelength) of interest is governed by the rise/fall time of the propagating signal. For example, the energy spectrum of a trapezoidal pulse is spread over an infinite frequency range; however, most of the signal energy is concentrated near the low-frequency region and decreases rapidly with the increase in frequency. Hence, ignoring the high-frequency components of the spectrum above a maximum frequency, $f_{\max}$, will not seriously alter the overall signal shape. Consequently, for all practical purposes, the width of the spectrum can be assumed to be finite. A practically used relationship between the desired $f_{\max}$ and t_r the (rise/fall time of the signal) can be expressed as [2], [4], [36], [66], [90]

$$f_{\max} \approx 0.35/t_r. \tag{1}$$

This implies that, for example, for a rise time of 0.1 ns, the maximum of frequency of interest is approximately 3 GHz or the minimum wavelength of interest is 10 cm. In some cases, the limit can be more conservatively set [90] as $f_{\max} \approx 1/t_r$.

In summary, the primary factors that influence the decision "whether high-speed signal distortion effects should be considered" are interconnect length, cross-sectional dimensions, signal slew rate, and the clock-speed. Other factors that also should be considered are logic levels, dielectric material, and conductor resistance. Electrically short interconnects can be represented by lumped models whereas electrically long interconnects need distributed or full-wave models.

The rest of the paper is organized as follows. In Section II, a brief description of high-speed effects and interconnect models is provided. Section III provides a detailed analysis of transmission line equations and derivation of a generic multiconductor transmission line stamp, suitable for inclusion in an MNA analysis. Section IV provides a review of circuit equations in the presence of distributed elements. Review of efficient techniques for discretization of Telegrapher's equations is given in Section V. Sections VI–VIII give a detailed account of simulation of interconnects using model-reduction techniques. Section IX provides references to related advanced topics.

II. High-Speed Interconnect Effects

High-speed effects influencing a signal propagating on an interconnect could be multifold, such as delay, rise time degradation, attenuation, crosstalk, skin effect, overshoots, undershoots, ringing, and reflection. In this section, we give a detailed account of each of these high-speed effects (which are also known as transmission line effects).

A. Propagation Delay

A signal traversing from one end of a transmission line to the other end takes a finite amount of time; in other words, it experiences a certain amount of *delay* (T_d). Fig. 3 illustrates the case of an ideal delay line. In addition, the signal may encounter rise time degradation as shown in Fig. 4, where the rise time at the receiver end (t_R) is larger than the rise time at the source end (t_r) [2], [4]. Rise-time degradation further adds to the overall delay experienced by the signal, as it influences the maximum and minimum attainable logic levels between the switching intervals.

B. Attenuation

The signal through an interconnect may suffer attenuation, due to ohmic or conductance losses. This is illustrated in Fig. 4. Ohmic losses are more pronounced at higher fre-

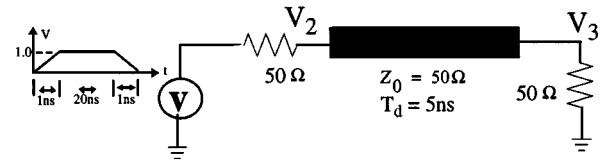

(a) Network with lossless transmission line

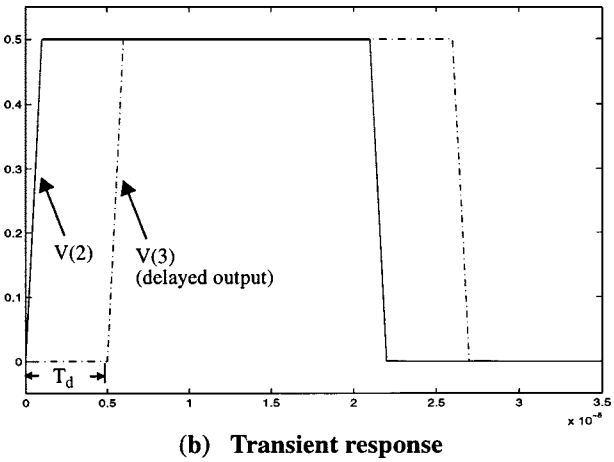

(b) Transient response

Fig. 3. Illustration of propagation delay.

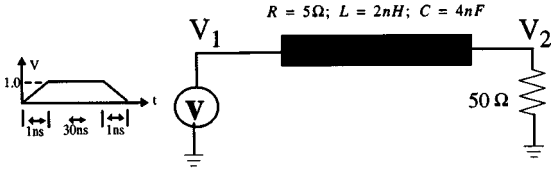

(a) Network with lossy transmission line

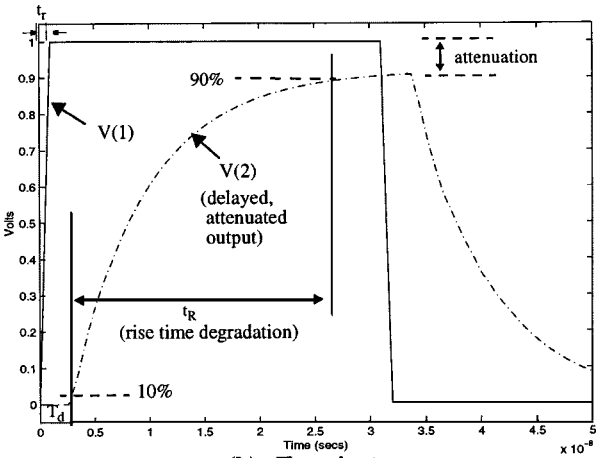

(b) Transient response

Fig. 4. Illustration of attenuation and rise-time degradation.

quencies due to the uneven current distributions. Conductance losses are proportional to the dielectric loss factor of the dielectric material and are also a function of the frequency. If the losses are high, the signals may not retain the specified logic levels during the transit through an interconnect and may result in false switching of digital circuitry.

C. Signal Reflection and Ringing

Signal reflection and the associated ringing can severely distort signal propagation at higher frequencies. The prime cause of reflection-related signal degradation is the discontinuity in characteristic impedance of the transmitting line. Such a discontinuity can be either distributed or lumped in nature. In the case of distributed discontinuity, the impedance variation on a line takes place over a certain length. For example, this can occur due to the change in the medium along the length of the signal trace, which may have to traverse several layers on a printed circuit board (impedance may not be well controlled from layer to layer). Following are some common causes of discontinuities: connectors between card-to-board, cable-to-card, leads between chip and chip carriers, or between card wiring and chip carriers, long vias, orthogonal wiring, flip-chip soldier balls, wire bonds, and redistribution lines, etc.

Another major contributor to the reflection related signal degradation is the impedance mismatch between the line characteristic impedance and source/terminating impedances. Fig. 5 illustrates these effects for the case of a lossless line. Fig. 5(b) and (c) shows the undershoots for relatively small and large delay lines. In general, undershoots occur when the terminating impedance is less than the characteristic impedance of the interconnect. Fig. 5(d) and (e) shows the phenomenon of overshoots, which occur when the terminating impedance is larger than the characteristic impedance of the line. As seen, the undershoots, overshoots, and the ringing experienced by the signal increases with the delay of the interconnect. Fig. 6 illustrates the ringing associated with a lossy line, for various cases of terminations.

1) Mechanism of Reflections: Consider the interconnect system shown in Fig. 7, which shows the simplest case of impedance variation from (Z_0) to (Z_0'). Such a variation results in part of the onward propagating signal (v_i) getting reflected (v_r). The coefficient of reflection (ρ) is given by $\rho = v_r/v_i = (Z_0' - Z_0)/(Z_0' + Z_0)$. As seen, the reflection will vanish when there is no mismatch $(Z_0 = Z_0')$. Care must be taken in high-speed designs to minimize the reflections, which otherwise may result in false switching.

D. Crosstalk

Crosstalk refers to the interaction between signals that are propagating on various lines in the system. An analogy of crosstalk could be the "the interference from other lines while talking on the phone." Crosstalk is mainly due to the dense wiring required by compact and high-performance systems. High-density and closely laid interconnects result in electromagnetic coupling between signal lines. The active signal energy is coupled to the quiet line through both mutual capacitance and inductances, resulting in noise voltage–currents. This may lead to inadvertent switching and system malfunctioning. Crosstalk is a major constraint while routing in high-speed designs. An example of crosstalk is given in Fig. 8. By its very nature, crosstalk analysis involves systems

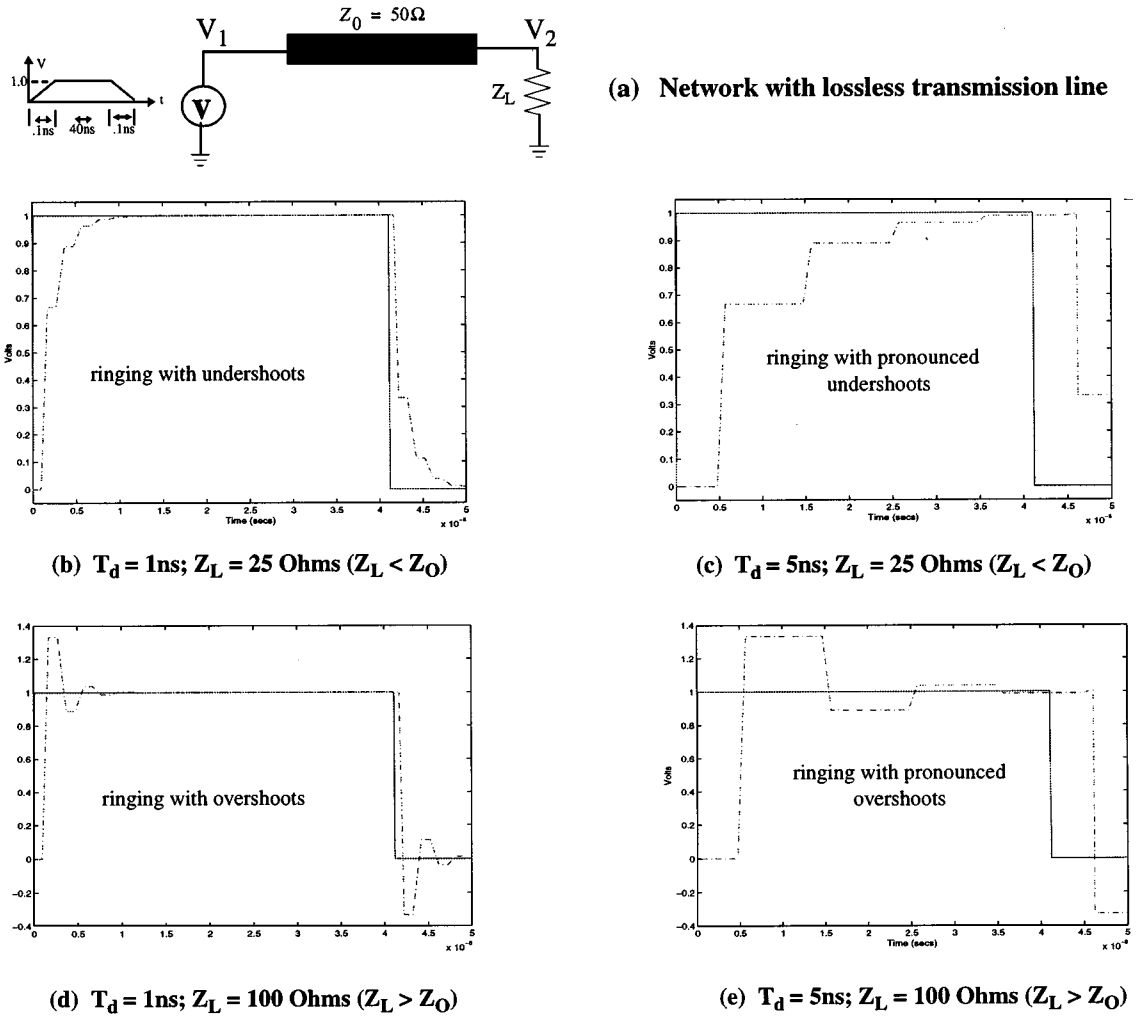

Fig. 5. Illustration of undershoots, overshoots, and ringing in lossless interconnects.

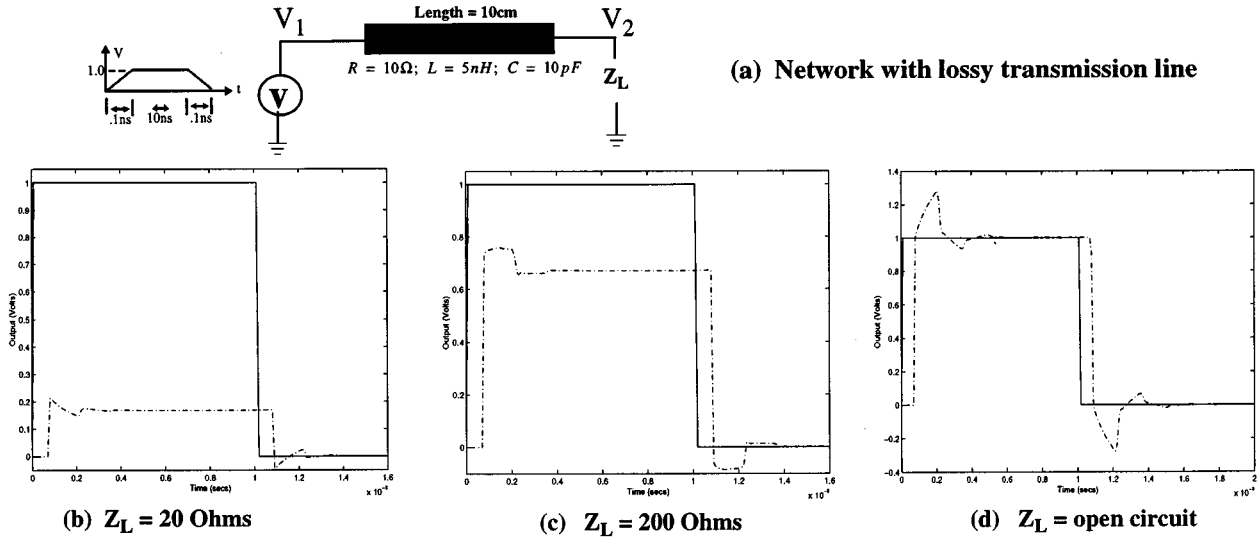

Fig. 6. Illustration of ringing in lossy interconnects.

of two or more conductors. Such systems are studied on the basis of dominant propagating modes. System behavior in response to any general excitation is then a linear combination of modal responses.

E. High-Speed Interconnect Models

Depending on the operating frequency, signal rise times, and nature of the structure, the interconnects can be mod-

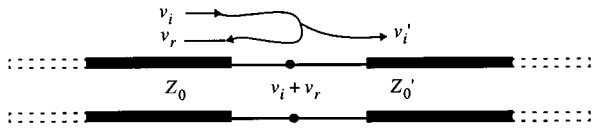

Fig. 7. Reflection due to impedance mismatch.

eled as lumped, distributed (frequency independent/dependent RLCG parameters, lossy, coupled), or full-wave models.

1) Lumped Models: At lower frequencies, the interconnect circuits could be modeled using lumped RC or RLC circuit models. RC circuit responses are monotonic in nature. However, in order to account for ringing in signal waveforms, RLC circuit models may be required. Usually lumped interconnect circuits extracted from layouts contain a large number of nodes that make the simulation highly CPU intensive (more details about lumped circuit modeling are given in Section V).

2) Distributed Transmission Line Models: At relatively higher signal-speeds, electrical length of interconnects becomes a significant fraction of the operating wavelength, giving rise to signal distorting effects that do not exist at lower frequencies. Consequently, the conventional lumped impedance interconnect models become inadequate and transmission line models based on quasi-transverse electromagnetic mode (TEM) assumptions are needed. The TEM approximation represents the ideal case, where both E and H fields are perpendicular to the direction of propagation and it is valid under the condition that the line cross section is much smaller than the wavelength. However, the inhomogeneties in practical wiring configurations give rise to E or H fields in the direction of propagation. If the line cross section or the extent of these nonuniformities remain a small fraction of the wavelength in the frequency range of interest, the solution to Maxwell's equations are given by the so-called quasi-TEM modes and are characterized by distributed R, L, C, G per unit length (p.u.l.) parameters [12] (discussed in detail in Section III).

In practical situations, owing to complex interconnect geometries and varying cross-sectional areas, the interconnects may need to be modeled as nonuniform lines. In this case, the p.u.l. parameters are functions of the distance, along the length of the transmission line [96]–[98].

3) Distributed Models with Frequency-Dependent Parameters: At low frequencies, the current in a conductor is distributed uniformly throughout its cross section. However, as the operating frequency increases, the current distribution gets uneven and starts getting concentrated more and more near the surface or edges of the conductor. This phenomenon can be categorized as follows: skin, edge, and proximity effects [12], [30], [99], [100]. The skin effect causes the current to concentrate in a thin layer near the conductor surface and this reduces the effective cross section available for signal propagation. This leads to an increase in the resistance to signal propagation and other related effects [9]. The edge effect causes the current to concentrate near the sharp edges of the conductor. The proximity effect causes the current to concentrate in the sections of ground plane that are close to the signal conductor. To account for these effects, modeling based on frequency-dependent p.u.l. parameters may be necessary. An illustration of frequency-dependent variation of R and L parameters for an example microstrip are given in Fig. 9.

4) PEEC and rPEEC Models: As switching speeds extend into the gigahertz range, two-dimensional (2-D) transmission line models become inadequate due to the spatial EM effects of three-dimensional structures. The modeling of these structures has been successfully accomplished using partial element equivalent circuit (PEEC) models. PEEC models are RLC circuits where individual resistances and capacitances are extracted from the geometry using a quasi-static (nonretarded) solution of Maxwell's equations. The rPEEC models include the retardation and provide full-wave solution. Simulation of these models is relatively CPU intensive as they involve large resultant networks [15]–[22].

III. Distributed Transmission Line Equations

Transmission line characteristics are in general described by Telegrapher's equations. Consider the transmission line system shown in Fig. 10(a). Telegrapher's equations for such a structure can be derived by discretizing the line into infinitesimal sections of length Δx and assuming uniform p.u.l. parameters of resistance (R), inductance (L), conductance (G), and capacitance (C). Each section then includes a resistance $R\Delta x$, inductance $L\Delta x$, conductance $G\Delta x$, and capacitance $C\Delta x$ [Fig. 10(b)]. Using Kirchhoff's current and voltage laws, one can write [12]

$$v(x+\Delta x, t) = v(x, t) - R\Delta x i(x, t) - L\Delta x \frac{\partial}{\partial t} i(x, t) \tag{2}$$

or

$$\frac{v(x+\Delta x, t) - v(x, t)}{\Delta x} = -Ri(x, t) - L\frac{\partial}{\partial t} i(x, t). \tag{3}$$

Taking the limit $\Delta x \to 0$, one gets

$$\frac{\partial}{\partial x} v(x, t) = -Ri(x, t) - L\frac{\partial}{\partial t} i(x, t). \tag{4}$$

Similarly, we can obtain the second transmission line equation

$$\begin{aligned} i(x+\Delta x, t) = {} & i(x, t) - G\Delta x v(x+\Delta x, t) \\ & - C\Delta x \frac{\partial}{\partial t} v(x+\Delta x, t). \end{aligned} \tag{5}$$

Substituting (2) in (5), we have

$$\begin{aligned} & i(x+\Delta x, t) \\ & = i(x, t) - G\Delta x \left(v(x, t) - R\Delta x i(x, t) - L\Delta x \frac{\partial}{\partial t} i(x, t) \right) \\ & \quad - C\Delta x \frac{\partial}{\partial t} \left(v(x, t) - R\Delta x i(x, t) \right. \\ & \qquad \left. - L\Delta x \frac{\partial}{\partial t} i(x, t) \right) \end{aligned} \tag{6}$$

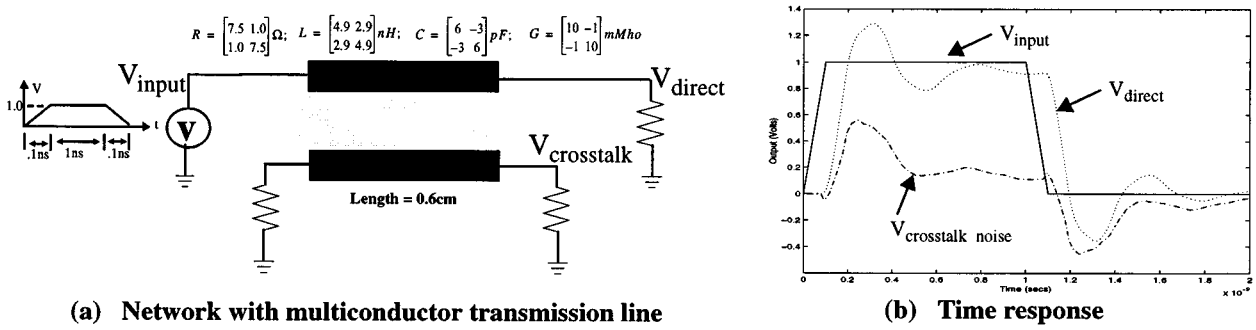

(a) Network with multiconductor transmission line (b) Time response

Fig. 8. Illustration of crosstalk.

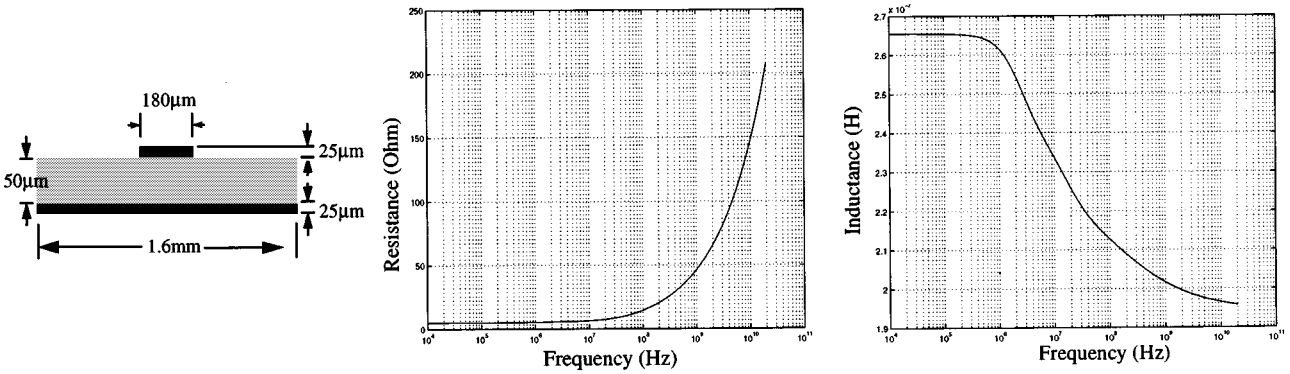

Fig. 9. An example of frequency-dependent variation of resistance and inductance.

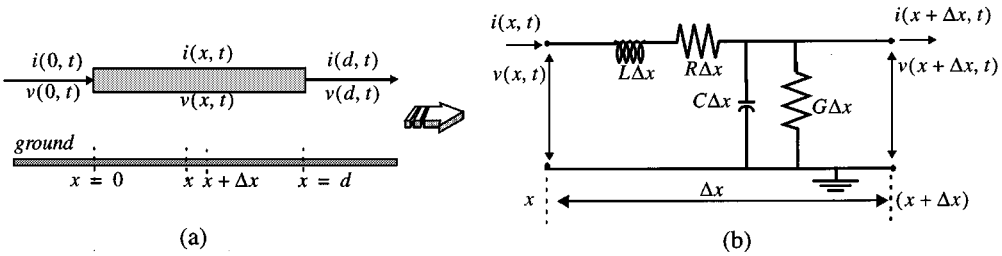

Fig. 10. Transmission line system.

or

$$\frac{i(x+\Delta x,\,t)-i(x,\,t)}{\Delta x} = -Gv(x,\,t)-C\frac{\partial}{\partial t}v(x,\,t)+\Delta x \cdot\left(GRi(x,\,t)+(GL+RC)\frac{\partial}{\partial t}i(x,\,t)+LC\frac{\partial^2}{\partial t^2}i(x,\,t)\right). \tag{7}$$

Taking the limit $\Delta x \to 0$, one gets

$$\frac{\partial}{\partial x}i(x,\,t) = -Gv(x,\,t) - C\frac{\partial}{\partial t}v(x,\,t). \tag{8}$$

Taking the Laplace transform of (4) and (8), one can write

$$\frac{\partial}{\partial x}V(x,\,s) = -(R+sL)I(x,\,s) = -ZI(x,\,s) \tag{9}$$

$$\frac{\partial}{\partial x}I(x,\,s) = -(G+sC)V(x,\,s) = -YV(x,\,s) \tag{10}$$

where Z and Y represent the p.u.l. impedance and admittances of the transmission line, given by

$$Z = R + sL, \qquad Y = G + sC. \tag{11}$$

The set of equations represented by (9) and (10) can be solved if they can be written in terms of one of the unknowns [either $\boldsymbol{V}(x,\,s)$ or $\boldsymbol{I}(x,\,s)$] as follows:

$$\frac{\partial^2}{\partial x^2}V(x,\,s) = ZYV(x,\,s) = \Upsilon^2 V(x,\,s) \tag{12}$$

$$\frac{\partial^2}{\partial x^2}I(x,\,s) = YZI(x,\,s) = \Upsilon^2 I(x,\,s) \tag{13}$$

where $\Upsilon(s)$ is the complex propagation constant, given by

$$\Upsilon(s) = \alpha + j\beta = \sqrt{ZY} = \sqrt{(R+jwL)(G+jwC)} \tag{14}$$

where α represents the real part of the propagation constant and is known as the *attenuation constant*, whose units are expressed in nepers/m. β represents the imaginary part of the propagation constant and is known as the *phase constant*, whose units are expressed in radians/m. The solution of (12)

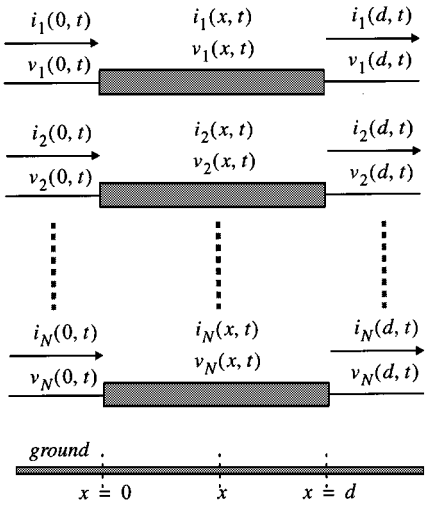

Fig. 11. Multiconductor transmission line system.

and (13) can be obtained as a combination of forward-reflected waves traveling on the line as

$$V(x,\, s) = V(0,\, s)e^{\pm \Upsilon(s)x} \tag{15}$$

$$I(x,\, s) = I(0,\, s)e^{\pm \Upsilon(s)x}. \tag{16}$$

The phase shift and attenuation experienced by the traveling waves are given by $e^{\pm j\beta(s)x}$ and $e^{\pm \alpha(s)x}$, respectively. If the lines are lossless, the propagation constant is given by $\Upsilon(s) = j\beta = \sqrt{ZY} = jw\sqrt{LC}$. The line in this case represents a *pure-delay* element.

A. Multiconductor Transmission Line System

Consider the multiconductor transmission line (MTL) system, with N coupled conductors, shown in Fig. 11.

Using steps similar to the case of single transmission line, we can derive the multiconductor transmission line equations. Per-unit-length parameters ($\boldsymbol{R}$, $\boldsymbol{L}$, $\boldsymbol{G}$, and $\boldsymbol{C}$) in this case become matrices and voltage–current variables become vectors represented by $\boldsymbol{v}$ and $\boldsymbol{i}$, respectively. Noting these changes, we can rewrite (4) and (8) as

$$\frac{\partial}{\partial x}\boldsymbol{v}(x,\, t) = -\boldsymbol{R}\boldsymbol{i}(x,\, t) - \boldsymbol{L}\frac{\partial}{\partial t}\boldsymbol{i}(x,\, t) \tag{17}$$

$$\frac{\partial}{\partial x}\boldsymbol{i}(x,\, t) = -\boldsymbol{G}\boldsymbol{v}(x,\, t) - \boldsymbol{C}\frac{\partial}{\partial t}\boldsymbol{v}(x,\, t). \tag{18}$$

The MTL equations represented by (17) and (18) are a set of $2N$ coupled first-order partial differential equations (PDE) and they can be put in a more concise form as

$$\frac{\partial}{\partial x}\begin{bmatrix}\boldsymbol{v}(x,\, t)\\ \boldsymbol{i}(x,\, t)\end{bmatrix} = -\begin{bmatrix}\boldsymbol{0} & \boldsymbol{R}\\ \boldsymbol{G} & \boldsymbol{0}\end{bmatrix}\begin{bmatrix}\boldsymbol{v}(x,\, t)\\ \boldsymbol{i}(x,\, t)\end{bmatrix} - \begin{bmatrix}\boldsymbol{0} & \boldsymbol{L}\\ \boldsymbol{C} & \boldsymbol{0}\end{bmatrix}\frac{\partial}{\partial t}\left(\begin{bmatrix}\boldsymbol{v}(x,\, t)\\ \boldsymbol{i}(x,\, t)\end{bmatrix}\right). \tag{19}$$

For the case of multiconductors, (9)–(11) are modified as

$$\frac{\partial}{\partial x}\boldsymbol{V}(x,\, s) = -\boldsymbol{Z}\boldsymbol{I}(x,\, s) \tag{20}$$

$$\frac{\partial}{\partial x}\boldsymbol{I}(x,\, s) = -\boldsymbol{Y}\boldsymbol{V}(x,\, s) \tag{21}$$

where $\boldsymbol{Z}$ and $\boldsymbol{Y}$ represent the impedance and admittance matrices, given by

$$\boldsymbol{Z} = \boldsymbol{R} + s\boldsymbol{L}, \qquad \boldsymbol{Y} = \boldsymbol{G} + s\boldsymbol{C}. \tag{22}$$

The $\boldsymbol{R}$, $\boldsymbol{L}$, $\boldsymbol{G}$, and $\boldsymbol{C}$ matrices are obtained by a 2-D solution of Maxwell's equations at appropriate positions, along the propagation axis. For this purpose, depending on the nature and geometry of the structure, and the desired accuracy, techniques based on quasi-static or full-wave approaches can be used. The $\boldsymbol{R}$, $\boldsymbol{L}$, $\boldsymbol{G}$, and $\boldsymbol{C}$ matrices are symmetric and positive definite [12], [90].

B. Multiconductor Transmission Line Stamp

In this section, we derive a stamp relating the terminal currents and voltages of MTL structures, suitable for inclusion in SPICE-like simulators. The transmission line stamp [63] is derived through *decoupling of MTL equations*.

Differentiating the partial differential equations given in (20) and (21) with respect to x, we have

$$\frac{\partial^2}{\partial x^2}\boldsymbol{V}(x,\, s) = -\boldsymbol{Z}\frac{\partial}{\partial x}\boldsymbol{I}(x,\, s) \tag{23}$$

$$\frac{\partial^2}{\partial x^2}\boldsymbol{I}(x,\, s) = -\boldsymbol{Y}\frac{\partial}{\partial x}\boldsymbol{V}(x,\, s). \tag{24}$$

Substituting (21) in (23) and (20) in (24), we get the following two sets of coupled wave equations:

$$\frac{\partial^2}{\partial x^2}\boldsymbol{V}(x,\, s) = \boldsymbol{Z}\boldsymbol{Y}\boldsymbol{V}(x,\, s) \tag{25}$$

$$\frac{\partial^2}{\partial x^2}\boldsymbol{I}(x,\, s) = \boldsymbol{Y}\boldsymbol{Z}\boldsymbol{I}(x,\, s). \tag{26}$$

Decoupling of equations in (25) or (26) can be achieved through the use of suitable modal transformation matrices [11]. For this purpose, introduce a transformation $\boldsymbol{W}$ relating the circuit voltages $\boldsymbol{V}$ and modal voltages $\tilde{\boldsymbol{V}}$ as

$$\boldsymbol{V}(x,\, s) = \boldsymbol{W}\tilde{\boldsymbol{V}}(x,\, s). \tag{27}$$

Hence, (25) can be rewritten as [for simplicity, we omit the accompanying term $(x,\, s)$]

$$\frac{\partial^2}{\partial x^2}\boldsymbol{W}\tilde{\boldsymbol{V}} = \boldsymbol{Z}\boldsymbol{Y}\boldsymbol{W}\tilde{\boldsymbol{V}} \tag{28}$$

or

$$\frac{\partial^2}{\partial x^2}\tilde{\boldsymbol{V}} = \left(\boldsymbol{W}^{-1}\boldsymbol{Z}\boldsymbol{Y}\boldsymbol{W}\right)\tilde{\boldsymbol{V}}. \tag{29}$$

For effective decoupling of equations to take place, the matrix product in parenthesis must lead to a diagonal matrix as

$$\boldsymbol{W}^{-1}\boldsymbol{Z}\boldsymbol{Y}\boldsymbol{W} = \begin{bmatrix}\Upsilon_1^2 & 0 & 0\\ 0 & \cdots & 0\\ 0 & 0 & \Upsilon_N^2\end{bmatrix} \tag{30}$$

where the diagonal matrix contains the eigenvalues of the product $\boldsymbol{ZY}$, which corresponds to the roots of the characteristic equation

$$\left|\Upsilon_k^2\boldsymbol{U} - \boldsymbol{Z}\boldsymbol{Y}\right| = 0, \qquad k = 1,\, 2,\, \ldots,\, N \tag{31}$$

where $\boldsymbol{U}$ represents the unity matrix (we assume the general case that there exist N distinct eigenvalues). Next, as is evident, the transformation matrix $\boldsymbol{W}$, which relates the circuit

voltages and modal voltages, consists of N linearly independent column vectors $(\boldsymbol{w_k})$, corresponding to the eigenvectors of product $\boldsymbol{ZY}$, given by

$$\left(\Upsilon_k^2\boldsymbol{U}-\boldsymbol{ZY}\right)\boldsymbol{w_k}=0, \qquad k=1, 2, \ldots, N. \tag{32}$$

[Similarly, we can write a transformation $\boldsymbol{T}$ relating the circuit currents $(\boldsymbol{I})$ and modal currents $(\tilde{\boldsymbol{I}})$ as $\boldsymbol{I}=\boldsymbol{T}\tilde{\boldsymbol{I}}$. Hence, (26) can be rewritten as $(\partial^2/\partial x^2)\tilde{\boldsymbol{I}}=(\boldsymbol{T}^{-1}\boldsymbol{YZT})\tilde{\boldsymbol{I}}$. The diagonalization of $\boldsymbol{YZ}$ leads to the same diagonal matrix Υ^2, represented by (30). (This can be easily proved by noting that $\boldsymbol{YZ}=(\boldsymbol{U})\boldsymbol{YZ}=(\boldsymbol{Z}^{-1}\boldsymbol{Z})\boldsymbol{YZ}=\boldsymbol{Z}^{-1}(\boldsymbol{ZY})\boldsymbol{Z}$. In other words, matrices $\boldsymbol{ZY}$ and $\boldsymbol{YZ}$ are similar or they have the same eigenvalues.) The transformation matrix $\boldsymbol{T}$ consists of the eigenvectors corresponding to the product $\boldsymbol{YZ}$.]

Having obtained the propagation constants, the solution of (29) can be written in the standard form as

$$\tilde{V}_k(x)=e^{-\Upsilon_k x}c_{ki}+e^{\Upsilon_k x}c_{kr}, \qquad k=1, 2, \ldots, N \tag{33}$$

where $\tilde{V}_k(x)$ represents the kth modal voltage and c_{ki}, c_{kr} are the corresponding constants, pertaining to incident and reflected waves, respectively. Equation (33) can be written in the matrix form as

$$\begin{bmatrix}\tilde{V}_1(x)\\ \tilde{V}_2(x)\\ \cdots\\ \tilde{V}_N(x)\end{bmatrix}=\begin{bmatrix}e^{-\Upsilon_1 x} & & & \\ & e^{-\Upsilon_2 x} & & \\ & & \cdots & \\ & & & e^{-\Upsilon_N x}\end{bmatrix}\begin{bmatrix}c_{1i}\\ c_{2i}\\ \\ \\ c_{Ni}\end{bmatrix}+\begin{bmatrix}e^{\Upsilon_1 x} & & & \\ & e^{\Upsilon_2 x} & & \\ & & \cdots & \\ & & & e^{\Upsilon_N x}\end{bmatrix}\begin{bmatrix}c_{1r}\\ c_{2r}\\ \cdots\\ c_{Nr}\end{bmatrix}. \tag{34}$$

Defining $\boldsymbol{E}(\boldsymbol{x})=\operatorname{diag}[e^{-\Upsilon_1 x}\cdots e^{-\Upsilon_N x}]$ and premultiplying both sides of (34) by the modal transformation matrix $\boldsymbol{W}$ [from (27)], we can write (34) in terms of circuit voltages as

$$\boldsymbol{V}(x)=\boldsymbol{W}[\boldsymbol{E}(x)]\boldsymbol{C}_1+\boldsymbol{W}[\boldsymbol{E}(x)]^{-1}\boldsymbol{C}_2 \tag{35}$$

where $\boldsymbol{C}_1$ and $\boldsymbol{C}_2$ are constant vectors, which can be determined from the terminal currents and voltages (i.e., at $x=0$ and $x=d$).

A relationship between the near-end $(x=0)$ and far-end $(x=d)$ voltages can be derived using (35) as

$$\begin{bmatrix}\boldsymbol{V}(0)\\ \boldsymbol{V}(d)\end{bmatrix}=\begin{bmatrix}\boldsymbol{W} & \boldsymbol{W}\\ \boldsymbol{WE}(d) & \boldsymbol{W}[\boldsymbol{E}(d)]^{-1}\end{bmatrix}\begin{bmatrix}\boldsymbol{C}_1\\ \boldsymbol{C}_2\end{bmatrix}. \tag{36}$$

Next, substituting (35) in (20), we have

$$-\boldsymbol{W}\Gamma[\boldsymbol{E}(x)]\boldsymbol{C}_1+\boldsymbol{W}\Gamma[\boldsymbol{E}(x)]^{-1}\boldsymbol{C}_2=-\boldsymbol{ZI}(x)$$

$$\Gamma=\begin{bmatrix}\Upsilon_1 & & \\ & \cdots & \\ & & \Upsilon_N\end{bmatrix} \tag{37}$$

or

$$\boldsymbol{I}(x)=\boldsymbol{W_i}[\boldsymbol{E}(x)]\boldsymbol{C}_1-\boldsymbol{W_i}[\boldsymbol{E}(x)]^{-1}\boldsymbol{C}_2, \quad \boldsymbol{W_i}=\boldsymbol{Z}^{-1}\boldsymbol{W}\Gamma. \tag{38}$$

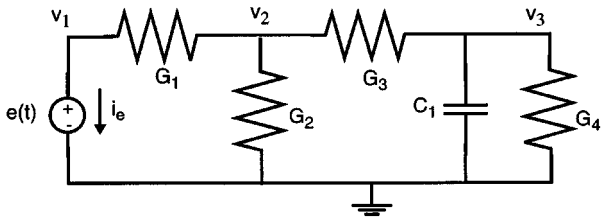

Fig. 12. Example circuit for MNA formulation.

A relationship between the near-end $(x=0)$ and far-end $(x=d)$ can be derived using (38) as

$$\begin{bmatrix}\boldsymbol{I}(0)\\ \boldsymbol{I}(d)\end{bmatrix}=\begin{bmatrix}\boldsymbol{W_i} & -\boldsymbol{W_i}\\ \boldsymbol{W_iE}(d) & -\boldsymbol{W_i}[\boldsymbol{E}(d)]^{-1}\end{bmatrix}\begin{bmatrix}\boldsymbol{C}_1\\ \boldsymbol{C}_2\end{bmatrix}. \tag{39}$$

Using (36) and (39) and eliminating the constants $\boldsymbol{C}_1$ and $\boldsymbol{C}_2$, we get

$$\begin{bmatrix}\boldsymbol{I}(0)\\ \boldsymbol{I}(d)\end{bmatrix}=\begin{bmatrix}\boldsymbol{W_i} & -\boldsymbol{W_i}\\ \boldsymbol{W_iE}(d) & -\boldsymbol{W_i}[\boldsymbol{E}(d)]^{-1}\end{bmatrix}\cdot\begin{bmatrix}\boldsymbol{W} & \boldsymbol{W}\\ \boldsymbol{WE}(d) & \boldsymbol{W}[\boldsymbol{E}(d)]^{-1}\end{bmatrix}^{-1}\begin{bmatrix}\boldsymbol{V}(0)\\ \boldsymbol{V}(d)\end{bmatrix}. \tag{40}$$

Assume that the y-parameter-based stamp of multiconductor stamp is required in the standard form, where current $\boldsymbol{I}(d)$ flows inwards. In this case, the expression for $\boldsymbol{I}(d)$ in (40) must be multiplied by -1. Noting this and simplifying (40), we can write the MTL stamp in terms of y-parameters as

$$\begin{bmatrix}\boldsymbol{I}(0)\\ -\boldsymbol{I}(d)\end{bmatrix}=\begin{bmatrix}\boldsymbol{Y}_{11} & Y_{12}\\ \boldsymbol{Y}_{21} & \boldsymbol{Y}_{22}\end{bmatrix}\begin{bmatrix}\boldsymbol{V}(0)\\ \boldsymbol{V}(d)\end{bmatrix}=\begin{bmatrix}\boldsymbol{W_iE}_1\boldsymbol{W}^{-1} & \boldsymbol{W_iE}_2\boldsymbol{W}^{-1}\\ \boldsymbol{W_iE}_2\boldsymbol{W}^{-1} & \boldsymbol{W_iE}_1\boldsymbol{W}^{-1}\end{bmatrix}\begin{bmatrix}V(0)\\ V(d)\end{bmatrix} \tag{41}$$

where

$$\boldsymbol{E}_1=\operatorname{diag}\left\{\frac{1+e^{(-2\Upsilon_k d)}}{1-e^{(-2\Upsilon_k d)}}\right\}$$

$$\boldsymbol{E}_2=\operatorname{diag}\left\{\frac{-2e^{(-\Upsilon_k d)}}{1-e^{(-2\Upsilon_k d)}}\right\}, \qquad k=1, 2, \ldots, N. \tag{42}$$

Matrix Exponential Stamp: An alternative form of the MTL stamp is also quite popular and it has the matrix exponential form [72], which is explained below. Equations (20) and (21) can be written in the hybrid form as

$$\frac{\partial}{\partial x}\begin{bmatrix}\boldsymbol{V}(x, s)\\ \boldsymbol{I}(x, s)\end{bmatrix}=(\boldsymbol{D}+s\boldsymbol{E})\begin{bmatrix}\boldsymbol{V}(x, s)\\ \boldsymbol{I}(x, s)\end{bmatrix}$$

$$\boldsymbol{D}=\begin{bmatrix}\boldsymbol{0} & -\boldsymbol{R}\\ -\boldsymbol{G} & \boldsymbol{0}\end{bmatrix}$$

$$\boldsymbol{E}=\begin{bmatrix}\boldsymbol{0} & -\boldsymbol{L}\\ -\boldsymbol{C} & \boldsymbol{0}\end{bmatrix}. \tag{43}$$

Using the terminal conditions, the solution of (43) can be written as

$$\begin{bmatrix}\boldsymbol{V}(d, s)\\ \boldsymbol{I}(d, s)\end{bmatrix}=e^{(\boldsymbol{D}+s\boldsymbol{E})d}\begin{bmatrix}V(0, s)\\ \boldsymbol{I}(0, s)\end{bmatrix}. \tag{44}$$

A relationship between the forms represented by (41) and (44) can be obtained as follows: Define $\boldsymbol{T}(s)$ as

$$\boldsymbol{T}(s)=\begin{bmatrix}\boldsymbol{T}_{11} & \boldsymbol{T}_{12}\\ \boldsymbol{T}_{21} & \boldsymbol{T}_{22}\end{bmatrix}=e^{(\boldsymbol{D}+s\boldsymbol{E})d}. \tag{45}$$

Using some algebraic manipulations, we can express the relationships between the hybrid parameters (44) and the y-parameters (41) as

$$\begin{aligned}\begin{bmatrix} \boldsymbol{I}(0) \\ -\boldsymbol{I}(d) \end{bmatrix} &= \begin{bmatrix} \boldsymbol{Y}_{11} & \boldsymbol{Y}_{12} \\ \boldsymbol{Y}_{21} & \boldsymbol{Y}_{22} \end{bmatrix} \begin{bmatrix} \boldsymbol{V}(0) \\ \boldsymbol{V}(d) \end{bmatrix} \\ &= \begin{bmatrix} -\boldsymbol{T}_{12}^{-1}\boldsymbol{T}_{11} & \boldsymbol{T}_{12}^{-1} \\ -\boldsymbol{T}_{21}+\boldsymbol{T}_{22}\boldsymbol{T}_{12}^{-1}\boldsymbol{T}_{11} & -\boldsymbol{T}_{22}\boldsymbol{T}_{12}^{-1} \end{bmatrix} \begin{bmatrix} \boldsymbol{V}(0) \\ \boldsymbol{V}(d) \end{bmatrix} \end{aligned} \quad (46)$$

$$\begin{aligned}\begin{bmatrix} \boldsymbol{V}(d) \\ \boldsymbol{I}(d) \end{bmatrix} &= \begin{bmatrix} \boldsymbol{T}_{11} & \boldsymbol{T}_{12} \\ \boldsymbol{T}_{21} & \boldsymbol{T}_{22} \end{bmatrix} \begin{bmatrix} \boldsymbol{V}(0) \\ \boldsymbol{I}(0) \end{bmatrix} \\ &= \begin{bmatrix} -\boldsymbol{Y}_{12}^{-1}\boldsymbol{Y}_{11} & \boldsymbol{Y}_{12}^{-1} \\ -\boldsymbol{Y}_{21}+\boldsymbol{Y}_{22}\boldsymbol{Y}_{12}^{-1}\boldsymbol{Y}_{11} & -\boldsymbol{Y}_{22}\boldsymbol{Y}_{12}^{-1} \end{bmatrix} \begin{bmatrix} V(0) \\ \boldsymbol{I}(0) \end{bmatrix}. \end{aligned} \quad (47)$$

Similarly, another useful representation of the MTL stamp is in terms of ABCD parameters, which can be written as

$$\begin{bmatrix} \boldsymbol{T}_{11} & -\boldsymbol{U} \\ \boldsymbol{T}_{21} & 0 \end{bmatrix} \begin{bmatrix} \boldsymbol{V}(0) \\ \boldsymbol{V}(d) \end{bmatrix} + \begin{bmatrix} \boldsymbol{T}_{12} & 0 \\ \boldsymbol{T}_{22} & -\boldsymbol{U} \end{bmatrix} \begin{bmatrix} \boldsymbol{I}(0) \\ \boldsymbol{I}(d) \end{bmatrix} = \begin{bmatrix} \boldsymbol{0} \\ \boldsymbol{0} \end{bmatrix}. \quad (48)$$

In the next section, we will review a generic formulation of distributed interconnect circuit equations, suitable for general purpose circuit simulators.

IV. Formulation of Circuit Equations

Prior to introducing interconnect simulation algorithms, it would be useful to review a generic formulation of circuit equations. For both frequency or time-domain analysis, the first step is to set up the *modified nodal analysis matrix (MNA)* [140]. For example, consider the circuit in Fig. 12. Let V_3 be the desired output. Using Kirchhoff's current law, the time-domain MNA and the output equations can be written as

$$\begin{bmatrix} 0 & 0 & 0 & 0 \\ 0 & 0 & 0 & 0 \\ 0 & 0 & C_1 & 0 \\ 0 & 0 & 0 & 0 \end{bmatrix} \begin{bmatrix} \dot{v}_1 \\ \dot{v}_2 \\ \dot{v}_3 \\ \dot{i}_e \end{bmatrix} + \begin{bmatrix} G_1 & -G_1 & 0 & 1 \\ -G_1 & G_1+G_2+G_3 & -G_3 & 0 \\ 0 & -G_3 & G_3+G_4 & 0 \\ 1 & 0 & 0 & 0 \end{bmatrix} \cdot \begin{bmatrix} v_1 \\ v_2 \\ v_3 \\ i_e \end{bmatrix} = \begin{bmatrix} 0 \\ 0 \\ 0 \\ 1 \end{bmatrix} [e(t)]$$

$$y = [0 \;\; 0 \;\; 1 \;\; 0] \begin{bmatrix} v_1 \\ v_2 \\ v_3 \\ i_e \end{bmatrix}.$$

The above equation, representing a simple three-node circuit, has the same form as any other MNA matrix representing a large linear lumped network. Hence, MNA and output equations for lumped linear networks can be written using a generic notation as

$$\begin{aligned} \boldsymbol{W}\dot{\boldsymbol{x}}(t)+\boldsymbol{G}\boldsymbol{x}(t) &= \boldsymbol{B}\boldsymbol{u}(t) \\ \boldsymbol{y} &= \boldsymbol{L}^T\boldsymbol{x}(t) \end{aligned} \quad (49)$$

where $\boldsymbol{B}$ and $\boldsymbol{L}$ are selector matrices, with entries (0 or 1), and the superscript "T" denotes the transpose. Let $\boldsymbol{b}(t) = \boldsymbol{B}\boldsymbol{u}(t)$. From (49), MNA equations in the frequency-domain can be written as

$$\begin{aligned} (\boldsymbol{G}+s\boldsymbol{W})\boldsymbol{X}(s) &= \boldsymbol{b}(s) \\ \boldsymbol{Y}(s) &= \boldsymbol{L}^T\boldsymbol{X}(s). \end{aligned} \quad (50)$$

For the case of nonlinear elements, MNA equations in (49) can be modified as

$$\begin{aligned} \boldsymbol{W}\dot{\boldsymbol{x}}(t)+\boldsymbol{G}\boldsymbol{x}(t)+\boldsymbol{F}(\boldsymbol{x}(t))-\boldsymbol{b}(t) &= \boldsymbol{0} \\ \boldsymbol{y} &= \boldsymbol{L}^T\boldsymbol{x}(t) \end{aligned} \quad (51)$$

where $\boldsymbol{F}(\boldsymbol{x}(t))$ is a nonlinear function of $\boldsymbol{x}$.

1) Formulation of Linear Subnetworks Containing Distributed Elements: Consider a linear subnetwork π containing distributed elements. Using (41), the frequency-domain equations of a distributed subnetwork containing n_d coupled conductors can be written as [63]

$$\boldsymbol{Y_d}(s)\boldsymbol{V_d}(s) = \boldsymbol{I_d}(s) \quad (52)$$

where $\boldsymbol{V_d}(s)$ and $\boldsymbol{I_d}(s)$ represent the Laplace-domain terminal voltages and currents of the distributed element, respectively, $\boldsymbol{Y_d}(s)$ represents the admittance matrix having complex dependency on frequency, which are described in terms of line parameters. Equation (50) representing the lumped linear network can be combined with (52) as

$$\begin{bmatrix} s\boldsymbol{W}_\pi+\boldsymbol{G}_\pi & \boldsymbol{L}_d \\ \boldsymbol{Y_d}\boldsymbol{L}_d^T & -\boldsymbol{U} \end{bmatrix} \begin{bmatrix} \boldsymbol{X}_\pi(s) \\ \boldsymbol{I_d}(s) \end{bmatrix} = \begin{bmatrix} \boldsymbol{b}_\pi \\ \boldsymbol{0} \end{bmatrix} \quad (53)$$

where

- $\boldsymbol{W}_\pi$, $\boldsymbol{G}_\pi \in \Re^{N_\pi \times N_\pi}$ are constant matrices describing the lumped memory and memoryless elements of subnetwork π, respectively, and $\Re^{N_\pi}$ is the node-space of subnetwork π;
- $\boldsymbol{L}_d$ is the selector matrix that maps the terminal currents of the distributed subnetwork to the nodal space of the linear subnetwork π, and $\boldsymbol{U}$ is the unity matrix;
- $\boldsymbol{b}_\pi \in \Re^{N_\pi}$ is a constant vector with entries determined by independent voltage–current sources of subnetwork π, and $\boldsymbol{X}_\pi(s) \in \Re^{N_\pi}$ is the vector of node voltage waveforms appended by independent voltage source currents, linear inductor current waveforms of linear subnetwork π.

Equation (53) can be concisely written as

$$\psi(s)\boldsymbol{X}(s) = \boldsymbol{b}(s). \quad (54)$$

2) Generic Formulation of Nonlinear Circuits with Distributed Elements: Consider a general network containing an arbitrary number of nonlinear and linear (lumped and distributed) components. For simplicity, let the linear components be grouped into a single linear subnetwork π as shown in Fig. 13.

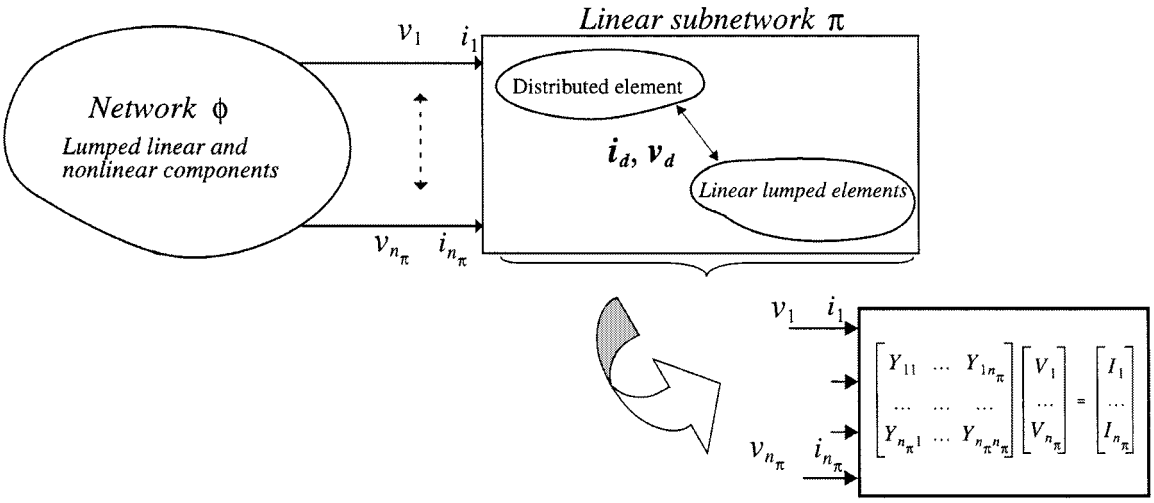

Fig. 13. Nonlinear network ϕ containing linear subnetwork π with distributed elements.

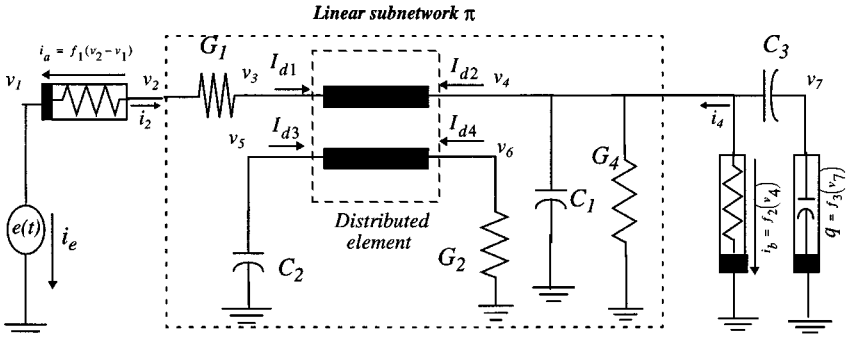

Fig. 14. Example circuit with lumped/distributed/measured and nonlinear devices.

Using (51), without loss of generality, the circuit equations [140] for the network ϕ can be written as

$$\boldsymbol{W}_\phi \frac{d}{dt}\dot{\boldsymbol{x}}_\phi(t) + \boldsymbol{G}_\phi \boldsymbol{x}_\phi(t) + \boldsymbol{L}_\pi \boldsymbol{i}_\pi(t) + \boldsymbol{F}(\boldsymbol{x}_\phi(t)) - \boldsymbol{b}_\phi(t) = 0 \qquad t \in [0, T] \tag{55}$$

where

- $\boldsymbol{W}_\phi$, $\boldsymbol{G}_\phi \in \Re^{N_\phi \times N_\phi}$ are constant matrices describing the lumped memory and memoryless elements of network ϕ, respectively, and $\boldsymbol{b}_\phi \in \Re^{N_\phi}$ is a constant vector with entries determined by the independent voltage and current sources;
- $\boldsymbol{F}(\boldsymbol{x}_\phi)$ is a function describing the nonlinear elements of the circuit, $\boldsymbol{x}_\phi(t) \in \Re^{N_\phi}$ is the vector of node voltage waveforms appended by independent voltage source current, linear inductor current, nonlinear capacitor charge, and nonlinear inductor flux waveforms, N_ϕ is the total number of variables in the MNA formulation, and n_π is the total number of ports in linear subnetwork π;
- $\boldsymbol{L}_\pi = [l_{i,j}]$ with elements $l_{i,j} \in \{0, 1\}$ where $i \in \{1, \ldots, N_\phi\}$, $j \in \{1, \ldots, n_\pi\}$ with a maximum of one nonzero in each row or column, is a selector matrix that maps $\boldsymbol{i}_\pi(t) \in \Re^{n_\pi}$ the vector of currents entering the linear subnetwork π, into the node space $\Re^{N_\phi}$ of the network ϕ.

The linear multiterminal subnetwork π can be characterized in the frequency-domain by its terminal behavior as

$$\boldsymbol{Y}_\pi(s)\boldsymbol{V}_\pi(s) = \boldsymbol{I}_\pi(s) \tag{56}$$

where $\boldsymbol{Y}_\pi(s)$ is the y-parameter matrix of subnetwork π, $\boldsymbol{V}_\pi(s)$ is the vector of terminal voltage nodes that connect the subnetwork to the network ϕ, and $\boldsymbol{I}_\pi(s)$ is the Laplace transform of $(\boldsymbol{i}_\pi(t))$.

3) Example: To illustrate the formulation scheme described in this section, consider the circuit shown in Fig. 14. The network equations can be written as follows.

The entities in (55) with respect to the given nonlinear network can be obtained as

$$\boldsymbol{G}_\phi = \begin{bmatrix} 0 & 0 & 0 & 0 & 1 & 0 \\ 0 & 0 & 0 & 0 & 0 & 0 \\ 0 & 0 & 0 & 0 & 0 & 0 \\ 0 & 0 & 0 & 0 & 0 & 0 \\ 1 & 0 & 0 & 0 & 0 & 0 \\ 0 & 0 & 0 & 0 & 0 & 1 \end{bmatrix}$$

$$\boldsymbol{W}_\phi = \begin{bmatrix} 0 & 0 & 0 & 0 & 0 & 0 \\ 0 & 0 & 0 & 0 & 0 & 0 \\ 0 & 0 & C_3 & -C_3 & 0 & 0 \\ 0 & 0 & -C_3 & C_3 & 0 & 1 \\ 0 & 0 & 0 & 0 & 0 & 0 \\ 0 & 0 & 0 & 0 & 0 & 0 \end{bmatrix}$$

$$\boldsymbol{F}(\boldsymbol{x}_\phi(t)) = \begin{bmatrix} -f_1(v_2 - v_1) \\ f_1(v_2 - v_1) \\ f_2(v_4) \\ 0 \\ 0 \\ -f_3(v_7) \end{bmatrix}, \qquad \boldsymbol{x}_\phi = \begin{bmatrix} v_1 \\ v_2 \\ v_4 \\ v_7 \\ i_e \\ q \end{bmatrix}$$

$$\boldsymbol{b}_\phi = \begin{bmatrix} 0 \\ 0 \\ 0 \\ 0 \\ e \\ 0 \end{bmatrix} \qquad \boldsymbol{L}_\pi = \begin{bmatrix} 0 & 0 \\ 1 & 0 \\ 0 & 1 \\ 0 & 0 \\ 0 & 0 \\ 0 & 0 \end{bmatrix}$$

$$\boldsymbol{i}_\pi(t) = \begin{bmatrix} i_2(t) \\ i_4(t) \end{bmatrix}.$$

The entities in (53), (54), and (56) characterizing the given linear subnetwork can be obtained as

$$\boldsymbol{G}_\phi + s\boldsymbol{W}_\pi = \begin{bmatrix} G_1 & -G_1 & 0 & 0 & 0 \\ -G_1 & G_1 & 0 & 0 & 0 \\ 0 & 0 & G_4 + sC_1 & 0 & 0 \\ 0 & 0 & 0 & sC_2 & 0 \\ 0 & 0 & 0 & 0 & G_2 \end{bmatrix}$$

$$\boldsymbol{L_d} = \begin{bmatrix} 0 & 0 & 0 & 0 \\ 1 & 0 & 0 & 0 \\ 0 & 1 & 0 & 0 \\ 0 & 0 & 1 & 0 \\ 0 & 0 & 0 & 1 \end{bmatrix}, \qquad \boldsymbol{X}_\pi(s) = \begin{bmatrix} V_2 \\ V_3 \\ V_4 \\ V_5 \\ V_6 \end{bmatrix}$$

$$\boldsymbol{Y}_d(s) = \begin{bmatrix} Y_{d11}(s) & Y_{d12}(s) & Y_{d13}(s) & Y_{d14}(s) \\ Y_{d21}(s) & Y_{d22}(s) & Y_{d23}(s) & Y_{d24}(s) \\ Y_{d31}(s) & Y_{d32}(s) & Y_{d33}(s) & Y_{d34}(s) \\ Y_{d41}(s) & Y_{d42}(s) & Y_{d43}(s) & Y_{d44}(s) \end{bmatrix}$$

$$\boldsymbol{I_d}(s) = \begin{bmatrix} I_{d1} \\ I_{d2} \\ I_{d3} \\ I_{d4} \end{bmatrix} \qquad \boldsymbol{Y}_\pi(s) = \begin{bmatrix} Y_{11}(s) & Y_{12}(s) \\ Y_{21}(s) & Y_{22}(s) \end{bmatrix}$$

$$\boldsymbol{I}_\pi(s) = \begin{bmatrix} I_2(s) \\ I_4(s) \end{bmatrix}, \qquad \boldsymbol{V}_\pi(s) = \begin{bmatrix} V_2(s) \\ V_4(s) \end{bmatrix}.$$

A. Interconnect Simulation Issues

Simulation of large interconnect networks is associated with two major bottlenecks: mixed frequency/time problem and CPU expense.

Mixed Frequency/Time Problem: The major difficulty in simulating high-frequency models such as distributed transmission lines is due to the fact that, while described in terms of partial differential equations, they are best represented in the frequency-domain (56). As seen, they do not have a direct representation in the time-domain. On the other hand, nonlinear devices can only be described in the time-domain (55). These simultaneous formulations are difficult to handle using a traditional ordinary differential equation solver such as SPICE [23], [140]–[151].

CPU Expense: Frequency-domain simulation of large linear networks is conventionally done by solving (50) or (53) at each frequency point using LU decomposition and forward–backward substitution. For time-domain simulation, integration techniques are used to convert a set of time-domain differential equations into a set of difference equations. For example, application of the trapezoidal rule to (51) leads to a nonlinear set of difference equation [151]

$$\left(\boldsymbol{G} + \frac{2}{\Delta t}\boldsymbol{W}\right)\boldsymbol{v}(t+\Delta t) + \boldsymbol{F}(\boldsymbol{v}(t+\Delta t)) = \left(\frac{2}{\Delta t}\boldsymbol{W} - \boldsymbol{G}\right)\boldsymbol{v}(t) + (\boldsymbol{b}(t) + \boldsymbol{b}(t+\Delta t)) - \boldsymbol{F}(\boldsymbol{v}(t)). \tag{57}$$

To solve (57) at each time point, Newton iterations are required, which may need several LU decompositions. This causes the CPU cost of a time-domain analysis to be expensive (note that $\boldsymbol{W}$ and $\boldsymbol{G}$ matrices for interconnect networks are usually very large).

The objectives of interconnect simulation algorithms are to address both mixed frequency/time problem as well as to handle large linear circuits without too much of CPU expense. There have been several algorithms proposed for this purpose, which are broadly classified into two main categories, as follows. 1) Approaches based on macromodeling each individual transmission line set. Techniques such as "method of characteristics" are grouped in this category and are discussed in detail in Section V. 2) Approaches based on model-order reduction (such as AWE, CFH, PRIMA) of the entire linear subnetwork containing lumped as well as distributed subnetworks and are discussed in detail in Sections VI–VIII. It is to be noted that the second approach can also be used in conjunction with the first approach.

V. Simulation Techniques Based on Transmission-Line Macromodels

In this approach, transmission-line networks described by Telegrapher's equations (partial differential equations) are translated into a set of ordinary differential equations (known as the macromodel), through some kind of discretization.

The conventional approach [12], [36] for discrete modeling of distributed interconnects is to divide the line into segments of length Δx, chosen to be small fraction of the wavelength. If each of these segments (assume that the line is discretized into "M" segments) is electrically small at the frequencies of interest (i.e., $\Delta x = L/M \ll \lambda$), then each segment can be replaced by lumped models. Generally the lumped structures used to discretize transmission lines contain the series elements $L\Delta x$ and $R\Delta x$, and shunt elements $G\Delta x$ and $C\Delta x$. The parameters (L, R, G, C are the p.u.l. inductance, resistance, conductance, and capacitance of the line, respectively (Fig. 10).

Distributed versus Lumped: Number of Lumped Segments Required: It is often of practical interest to know how many lumped segments are required to reasonably approximate a

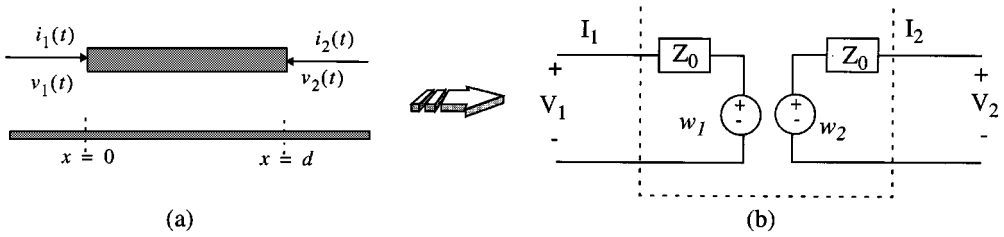

Fig. 15. Macromodel using Method of Characteristics.

distributed model. For illustration, consider LC segments, which can be viewed as low-pass filters. For a reasonable approximation, this filter must pass at least some multiples of the highest frequency $f_{\max}$ of the propagating signal (say ten times, $f_0 \geq 10 f_{\max}$). In order to relate these parameters, we make use of the 3-dB passband frequency of the LC filter given by [2], [4]

$$f_0 = \frac{1}{\pi\sqrt{LdCd}} = \frac{1}{\pi\tau d} \tag{58}$$

where d is the length of the line and $\tau = \sqrt{LC}$ represents the delay p.u.l. From (1), we have $f_{\max} = 0.35/t_r$ and using (58), we can express the relation $f_0 \geq 10 f_{\max}$ in terms of the delay of the line and the rise time as $1/\pi\tau d \geq 10 \times 0.35/t_r$, or

$$t_r \geq 3.5(\pi\tau d) \approx 10\tau d. \tag{59}$$

In other words, the delay allowed per segment is approximately $t_r/10$. Hence, the total number of segments (N) needed to accurately represent a total delay of τd is given by

$$N = \tau d/(t_r/10) = 10\tau d/t_r. \tag{60}$$

In the case of RLC segments, in addition to satisfying (59), the series resistance of each segment must also be accounted.

Example: Consider a digital signal with rise time of 0.2 ns propagating on a lossless wire of length 10 cm, with a p.u.l. delay of 70.7 ps (this can be represented by a distributed model with p.u.l. parameters of $L = 5$ nh/cm and $C = 1$ pF/cm). If the same circuit were to be represented by lumped segments, one needs $N = (10 \times 70.7e^{-12} \times 10/(0.2e^{-9}) \approx$ 35 sections. It is to be noted that using more sections does not clean up ripples completely but helps to reduce the first overshoot (Gibb's phenomenon). Ripples can be reduced when losses are properly taken into account.

One of the major drawbacks of the above conventional discretization is that it requires a large number of sections, especially for circuits with high operating speeds and sharper rise times. This leads to large circuit sizes and the simulation becomes CPU inefficient. In order to overcome these difficulties, several techniques for efficient discretization were proposed in the literature. These methods can be broadly classified, based on the passivity property (details concerning passivity of macromodels can be found in Section VIII-F) as follows. 1) Macromodels with no guarantee of passivity: A sample of such techniques are *method of characteristics*, *transfer function approximation* and *Chebyshev polynomial-based approximation*, and are discussed in Section V-A–V-C. 2) Macromodels with guaranteed passivity by construction of macromodels: A sample of such techniques are *compact finite differences*, *integrated congruent transform*, and *exponential Padé-based matrix-rational approximation*, and are discussed in Section V-D–V-F.

A. Method of Characteristics

The method of characteristics (MC) [43]–[45] transforms partial differential equations of a transmission line into ordinary differential equations containing time-delayed controlled sources.

Consider the case of two conductor transmission lines, as shown in Fig. 15(a). An analytical solution, in terms of y-parameters for (9) or (10) can be derived [43] as

$$\boldsymbol{I} = \boldsymbol{Y}\boldsymbol{V}$$
$$\begin{bmatrix} I_1 \\ I_2 \end{bmatrix} = \frac{1}{Z_0(1-e^{-2\gamma d})} \begin{bmatrix} 1+e^{-2\gamma d} & -2e^{-\gamma d} \\ -2e^{-\gamma d} & 1+e^{-2\gamma d} \end{bmatrix} \begin{bmatrix} V_1 \\ V_2 \end{bmatrix} \tag{61}$$

where γ is the propagation constant, Z_0 is the characteristic impedance, V_1 and I_1 are the terminal voltage and current at the near end of the line, and V_2 and I_2 are the terminal voltage and current at the far end of the line. The y-parameters of the transmission line are complex functions of s, and in most cases cannot be directly transformed into an ordinary differential equation in the time domain. The MC succeeded in doing such a transformation, but only for lossless transmission lines. Although this method was originally developed in the time domain using what was referred to as characteristic curves (hence, the name), a short alternative derivation in the frequency domain will be presented here. By rearranging the terms in (61), we can write

$$\begin{aligned} V_1 &= Z_0 I_1 + e^{-\gamma d}[2V_2 - e^{-\gamma d}(Z_0 I_1 + V_1)] \\ V_2 &= Z_0 I_2 + e^{-\gamma d}[2V_1 - e^{-\gamma d}(Z_0 I_2 + V_2)]. \end{aligned} \tag{62}$$

Next, (62) can be rewritten as

$$\begin{aligned} V_1 - Z_0 I_1 &= W_1 \\ V_2 - Z_0 I_2 &= W_2 \end{aligned} \tag{63}$$

where

$$\begin{aligned} W_1 &= e^{-\gamma d}[2V_2 - e^{-\gamma d}(Z_0 I_1 + V_1)] \\ W_2 &= e^{-\gamma d}[2V_1 - e^{-\gamma d}(Z_0 I_2 + V_2)]. \end{aligned} \tag{64}$$

Using (62) and (64), a recursive relation for W_1 and W_2 can be obtained as

$$\begin{aligned} W_1 &= e^{-\gamma d}[2V_2 - W_2] \\ W_2 &= e^{-\gamma d}[2V_1 - W_1]. \end{aligned} \tag{65}$$

A lumped model of the transmission line can then be deduced from (62) and (65), as in Fig. 15(b).

If the lines were lossless (in which case the propagation constant is purely imaginary; $\gamma = j\beta$), the frequency domain expression (65) could be analytically converted into time-domain using the inverse Laplace transform as

$$w_1(t+\tau) = 2v_2(t) - w_2(t)$$
$$w_2(t+\tau) = 2v_1(t) - w_1(t) \tag{66}$$

where $e^{-j\beta d}$ is replaced by a time shift (or delay). Each transmission line can, therefore, be modeled by two impedances and two voltage controlled voltage sources with time delay. Since this transmission line model is in the time domain, it can be easily linked to transient simulators.

For lossy lines, the propagation constant is not purely imaginary and, hence, cannot be replaced by a pure delay. In that case analytical expressions for w_1 and w_2 cannot be found in the time domain. To handle such cases, classical MC can be extended through Padé synthesis of characteristic impedance and complex propagation constant [44]. In the case of multiconductor transmission lines, MC can be applied through decoupling of MTL equations [12].

B. Transfer Function Approximation

Least square approximation-based techniques [111] derive a transfer-function representation for the frequency response of transmission line subnetworks. The method fits data from sample frequency points, to a complex rational function $H(s)$, where

$$H(s) = c + \sum_{i=1}^{q} \frac{k_1}{s - p_i} \tag{67}$$

where p_i and k_i are the ith pole–residue pair, q is the total number system poles, and c is quotient. In order to obtain a stable-model (poles restricted to the left-half plane), the real part [even part of $H(s = jw)$] is fitted to the real part of data samples. Let the real part of (67) be approximated as

$$\mathrm{Re}(H(s)) = \frac{A(s)}{B(s)} = \frac{\sum_{i=0}^{q} a_1 (w^2)^i}{\sum_{i=1}^{q} b_i (w^2)^i}. \tag{68}$$

Writing (68) at several frequency points, $(0,\ w_1,\ \ldots w_N)$, and expressing it in a matrix form, we get the matrices in (69) at the bottom of the page. Expressing (69) in a simple notation

$$\Theta \boldsymbol{Z} = \theta. \tag{70}$$

The least square solution of (70) is given by

$$\Theta^t \Theta \boldsymbol{Z} = \Theta^t \theta. \tag{71}$$

Poles of the system are obtained by computing the roots of the denominator polynomial $B(s)$ and they belong to the LHS plane only, since they are obtained from an even function (68). If any poles are purely imaginary, they are rejected. Next, the residues are obtained by matching the real and imaginary parts of (67) to the sampled data, as follows:

$$\begin{bmatrix} 1 & -1/p_1 & \cdots & -1/p_q \\ 1 & \dfrac{-1/p_1}{1+(w_1/p_1)^2} & \cdots & \dfrac{-1/p_q}{1+(w_1/p_q)^2} \\ \vdots & \cdots & \vdots \ \cdots & \vdots \\ 1 & \dfrac{1}{1+(w_N/p_1)^2} & \cdots & \dfrac{1}{1+(w_N/p_q)^2} \\ 0 & \dfrac{-w_1/p_1}{1+(w_1/p_1)^2} & & \dfrac{-w_1/p_q}{1+(w_1/p_q)^2} \\ \vdots & \vdots & \vdots & \vdots \\ & \dfrac{-w_N/p_1}{1+(w_N/p_1)^2} & & \dfrac{-w_N/p_q}{1+(w_N/p_q)^2} \end{bmatrix} \cdot \begin{bmatrix} c \\ k_1 \\ \vdots \\ k_q \end{bmatrix} = \begin{bmatrix} \mathrm{Re}(H(0)) \\ \mathrm{Re}(H(w_1)) \\ \vdots \\ \mathrm{Re}(H(w_N)) \\ \mathrm{Im}(H(w_1)) \\ \vdots \\ \mathrm{Im}(H(w_N)) \end{bmatrix}. \tag{72}$$

Here, the solution for the residues are obtained by solving the least square approximation, similar to the equations in (71). Once the pole–residue model is obtained, it can be easily converted to a time-domain macromodel described in terms of ordinary-differential equations.

Least square approximation provides higher flexibility in modeling all types of interconnect models. However, the so-

$$\begin{bmatrix} 1 & 0 & \cdots & 0 & 0 & \cdots & 0 \\ 1 & w_1^2 & \cdots & w_1^{2q} & -w_1^2\mathrm{Re}(H(w_1)) & \cdots & -w_1^{2q}\mathrm{Re}(H(w_1)) \\ \vdots & \vdots & \cdots & \vdots & \vdots & \cdots & \vdots \\ 1 & w_N^2 & & w_N^{2q} & -w_N^2\mathrm{Re}(H(w_N)) & \cdots & -w_N^{2q}\mathrm{Re}(H(w_N)) \end{bmatrix} \begin{bmatrix} a_0 \\ \vdots \\ a_q \\ b_1 \\ \vdots \\ b_q \end{bmatrix} = \begin{bmatrix} \mathrm{Re}(H(0)) \\ \mathrm{Re}(H(w_1)) \\ \vdots \\ \mathrm{Re}(H(w_N)) \end{bmatrix} \tag{69}$$

lution of (71) can be ill-conditioned. Also, the algorithm does not guarantee a passive macromodel.

C. Chebyshev Polynomials

One of the efficient approaches for discretization is to express the variations in space for voltages and currents of a transmission line system in terms of *known basis functions*, such as Chebyshev, [91], [37] or Wavelet polynomials. For example, consider the single transmission line equations (4) and (8). Assume that the voltage $v(x, t)$ and the current $i(x, t)$ can be expanded in the form

$$v(x, t)=\sum_{n=0}^{N} a_n(t)T_n(x), \qquad i(x, t)=\sum_{n=0}^{N} b_n(t)T_n(x) \tag{73}$$

where $T_n(x)$ is the nth degree Chebyshev polynomial; $a_n(t)$ and $b_n(t)$ are the unknown variables. The derivatives of $v(x, t)$ and $i(x, t)$ with respect to x are also expanded using Chebyshev polynomials as

$$\begin{aligned}\frac{\partial}{\partial x} v(x, t) &= \sum_{n=0}^{N} \widehat{a}_n(t)T_n(x)\\ \frac{\partial}{\partial x} i(x, t) &= \sum_{n=0}^{N} \widehat{b}_n(t)T_n(x)\end{aligned} \tag{74}$$

where $a_n(t)$, $b_n(t)$ are related to $a_n(t)$ and $b_n(t)$ as

$$\begin{aligned}a_n(t) &= \frac{1}{2n}\left(\hat{a}_{n-1}(t) - \hat{a}_{n+1}(t)\right)\\ b_n(t) &= \frac{1}{2n}\left(\hat{b}_{n-1}(t) - \hat{b}_{n+1}(t)\right).\end{aligned} \tag{75}$$

Using (73) and (74) and the orthogonal properties Chebyshev polynomials, the Telegrapher's equations (4), (8) can be converted to a set of ordinary differential equations in terms of the unknown coefficients $a_n(t)$ and $b_n(t)$.

One of the advantages of the algorithm is that it can also be applied for interconnects with nonuniform line parameters by expanding line parameters as Chebyshev polynomials with respect to position x. Chebyshev approximations are able to achieve better accuracy with fewer variables when compared to direct lumped RLC segmentation. However, the algorithm does not guarantee the passivity of the resulting macromodel. Similarly, an alternative approximation strategy can be adopted based on expansions of $v(x, t)$ and $i(x, t)$ in terms of *wavelet basis functions* [88], [89].

D. Compact Finite-Differences-Based Approximation

Compact finite-differences (CFD) [150]-based approximations were suggested in the literature to convert Telegrapher's equations into ordinary differential equations [90]. For the purpose of simplicity, consider the case of a single transmission line system, represented by (9) and (10). The variations in space for voltages and currents of a transmission line system can be expressed as

$$\begin{aligned}V(x, s) &= \sum_{m=1}^{P} V_m(s)A_m(x)\\ I(x, s) &= \sum_{n=1}^{Q} I_n(s)B_n(x)\end{aligned} \tag{76}$$

where P and Q are the degrees of freedom of approximation, while $A_m(x)$ and $B_n(x)$ are the known expansion functions. Assume that the line is divided into M equal segments of length Δx. The unknown voltages $V(x)$ are represented in terms of values at nodes corresponding to $x = i\Delta x$; $(i = 0, 1\cdots M)$. The current distribution $I(x)$ is described in terms of its values at the centers of the M segments, $x = (i - 1/2)\Delta x$; $(i = 0, 1\cdots M)$. Next, spatial derivatives of $V(x, s)$ and $I(x, s)$ can be approximated using compact central difference operator as

$$\begin{aligned}&\alpha_1 \left.\frac{\partial f(x)}{\partial x}\right|_{i+1} + \alpha_2 \left.\frac{\partial f(x)}{\partial x}\right|_{i} + \alpha_1 \left.\frac{\partial f(x)}{\partial x}\right|_{i-1}\\ &\quad = \frac{f_{i+1/2} - f_{i-1/2}}{\Delta x}\end{aligned} \tag{77}$$

where i denotes the node where the operator is centered, $f(x)$ represents either or $V(x)$ or $I(x)$. The unknown coefficients α_1 and α_2 are computed such that the desired truncation error criteria is satisfied. For example, fourth order approximation is achieved when $\alpha_1 = 1/24$, $\alpha_2 = 11/12$. Performing discretization operation on TL equations (9), (10) results in a discrete form [90]

$$\begin{aligned}&-\alpha_1 Z_{i+3/2}I_{i+3/2} - \alpha_2 Z_{i+1/2}I_{i+1/2} - \alpha_1 Z_{i-1/2}I_{i-1/2}\\ &\quad = \frac{V_{i+1} - V_i}{\Delta x}, \qquad i = 0, 1\cdots M-2\\ &-\alpha_1 Y_{i+1}V_{i+1} - \alpha_2 Y_i V_i - \alpha_1 Y_{i-1}V_{i-1}\\ &\quad = \frac{I_{i+1/2} - I_{i-1/2}}{\Delta x}, \qquad i = 0, 1\cdots M-1\end{aligned} \tag{78}$$

where $Z_i = Ri\Delta x + sLi\Delta x$ and $Y_i = Gi\Delta x + sCi\Delta x$. Using suitable corrections for end-points, the set of equations represented by (78) can be converted to the standard MNA form.

One of the advantages of the algorithm is that it can achieve better accuracy with fewer variables when compared to direct lumped RLC segmentation. Also, the algorithm guarantees the passivity of the macromodel by construction [90].

E. Integrated Congruence Transform

Consider an m-conductor system and the TL equations represented by (19), which can be expressed after slight modification, in the Laplace-domain as

$$\left(s\boldsymbol{P} + \boldsymbol{Q} + \boldsymbol{T}\frac{d}{dx}\right)\boldsymbol{Z}(x, s) = 0 \tag{79}$$

where

$$\boldsymbol{Z}(x,\,s)=\begin{bmatrix}\boldsymbol{I}(x,\,s)\\ \boldsymbol{V}(x,\,s)\end{bmatrix},\qquad \boldsymbol{P}=\begin{bmatrix}\boldsymbol{L} & \boldsymbol{0}\\ \boldsymbol{0} & \boldsymbol{C}\end{bmatrix}$$
$$\boldsymbol{Q}=\begin{bmatrix}\boldsymbol{R} & \boldsymbol{0}\\ \boldsymbol{0} & \boldsymbol{G}\end{bmatrix},\qquad \boldsymbol{T}=\begin{bmatrix}\boldsymbol{0} & \boldsymbol{1}\\ \boldsymbol{1} & \boldsymbol{0}\end{bmatrix} \tag{80}$$

and are $\boldsymbol{I}(x,\,s)$, $\boldsymbol{V}(x,\,s)$ the vector of currents and voltages along the length of the line, of dimension $m\times 1$ each. Next, define a transformation as

$$\boldsymbol{Z}(x,\,s)=\boldsymbol{u}(x)\times\hat{z}(s) \tag{81}$$

where

$$\boldsymbol{u}(x)|_{2m\times n}=\begin{bmatrix}\boldsymbol{u}_i(x)|_{m\times n}\\ \boldsymbol{u}_v(x)|_{m\times n}\end{bmatrix}=\begin{bmatrix}\boldsymbol{u}_{i1}(x)\cdots\boldsymbol{u}_{in}(x)\\ \boldsymbol{u}_{v1}(x)\cdots\boldsymbol{u}_{vn}(x)\end{bmatrix}$$
$$\hat{z}(s)|_{n\times 1}=\begin{bmatrix}\hat{z}_1(s)\\ \cdots\\ \hat{z}_n(s)\end{bmatrix}. \tag{82}$$

Note that the transformation matrix $\boldsymbol{u}(x)$ is a function of x only, and not dependent on s. Substituting (81) in (79), premultiplying by the transpose of $\boldsymbol{u}(x)$ and integrating them with respect to the normalized variable x (from 0 to 1), we get

$$\left(s\hat{\boldsymbol{P}}+\hat{\boldsymbol{Q}}+\hat{\boldsymbol{T}}\right)\hat{z}(s)=0 \tag{83}$$

where

$$\hat{\boldsymbol{P}}=\int_0^1\boldsymbol{u}^T(x)\boldsymbol{P}(\boldsymbol{x})\boldsymbol{u}(x)\,dx$$
$$\hat{\boldsymbol{Q}}=\int_0^1\boldsymbol{u}^T(x)\boldsymbol{Q}(x)\boldsymbol{u}(x)\,dx$$
$$\hat{\boldsymbol{T}}=\int_0^1\boldsymbol{u}^T(x)\boldsymbol{T}\frac{d\boldsymbol{u}(x)}{dx}(x)\,dx. \tag{84}$$

The transformation defined by the set of equations (81)–(84) is called the integrated congruence transform [86]. Expanding the expressions for $\hat{\boldsymbol{P}}$, $\hat{\boldsymbol{Q}}$, $\hat{\boldsymbol{T}}$ and with some mathematical manipulations, (83) can be translated into a set of ordinary differential equations. It can be proved that integrated congruence transform-based approximation preserves the passivity [86].

F. Exponential Padé-based Matrix-Rational Approximation

This algorithm directly converts partial differential equations into time-domain macromodels based on Padé rational approximations of exponential matrices [39], [40], [87]. In this technique, coefficients describing the macromodel are computed *a priori* and analytically, using closed-form Padé approximant of exponential matrices. Since closed-form relations are used, this technique does not suffer from the usual ill-conditioning experienced with the direct application of Padé approximations. Hence, it allows a higher order of approximation. Also, it guarantees the passivity of the resulting macromodel.

Matrix-Rational Approximation: Consider the exponential form of Telegrapher's equations describing the multiconductor transmission lines, given by (44)

$$\begin{bmatrix}\boldsymbol{V}(d,\,s)\\ \boldsymbol{I}(d,\,s)\end{bmatrix}=e^{\boldsymbol{Z}}\begin{bmatrix}\boldsymbol{V}(0,\,s)\\ \boldsymbol{I}(0,\,s)\end{bmatrix},\qquad \boldsymbol{Z}=(\boldsymbol{D}+s\boldsymbol{E})d$$
$$\boldsymbol{D}=\begin{bmatrix}\boldsymbol{0} & -\boldsymbol{R}\\ -\boldsymbol{G} & \boldsymbol{0}\end{bmatrix},\qquad \boldsymbol{E}=\begin{bmatrix}\boldsymbol{0} & -\boldsymbol{L}\\ -\boldsymbol{C} & \boldsymbol{0}\end{bmatrix} \tag{85}$$

where d is the length of the line. The matrix $e^{\boldsymbol{Z}}$ is approximated using matrix-rational function as

$$\boldsymbol{P}_{N,\,M}(\boldsymbol{Z})e^{\boldsymbol{Z}}\approx\boldsymbol{Q}_{N,\,M}(\boldsymbol{Z}) \tag{86}$$

where $\boldsymbol{P}_{N,\,M}(\boldsymbol{Z})$ and $\boldsymbol{Q}_{N,\,M}(\boldsymbol{Z})$ are polynomial matrices expressed in terms of closed-form Padé rational functions [39] as

$$\boldsymbol{P}_{N,\,M}(\boldsymbol{Z})=\sum_{j=0}^{N}\frac{(M+N-j)!N!}{(M+N)!j!(N-j)!}(-\boldsymbol{Z})^j$$
$$\boldsymbol{Q}_{N,\,M}(\boldsymbol{Z})=\sum_{j=0}^{M}\frac{(M+N-j)!M!}{(M+N)!j!(M-j)!}\boldsymbol{Z}^j. \tag{87}$$

With some mathematical manipulations, (86) can be translated into a macromodel represented by a set of ordinary differential equations, in a closed form. Since all the coefficients in the macromodel are known *a priori*, in terms of the p.u.l. parameters, the macromodel can be easily stenciled into a circuit simulator as the stamp of the transmission line. The fact that the coefficients $\boldsymbol{P}_{N,\,M}(\boldsymbol{Z})$ and $\boldsymbol{Q}_{N,\,M}(\boldsymbol{Z})$ are known *a priori* in closed form, provides substantial computational advantage for this algorithm.

It can be proved that the matrix-rational function-based approximation preserves the passivity of reduced model [39]. Also, the extension of the above matrix-rational approximation-based technique to handle frequency-dependent parameters can be found in [40].

VI. Model-Reduction Based Simulation Algorithms

Interconnect networks generally tend to have a large number of poles, spread over a wide-frequency range. Even though the majority of these poles would normally have very little effect on simulation results, however, they make the simulation to be CPU extensive by forcing the simulator to take smaller step sizes.

Dominant Poles: Dominant poles are those that are close to the imaginary axis and significantly influence the time as well as the frequency characteristics of the system. The moment-matching techniques (*MMT*s) [59]–[75] capitalize on the fact that irrespective of the presence of a large number of poles in a system, only the dominant poles are sufficient to accurately characterize a given system. This effect is demonstrated in Fig. 16, where it is clear that pole P_2 will have little effect on the final transient result.

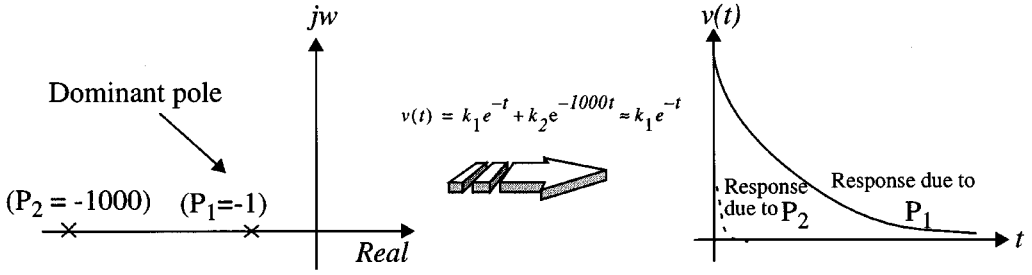

Fig. 16. Illustration of dominant poles.

A brief mathematical description of the underlying concepts of MMTs is given below. Consider a single input/single output system and let $H(s)$ be the transfer function. $H(s)$ can be represented in a rational form as

$$H(s) = \frac{P(s)}{Q(s)} \tag{88}$$

where $P(s)$ and $Q(s)$ are polynomials in s. Equivalently, (88) can be written as

$$H(s) = c + \sum_{i=1}^{N_p} \frac{k_i}{s - p_i} \tag{89}$$

where p_i and k_i are the ith pole–residue pair, N_p is the total number of system poles, and c is the direct coupling constant. The time-domain impulse response can be computed in a closed form using inverse Laplace transform as

$$h(t) = c\delta t + \sum_{i=1}^{N_p} k_i e^{p_i t}. \tag{90}$$

In case of large networks N_p, the total number of poles can be of the order of thousands. Computing all N_p, the poles will be highly CPU intensive even for a small network and for large networks it is completely impractical. Model-reduction techniques address the above issue by deriving a reduced-order approximation $\hat{H}(s)$ in terms of dominant poles, instead of trying to compute all the poles of a system. Assuming that only L dominant poles were extracted, (88) can be rewritten to obtain approximate frequency/time responses, as

$$H(s) \approx \hat{H}(s) = \frac{\hat{P}(s)}{\hat{Q}(s)} = \hat{c} + \sum_{i=1}^{L} \frac{\widehat{k}_i}{s - \widehat{p}_i} \tag{91}$$

$$h(t) \approx \hat{h}(t) = \hat{c}\delta t + \sum_{i=1}^{L} \widehat{k}_i e^{\widehat{p}_i t}. \tag{92}$$

Moments of the Response: Consider the Taylor series expansion of a given transfer-function, $H(s)$, at point, $s = 0$

$$\begin{aligned} H(s) &\approx \hat{H}(s) \\ &= H(0) + s\frac{(H(0))^{(1)}}{1!} + s^2\frac{(H(0))^{(2)}}{2!} \\ &\quad + \cdots + s^n\frac{(H(0))^{(n)}}{n!} \end{aligned} \tag{93}$$

where the superscript (n) denotes the nth derivative. Using a simpler notation, we can rewrite (93) as

$$\begin{aligned} H(s) &\approx \hat{H}(s) \\ &= m_0 + m_1 s + m_2 s^2 + \cdots + m_n s^n \\ &= \sum_{i=0}^{n} s^i m_i, \qquad m_i = \frac{H(0)^{(i)}}{i!}. \end{aligned} \tag{94}$$

The coefficients of Taylor series expansion (m_i) are also identical to the *time-domain moments* of the impulse response $h(t)$. This can be easily seen by using the Laplace transform of $h(t)$ [77]

$$\begin{aligned} H(s) &= \int_0^\infty h(t)e^{-st}\,dt \\ &= \int_0^\infty h(t)\left[1 - st + \frac{s^2t^2}{2!} - \cdots\right]dt \\ &= \int_0^\infty h(t)\,dt + s\int_0^\infty (-1)th(t)\,dt \\ &\quad + s^2\int_0^\infty \frac{t^2h(t)}{2!}\,dt + \cdots \\ &= \sum_{i=0}^{\infty} s^i\left(\frac{(-1)^i}{i!}\int_0^\infty t^i h(t)\,dt\right). \end{aligned} \tag{95}$$

Due to this analogy, the coefficients of Taylor series expansion, (m_i), are generally referred to as *moments*.

It has been shown that the moments provide an estimation of delay and rise times [57], [58]. Elmore delay [57], which approximates the midpoint of the monotonic step response waveform by the mean of the impulse response, essentially matches the first moment of the response. This can be considered as one of the basic forms of approximation. However, in order to get accurate prediction of interconnect effects, it is essential that the reduced-order model must match (or preserve) as many moments as possible.

Several algorithms can be found in the literature for reduction of large interconnect subnetworks [59]–[94]. They can be broadly classified into two categories: 1) approaches based on explicitly matching the moments to a reduced-order model and 2) approaches based on implicitly matching the moments. The techniques such as AWE belong to the first category and are discussed in Section VII. Techniques such as PVL, PRIMA, which are based on Krylov subspace formulation, belong to the second category and are discussed in Section VIII.

VII. Model-Reduction Based on Explicit Moment-Matching

These techniques employ Padé approximation, based on explicit moment-matching to extract the dominant poles and residues of a given system [8], [59]–[63].

A. Padé Approximation

Consider a system-transfer function $H(s)$ that is approximated by a rational function $\hat{H}(s)$ as

$$H(s) \approx \hat{H}(s) = \frac{a_0 + a_1 s + a_2 s^2 + \cdots + a_L s^L}{1 + b_1 s + \cdots + b_M s^M} = \frac{P_L(s)}{Q_M(s)} \tag{96}$$

where $a_0, \ldots, a_L, b_1, \ldots, b_M$ are the unknowns (total of $L+M+1$ variables). Consider the Taylor series expansion of $H(s)$ at $(s=0)$, in terms of its moments. Matching $H(s)$ to the rational function approximation given in (96) (hence, the name moment-matching techniques, which is also known as Padé approximation), we get

$$\frac{a_0 + a_1 s + a_2 s^2 + \cdots + a_L s^L}{1 + b_1 s + \cdots + b_M s^M} = m_0 + m_1 s + m_2 s^2 + \cdots + m_{(L+M)} s^{L+M}. \tag{97}$$

Cross multiplying and equating the coefficients of similar powers of s starting from s^{L+1} to s^{L+M} on both sides of (97), we can evaluate the denominator polynomial coefficients as

$$\begin{bmatrix} m_{L-M+1} & m_{L-M+2} & \cdots & m_L \\ m_{L-M+2} & \cdots & \cdots & m_{L+1} \\ \cdots & \cdots & \cdots & \cdots \\ m_L & m_{L+1} & \cdots & m_{L+M-1} \end{bmatrix} \begin{bmatrix} b_M \\ b_{M-1} \\ \cdots \\ b_1 \end{bmatrix} = - \begin{bmatrix} m_{L+1} \\ m_{L+2} \\ \cdots \\ m_{L+M} \end{bmatrix}. \tag{98}$$

The numerator coefficients can be found by equating the remaining powers of s (from s^0 to s^L) as

$$\begin{aligned} a_0 &= m_0 \\ a_1 &= m_1 + b_1 m_0 \\ &\cdots \\ a_L &= m_L + \sum_{i=1}^{\min(L,M)} b_i m_{L-i}. \end{aligned} \tag{99}$$

Equations (98) and (99) yield an approximate transfer function in terms of rational polynomials.

Alternatively, an equivalent pole–residue model can be found as follows. Poles p_i are obtained by applying a root-solving algorithm on denominator polynomial $\hat{Q}(s)$. In order to obtain k_i, the approximate transfer function given by (91) is expanded using Maclaurin series as

$$\hat{H}(s) = \hat{c} - \sum_{n=0}^{\infty} s^n \left(\sum_{i=1}^{L} \frac{\widehat{k}_i}{\widehat{p}_i^{\,n+1}} \right). \tag{100}$$

Comparing $\hat{H}_s$ from (94) and (100), we note that

$$\begin{aligned} m_0 &= \hat{c} - \sum_{i=1}^{L} = \frac{\widehat{k}_i}{\hat{p}_i} \\ &\cdots \\ m_i &= - \sum_{i=1}^{L} \frac{\widehat{k}_i}{\hat{p}_i^{\,i+1}}. \end{aligned} \tag{101}$$

Residues can be evaluated by writing the equations in (101) in a matrix form as

$$\begin{bmatrix} \hat{p}_1^{-1} & \hat{p}_2^{-1} & & \hat{p}_L^{-1} & -1 \\ \hat{p}_1^{-2} & \hat{p}_2^{-2} & & \hat{p}_L^{-2} & 0 \\ & & \cdots & & \\ & & \cdots & & \\ \hat{p}_1^{-L-1} & \hat{p}_2^{-L-1} & & \hat{p}_L^{-L-1} & 0 \end{bmatrix} \begin{bmatrix} \widehat{k}_1 \\ \widehat{k}_2 \\ \cdots \\ \widehat{k}_L \\ \hat{c} \end{bmatrix} = - \begin{bmatrix} m_0 \\ m_1 \\ \cdots \\ m_{L-1} \\ m_L \end{bmatrix}. \tag{102}$$

In the above equations $\hat{c}$ represents the direct coupling between input and output. More accurate ways to compute $\hat{c}$ can be found in [8].

B. Computation of Moments

Having outlined the concept of MMTs, we need to evaluate the moments of the system, which are required by (98)–(102). Consider the simple case of lumped circuits and the corresponding MNA equations represented by (50). Expanding the vector $\boldsymbol{X}(s)$ using the Taylor series, we have

$$[\boldsymbol{G} + s\boldsymbol{W}][\boldsymbol{M_0} + \boldsymbol{M_1} s + \boldsymbol{M_2} s^2 + \cdots] = [\boldsymbol{b}] \tag{103}$$

where $\boldsymbol{M_i}$ represents the ith moment-vector. Equating coefficients of similar powers of s on both sides of (103), we obtain the following relationships:

$$\begin{aligned} \boldsymbol{G M_0} &= \boldsymbol{b} \\ \boldsymbol{G M_i} &= -\boldsymbol{W M_{i-1}}, \qquad i > 0. \end{aligned} \tag{104}$$

The above equations give a closed form relationship for the computation of moments. The moments of a particular output of interest [which are represented in (96)–(102)] are picked from moment-vectors $\boldsymbol{M_i}$. As seen, (104) requires only one LU decomposition and few forward–backward substitutions during the recursive computation of higher order moments. Since the major cost involved in linear circuit simulation is due to LU decomposition, MMTs yield very high-speed advantage (100 to 1000 times) compared to conventional simulators.

Generalized Computation of Moments: In the case of networks containing transmission lines, moment-computation is not straightforward. A generalized relation for recursive computation of higher order moments can be derived as follows [62], [63], [67], [69], [72]. Considering the MNA equations containing MTL stamps (54) and expanding $\psi(s)$ and

$\boldsymbol{X}(s)$ in Taylor series at an expansion point $s=\alpha$, we get [72]

$$\left[\psi(\alpha)+\frac{\psi^{(1)}\big|_{s=\alpha}}{1!}(s-\alpha)+\cdots+\frac{\psi^{(n)}\big|_{s=\alpha}}{n!}(s-\alpha)^n\right]\cdot[\boldsymbol{M_0}+\boldsymbol{M_1}(s-\alpha)+\cdots+\boldsymbol{M}_n(s-\alpha)^n]=[\boldsymbol{b}] \quad (105)$$

where $\psi^{(n)}$ denotes the nth derivative of $\psi(s)$ and $\boldsymbol{M}_n$ denotes the nth moment of $\boldsymbol{X}(s)$ at $s=\alpha$. Equating coefficients of similar powers of $s-\alpha$ on both sides of (105), we have

$$\begin{aligned}[\psi]\boldsymbol{M}_0&=\boldsymbol{b}\\ [\psi]\boldsymbol{M}_1+\frac{\psi^{(1)}}{1!}\boldsymbol{M}_0&=0\\ \Rightarrow\Rightarrow[\psi]\boldsymbol{M}_1&=-\frac{\psi^{(1)}}{1!}\boldsymbol{M}_0\\ [\psi]\boldsymbol{M}_2+\frac{\psi^{(1)}}{1!}\boldsymbol{M}_1+\frac{\psi^{(2)}}{2!}\boldsymbol{M}_0&=0\\ \Rightarrow\Rightarrow[\psi]\boldsymbol{M}_2&=-\left(\frac{\psi^{(1)}}{1!}\boldsymbol{M}_1+\frac{\psi^{(2)}}{2!}\boldsymbol{M}_0\right)\\ \Rightarrow\Rightarrow[\psi]\boldsymbol{M}_2&=-\sum_{r=1}^{2}\frac{\left(\psi^{(r)}\right)\boldsymbol{M_{2-r}}}{r!}.\end{aligned} \quad (106)$$

Generalizing (106), a recursive relation for any nth higher order moment can be obtained as

$$\begin{aligned}[\psi(\alpha)]\boldsymbol{M}_0&=\boldsymbol{b}\\ [\psi(\alpha)]\boldsymbol{M_n}&=-\sum_{r=1}^{n}\frac{\left(\psi^{(r)}\big|_{s=a}\right)\boldsymbol{M_{n-r}}}{r!}.\end{aligned} \quad (107)$$

It can be seen that the coefficient on the left-hand side of (107) does not change during higher order moment computation. Hence, it requires only one LU decomposition and n forward–backward substitutions to compute n moments. Also, it is easy to note that the lumped networks are a special case of (107) [where $\psi^{(r)}=0$ for $r\geq 2$, in which case (107) reduces to the form given by (104)]. Next, (107) requires the derivatives of (ψ). These can be obtained using (53) as

$$[\psi]^{(1)}=\begin{bmatrix}\boldsymbol{W}_\pi & \boldsymbol{0}\\ \boldsymbol{Y_d^{(1)}L_d^t} & \boldsymbol{0}\end{bmatrix},\qquad [\psi]^{(r)}=\begin{bmatrix}\boldsymbol{0} & \boldsymbol{0}\\ \boldsymbol{Y_d^{(r)}L_d^t} & \boldsymbol{0}\end{bmatrix}\quad (r\geq 2). \quad (108)$$

The derivatives $\boldsymbol{Y_d^{(r)}}$ can be obtained as a function of the derivatives of the entries on the RHS of (46) and proper application of Leibnitz's theorem. However, this requires the derivatives of the exponential stamp represented by (45). A brief review of computation of these derivatives [72] is given below.

Transmission Line Moments: Consider the exponential stamp represented by (45). We wish to expand the exponential matrix in Taylor series, as follows:

$$e^{(\boldsymbol{D}+\boldsymbol{sE})d}=\boldsymbol{F_0}+\boldsymbol{F_1}s+\cdots+\boldsymbol{F}_n s^n. \quad (109)$$

From the property of matrix exponentiation of an arbitrary matrix $\boldsymbol{A}$, we have

$$e^{\boldsymbol{A}}=1+\frac{\boldsymbol{A}}{1!}+\frac{\boldsymbol{A}^2}{2!}+\cdots+\frac{\boldsymbol{A}^n}{n!}. \quad (110)$$

Let

$$\boldsymbol{A}=(\boldsymbol{D}+s\boldsymbol{E})d. \quad (111)$$

Hence, (110) can be rewritten as

$$e^{(\boldsymbol{D}+s\boldsymbol{E})d}=1+\frac{(\boldsymbol{D}+s\boldsymbol{E})\,d}{1!}+\frac{((\boldsymbol{D}+s\boldsymbol{E})\,d)^2}{2!}+\cdots+\frac{((\boldsymbol{D}+s\boldsymbol{E})\,d)^n}{n!}. \quad (112)$$

Expanding the RHS of (112) further, and collecting the terms in powers of s, we have

$$\begin{aligned}&e^{(\boldsymbol{D}+s\boldsymbol{E})d}\\ &=\left[\frac{\boldsymbol{I}}{0!}+\frac{\boldsymbol{D}d}{1!}+\frac{1}{2!}\boldsymbol{D}^2d^2+\cdots\right]\\ &\quad+s\left[\frac{\boldsymbol{E}d}{1!}+\frac{1}{2!}(\boldsymbol{DE}+\boldsymbol{ED})d^2\right.\\ &\qquad\left.+\frac{1}{3!}(\boldsymbol{D}^2\boldsymbol{E}+\boldsymbol{DED}+\boldsymbol{ED}^2)d^3+\cdots\right]\\ &\quad+s^2\left[\frac{1}{2!}\boldsymbol{E}^2d^2+\frac{1}{3!}(\boldsymbol{DE}^3+\boldsymbol{EDE}^2\right.\\ &\qquad\left.+\boldsymbol{E}^2\boldsymbol{DE}+\boldsymbol{E}^3\boldsymbol{D})d^3+\cdots\right].\end{aligned} \quad (113)$$

Equating (109) with (113) gives

$$\begin{aligned}\boldsymbol{F_0}&=\frac{\boldsymbol{I}}{0!}+\frac{\boldsymbol{D}d}{1!}+\frac{1}{2!}\boldsymbol{D}^2d^2+\cdots\\ &=\boldsymbol{F}_{0,0}+\boldsymbol{F}_{0,1}+\boldsymbol{F}_{0,2}+\cdots\\ \boldsymbol{F}_1&=\frac{\boldsymbol{E}d}{1!}+\frac{1}{2!}(\boldsymbol{DE}+\boldsymbol{ED})\,d^2\\ &\quad+\frac{1}{3!}(\boldsymbol{D}^2\boldsymbol{E}+\boldsymbol{DED}+\boldsymbol{ED}^2)\,d^3+\cdots\\ &=\boldsymbol{F}_{1,0}+\boldsymbol{F}_{1,1}+\boldsymbol{F}_{1,2}+\cdots\\ \boldsymbol{F}_2&=\frac{1}{2!}\boldsymbol{E}^2d^2+\cdots+\cdots\\ &=\boldsymbol{F}_{2,0}+\boldsymbol{F}_{2,1}+\boldsymbol{F}_{2,2}+\cdots\end{aligned} \quad (114)$$

and so on. From the above results, a recursive relationship for generating transmission line moments can be obtained as

$$\boldsymbol{F}_i=\sum_{j=0}^{\infty}\boldsymbol{F}_{i,j},\qquad \boldsymbol{F}_{i,j}=\frac{(\boldsymbol{DF}_{i,j-1}+\boldsymbol{EF}_{i-1,j})\,d}{i+j}$$
$$i\geq 0,\quad j\geq 0,\quad (i+j)\neq 0$$
$$\boldsymbol{F}_{i,j}=0\qquad (i<0 \text{ or } j<0),\qquad \boldsymbol{F}_{0,0}=\boldsymbol{I}. \quad (115)$$

Convergence of (115), in practice requires 20–30 terms. It is to be noted that the convergence of the series represented by (110) can suffer, if for the first few terms $\boldsymbol{A}^n$ grows quicker than $n!$. In order to control this problem, note that the growth of $\boldsymbol{A}^n$ depends on its eigenvalues. If all the eigenvalues of $\boldsymbol{A}$ are within the unit circle in the complex plane, then $\boldsymbol{A}^n$ will decay with increasing n, leading to fast convergence. From (110) one can see that the eigenvalues of $\boldsymbol{A}$

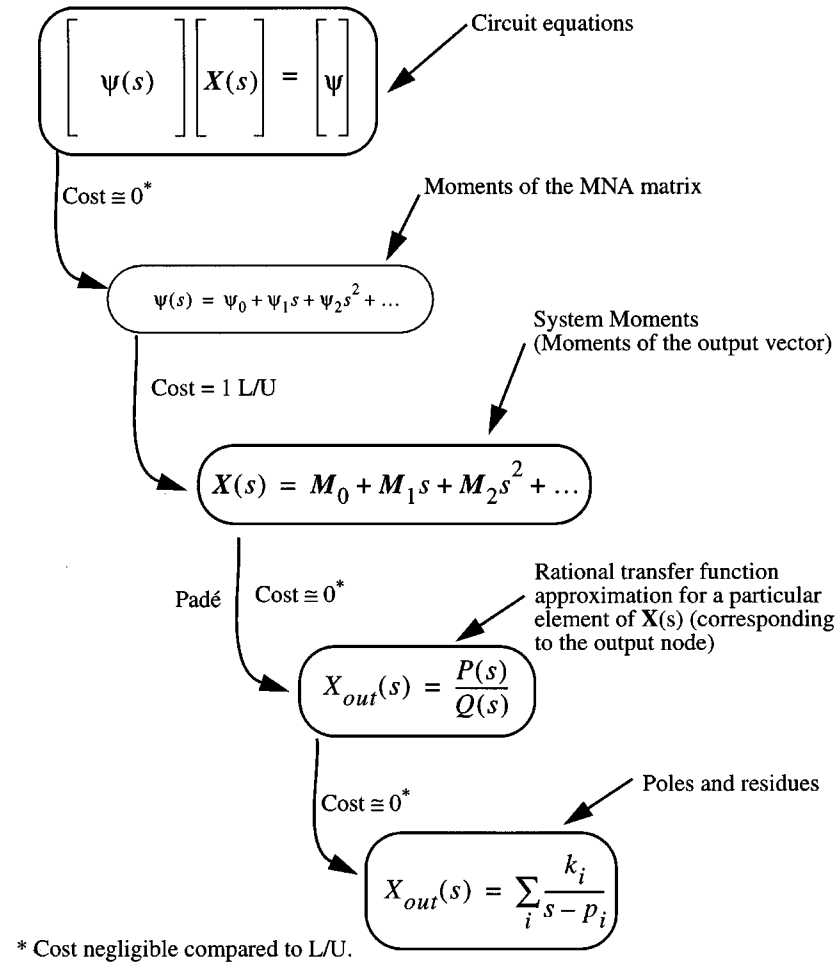

Fig. 17. Summary of the steps involved in the MMT algorithm.

can be controlled by varying the length d. By restricting d to be small enough, such that the eigenvalues of $(\boldsymbol{D}+s\boldsymbol{E})\,d$ will also be small (over a given frequency range), so as not to cause truncation errors or slow convergence. This can be achieved efficiently, by noting that

$$e^{(\boldsymbol{D}+s\boldsymbol{E})d} = e^{(((\boldsymbol{D}+s\boldsymbol{E})d)/2)}e^{(((\boldsymbol{D}+s\boldsymbol{E})d)/2)}. \tag{116}$$

In other words, moments of a line can be generated by squaring half-line moments. Let Φ represent the half-line moments, then

$$\begin{aligned} e^{(\boldsymbol{D}+s\boldsymbol{E})d} &= \boldsymbol{F_0} + \boldsymbol{F_1}s + \cdots + \boldsymbol{F}_n s^n \\ &= (\Phi_{\mathbf{0}} + \Phi_{\mathbf{1}}s + \cdots + \Phi_n s^n) \\ &\quad \cdot (\Phi_{\mathbf{0}} + \Phi_{\mathbf{1}}s + \cdots + \Phi_n s^n) \end{aligned} \tag{117}$$

which will give

$$\boldsymbol{F}_r = \sum_{i=0}^{r} \Phi_i \Phi_{r-i}. \tag{118}$$

The line can be subdivided by power of 2 (i.e., two sections, four sections, eight sections ...) and the moments of the smallest section that meets the convergence requirements are calculated. From these, the moments of the entire line can be recursively calculated with the help of (118).

A summary of the steps involved in the Padé-based circuit reduction is given in Fig. 17.

C. Limitations of Single Expansion MMT Algorithms

Obtaining a lower order approximation of the network transfer function using a single Padé expansion is commonly referred as *asymptotic waveform evaluation (AWE)* in the literature. However, due to the inherent limitations of Padé approximants, MMTs based on single expansion often give inaccurate results. The following is a list of those properties that have the most impact on MMTs.

- The matrix in (98) (known as Toeplitz matrix) becomes increasingly ill-conditioned as its size increases. This implies that one can only expect to detect six to eight accurate poles from a single expansion.
- Padé often produces unstable poles on the right-hand side of the complex plane.
- Padé accuracy deteriorates as we move away from the expansion point.
- Padé provides no estimates for error bounds.

In addition, there is no guarantee that the reduced-model obtained as above is passive. Passivity implies that a network cannot generate more energy than it absorbs, and no passive termination of the network will cause the system to go unstable [83]–[92]. The loss of passivity can be a serious

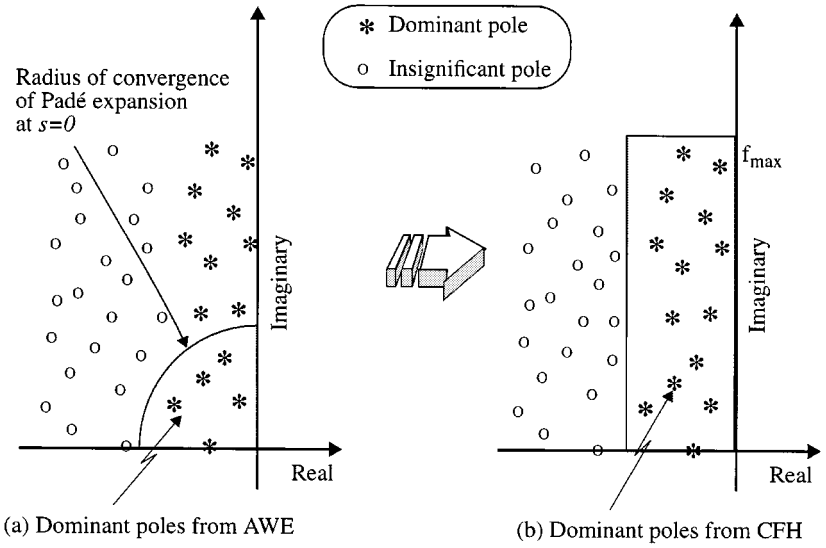

Fig. 18. Illustration of CFH.

problem because transient simulations of reduced networks may encounter artificial oscillations.

In systems containing distributed elements the number of dominant poles will be significantly higher, and it is very difficult to capture all of them with a single Padé expansion. This lead to the development of multipoint expansion techniques such as *complex frequency hopping (CFH)*, which are summarized in the next section.

D. Complex Frequency Hopping

CFH extends the process of moment matching to multiple expansion points (*hops*) in the complex plane near or on the imaginary axis using a binary search algorithm [72]. With a minimized number of frequency point expansions, enough information is obtained to enable the generation of an approximate transfer function that matches the original function up to a predefined highest frequency of interest. Using the information from all the expansion points, CFH extracts a dominant pole-set as illustrated in Fig. 18(b). In addition, CFH provides an error criterion for the selection of accurate poles and transfer functions.

Selection and Minimization of Hops in CFH: A Padé approximation is accurate only near the point of expansion and its accuracy decreases as we move away from the *point of expansion (hop)*. In order to validate the accuracy of such an approximation, at least two expansion points are necessary. Accuracies of these two expansions can be verified by matching the poles generated at these two hops [72] (referred as *pole-matching-based approach*). Alternatively, the two hops can be verified for their accuracy by comparing the value of the transfer functions due to both these hops at a point intermediate to them (referred as *transfer-function-based approach*) [73]. CFH relies on a binary search algorithm to determine the expansion points and to minimize the number of expansions. The steps involved in the binary search algorithm for both the above approaches are summarized as follows.

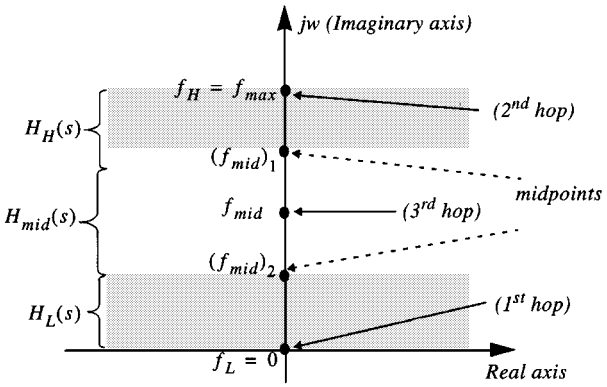

Fig. 19. Graphical illustration of transfer-function-based search algorithm.

1) Transfer-Function-Based Approach: In this approach the transfer functions obtained at various hops (expansions) are used to ensure the accuracy of the reduced-order model up to the highest frequency of interest. Steps involved in the algorithm are given in Figs. 19 and 20. It is to be noted that the computational effort needed for a comparison as required by *Step 5* is trivial as the responses can be computed in a closed-form using the transfer functions generated in *Steps 2* and *3*. Here, ε_{th} is a predefined threshold for the relative error in the transfer functions. At the completion of the binary search algorithm, a set of transfer functions are generated. When evaluating the frequency response at a frequency point α, only the transfer function that is valid in the region containing α is used. This is repeated for all other frequency points to obtain the frequency response of the system.

2) Pole-Matching-Based Approach: In this approach, poles of the transfer function are explicitly evaluated at each hop and the hops are verified for their accuracy by comparing the poles from two adjacent hops using a binary search algorithm. If a matching pole is found between two adjacent expansions, then the binary search is stopped. The distance between the matching pole and the expansion point

- *Step 1:* Set $f_L = 0$ and $f_H = f_{max}$ (Fig. 19).
- *Step 2:* Expand system's response at frequency $f_L = 0$. Determine the coefficients of the corresponding transfer function $H_L(s)$ using (98) and (99).
- *Step 3:* Expand system's response at $f_H = f_{max}$. Determine the coefficients of the corresponding transfer function $H_H(s)$.
- *Step 4:* Set $f_{mid} = \frac{1}{2}(f_L + f_H)$. Calculate $H_L(j2\pi f_{mid})$ and $H_H(j2\pi f_{mid})$ using the transfer function coefficients obtained in Steps 2 and 3.
- *Step 5:* If $|H_H(j2\pi f_{mid}) - H_L(j2\pi f_{mid})| < \varepsilon_{th}$, Go To Step 6. Otherwise expand at f_{mid} and obtain $H_{mid}(s)$.
- *Step 6:* If the threshold condition specified by step 5 is satisfied, STOP. ELSE repeat steps 2-5 between every two consecutive frequency points (e.g., between f_L & f_{mid} and f_{mid} & f_H).

Fig. 20. Transfer-function-based binary search algorithm.

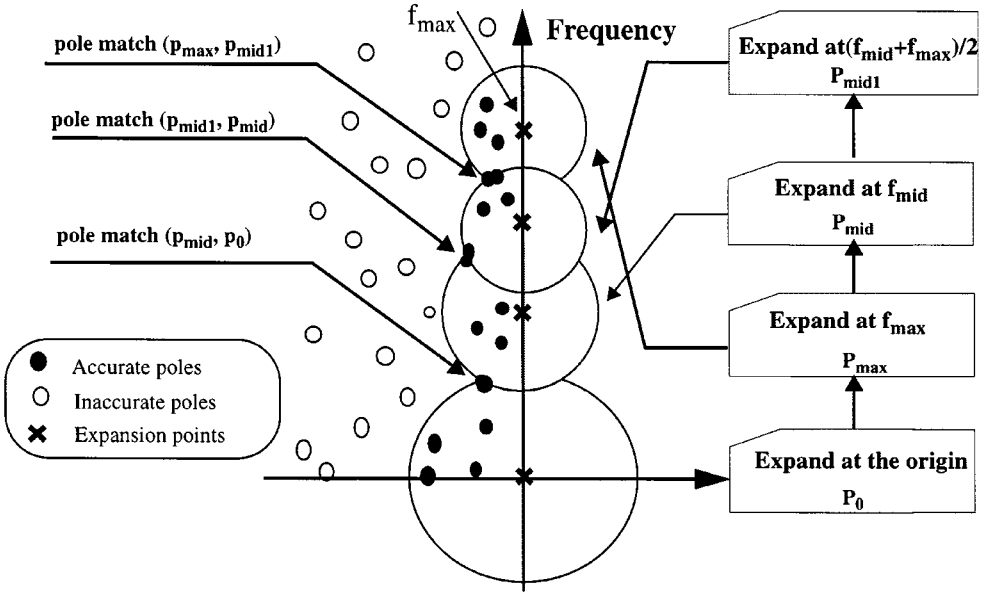

Fig. 21. Pole-matching-based binary search algorithm.

under consideration defines the radius of accuracy for the corresponding expansion. All the poles that are within the radius of accuracy are treated as accurate poles and are retained in the final pole-set. The poles that are outside the radius of accuracy are considered as inaccurate poles and are discarded. Fig. 21 illustrates the idea of the pole search. Steps involved in this approach are identical to the one given in Fig. 20, except for the matching criterion, which is based on poles here. Once a set of dominant poles are obtained, residues of the system are obtained using (102). Further details of CFH and its search algorithms can be found in [72] and [73].

E. Reduced-Order Models of Multiport Linear Networks

So far we looked into the model-reduction of single input-single output systems. In this section, a discussion pertaining to the multiport networks is given. Consider the general multiport interconnect linear subnetwork shown in Fig. 22 [this corresponds to the linear subnetwork π that is described during the general formulation (56) in Section V]. Such a network can be characterized in terms of y (admittance), z (impedance), h (hybrid) or s (scattering) parameters. For the purpose of simplicity of presentation, only the discussion with respect to y parameters is considered in this paper (the idea presented here can be easily

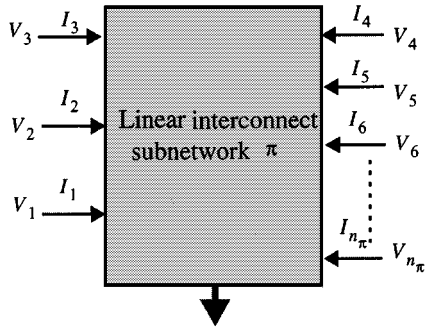

Fig. 22. Multiport linear subnetwork π.

extended to other types of characterization). The network can be characterized using y-parameters as

$$\begin{bmatrix} Y_{11} & Y_{12} & \cdots & Y_{1n_\pi} \\ \cdots & \cdots & \cdots & \cdots \\ Y_{n_\pi 1} & Y_{n_\pi 2} & \cdots & Y_{n_\pi n_\pi} \end{bmatrix} \begin{bmatrix} V_1 \\ \cdots \\ V_{n_\pi} \end{bmatrix} = \begin{bmatrix} I_1 \\ \cdots \\ I_{n_\pi} \end{bmatrix}. \tag{119}$$

Using model-reduction techniques, each entry Y_{jk} in (119) can be approximated by a q-pole lower order model having a general form as follows:

$$Y_{ij}(s) = c^{i,j} + \sum_{a=1}^{q^{i,j}} \frac{k_a^{i,j}}{s - p_a^{i,j}}, \qquad 1 \le (i,j) \le n_\pi \tag{120}$$

where $p_a^{i,j}$ and $k_a^{i,j}$ are the ath dominant pole–residue pair at a port j due to an input excitation at port i, $c^{i,j}$ is the direct coupling constant, and $q^{i,j}$ is the number of dominant poles used for approximating Y_{ij}.

There are two main approaches available in the literature to obtain the matrix-transfer function represented by (119) and (120). In the first approach, a common set of poles obtained for any one of the entries Y_{ij} are used for the computation of residues of all other entries [64], [66]. However, this can lead to inaccurate results, since the residue computation using (102) is very sensitive to the location of poles of each Y_{jk}. In the second approach, separate set of poles are used for the computation of residues of each entry [68]. This approach can lead to a macromodel with a very large number of poles. However, it is to be noted that the nonlinear simulation time using general purpose simulators is superlinearly proportional to the number of states involved (the number of states is generally given by $Total\ number\ of\ states = Total\ number\ of\ poles \times Total\ number\ of\ ports$). Hence, the second approach can become inefficient in the presence of a large number of ports. Both these difficulties can be addressed using the Block CFH technique [76], which provides schemes to minimize the number of poles, as well as to improve the accuracy of residues.

Selection of Dominant Pole-Set: In order to minimize the number of poles in the matrix-transfer function, the following two propositions can be used.

1) In general, the pole-set corresponding to any individual transfer impedances (Y_{ij}) is a subset of the union of all driving point impedances (Y_{ii}) [158].
2) CFH accurately computes the dominant poles of a system. Generally in a system with a large number of dominant poles (20–40), pole-sets belonging to different driving point admittances (Y_{ii}) obtained using CFH contain mostly identical poles and with only a very small number of poles differing among these sets.

Residue Computation Algorithm: Residue computation algorithm [76], which combines the merits of two different approaches of CFH, namely, *transfer-function-based approach* and *pole-matching-based approach*. The transfer-function-based approach collects a set of transfer functions that *accurately matches the frequency response up to the highest frequency of interest*. On the other hand, pole-matching-based approach *collects all the dominant poles accurately up to the highest frequency of interest*. In this algorithm, the relationship between frequency response and pole–residue model of the system is used to compute the residues (this idea is illustrated in Fig. 23) as

$$c + \sum_{i=0}^{q} \frac{k_i}{s - p_i} = H(s) \tag{121}$$

where q is the total number of dominant poles (p_i) extracted using CFH and (k_i) are the corresponding unknown residues, c is the direct coupling constant, and $H(s)$ represents the frequency response obtained using the transfer-function-based approach.

In order to compute the unknown residues, a set of linear equations can be formulated using (121), spanning many frequency points in the region of interest as shown below:

$$c + \sum_{i=0}^{q} \frac{k_i}{s - p_i} = H(s) \tag{122}$$

$$c + \frac{k_1}{s_m - p_1} + \frac{k_2}{s_m - p_2} + \cdots + \frac{k_q}{s_m - p_q} = H(s_m) \tag{123}$$

where s_m represents the mth frequency point. In the case of complex poles, both the pole as well as its conjugate should be used while formulating (123). Let N_m be the total number of frequency points matched. Next, equating both the real and imaginary parts of (123) separately, we obtain a new set of linear equations as

$$\boldsymbol{AK} = \boldsymbol{H} \tag{124}$$

where $\boldsymbol{K} \in \Re^{q \times 1}$ is a vector containing the unknowns corresponding to the real and imaginary parts of residues, $\boldsymbol{H} \in \Re^{2N_m \times 1}$ is a vector containing real and imaginary parts of the frequency responses represented by $\boldsymbol{H}(s_m)$, and $\boldsymbol{A} \in \Re^{2N_m \times q}$ consists of entries contributed by the LHS of (123). In case the direct coupling constant is computed by adding it as one more variable in (124), then the order of matrix/vectors indicated above will change from q to $q+1$.

Next, the solution of (124) is needed to evaluate unknown residues $\boldsymbol{K}$. In order to improve the accuracy of residues, it

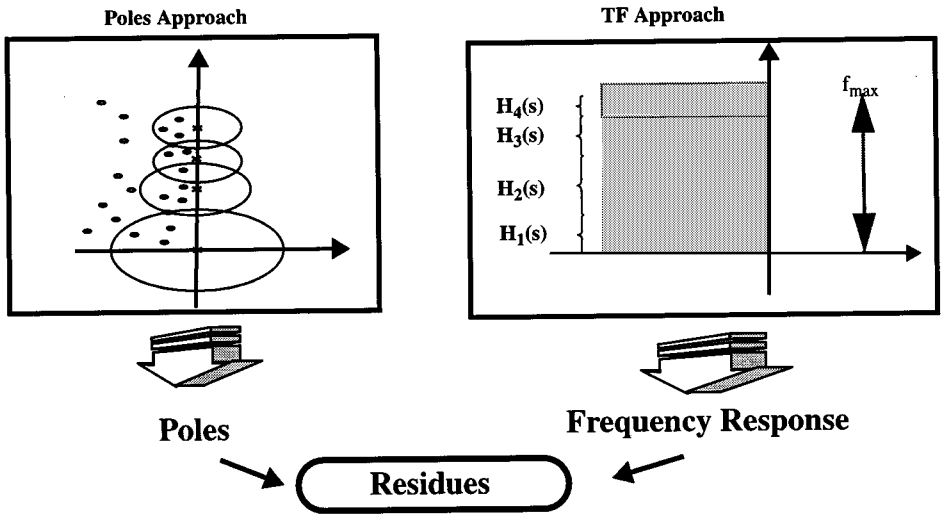

Fig. 23. Illustration of the new residue computation algorithm.

is necessary to match as many frequency points as possible using (123). However, in the case of choosing a number of frequency points higher than the number of unknown residues, matrix $\boldsymbol{A}$ will not be square. To overcome this difficulty, (124) is solved using the least mean square error algorithm and the solution is given by a new set of normal equations

$$\boldsymbol{A_s K} = \boldsymbol{A}^t \boldsymbol{H} \tag{125}$$

where

$$\boldsymbol{A_s} = \boldsymbol{A}^t \boldsymbol{A} \tag{126}$$

is a square matrix of order $q \times q$. $\boldsymbol{A}^t$ represents the transpose of $\boldsymbol{A}$. Formulating the residue equations in the form given by (125) leads to additional computational savings as the *number of equations to be solved remains equal to the number of unknown residues despite the increase in matched frequency points*.

In the multiport CFH algorithm, an accurate frequency-response for each of the entries in the $\boldsymbol{Y}$ matrix is obtained using complex frequency hopping based on transfer-function approach. Next, an accurate pole-set is obtained as the union of driving point impedances. Using these accurate poles and frequency responses, residues for each Y_{ij} is obtained through the residue computation algorithm.

F. Interface to Circuit Simulators

In this section, a review of techniques to link reduced-order models to nonlinear SPICE-like simulators is described. The reduced-order model for the linear subnetwork is obtained as shown in (127) at the bottom of the page, where q is the number of poles in the common pole-set P. $k^{i,j}$ and $c^{i,j}$ represent residue and the direct coupling constant for the parameter Y_{ij}, respectively. Derivation of differential equations from reduced-order interconnect models is referred as *macromodel synthesis*. The differential equations can be easily linked to nonlinear simulators as they are described in time-domain. This process is illustrated in Fig. 24. In general, a set of first-order differential equations in the state–space domain can be described as

$$\begin{aligned} \left[\dot{\boldsymbol{X}}\right] &= [\boldsymbol{A}][\boldsymbol{X}] + [\boldsymbol{B}][\boldsymbol{U}] \\ [\boldsymbol{Y}] &= [\boldsymbol{C}][\boldsymbol{X}] + [\boldsymbol{D}][\boldsymbol{U}] \end{aligned} \tag{128}$$

where $\boldsymbol{A} \in \Re^{n \times n}$ is a state-matrix, $\boldsymbol{B} \in \Re^{n \times n_\pi}$ is a matrix that relates the inputs to state-variables, $\boldsymbol{C} \in \Re^{n_\pi \times n}$ is a matrix relating state variables to the outputs ($\boldsymbol{Y}$), $\boldsymbol{D} \in \Re^{n_\pi \times n_\pi}$ is a matrix relating inputs directly to the output, $\boldsymbol{X}$ is the state vector of length n, and $\boldsymbol{U}$ is the input vector of length n_π (where n_π is the number of ports).

Given a matrix-transfer function described by (127), several forms of time-domain realization can be obtained. For the purpose of illustration, macromodel synthesis using Jordan-canonical [152], [153] form of realization is given

$$\boldsymbol{Y}_\pi(s) = \begin{bmatrix} c^{1,1} + \sum_{i=1}^{q} \dfrac{k_i^{1,1}}{s - p_i} & \cdots & c^{1,2} + \sum_{i=1}^{q} \dfrac{k_i^{1,2}}{s - p_i} & \cdots & \cdots & c^{1,n_\pi} + \sum_{i=1}^{q} \dfrac{k_i^{1,n_\pi}}{s - p_i} \\ \cdots & & & \cdots & \cdots & \\ c^{n_\pi,1} + \sum_{i=1}^{q} \dfrac{k_i^{n_\pi,1}}{s - p_i} & & c^{n_\pi,1} + \sum_{i=1}^{q} \dfrac{k_i^{n_\pi,2}}{s - p_i} & \cdots & \cdots & c^{n_\pi,n_\pi} + \sum_{i=1}^{q} \dfrac{k_i^{n_\pi,n_\pi}}{s - p_i} \end{bmatrix} \tag{127}$$

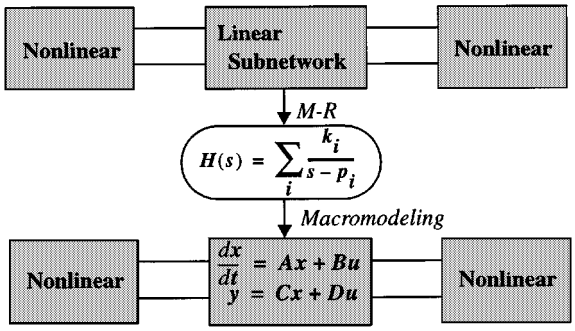

Fig. 24. Illustration of macromodel synthesis for nonlinear simulation.

below. Consider a two-port network containing two common poles, whose transfer function is described by

$$\begin{bmatrix} c^{1,1} + \sum_{a=1}^{2} \frac{k_a^{1,1}}{s-p_a} & c^{1,2} + \sum_{a=1}^{2} \frac{k_a^{1,2}}{s-p_a} \\ c^{2,1} + \sum_{a=1}^{2} \frac{k_a^{2,1}}{s-p_a} & c^{2,2} + \sum_{a=1}^{2} \frac{k_a^{2,2}}{s-p_a} \end{bmatrix} \begin{bmatrix} V_1 \\ V_2 \end{bmatrix} = \begin{bmatrix} I_1 \\ I_2 \end{bmatrix}.$$

A Jordan-canonical [152], [153] form of realization for this case would need four state variables, and it can be represented as

$$\begin{bmatrix} \dot{x}_1 \\ \dot{x}_2 \\ \dot{x}_3 \\ \dot{x}_4 \end{bmatrix} = \begin{bmatrix} p_1 & 0 & 0 & 0 \\ 0 & p_1 & 0 & 0 \\ 0 & 0 & p_2 & 0 \\ 0 & 0 & 0 & p_2 \end{bmatrix} \begin{bmatrix} x_1 \\ x_2 \\ x_3 \\ x_4 \end{bmatrix} + \begin{bmatrix} 1 & 0 \\ 0 & 1 \\ 1 & 0 \\ 0 & 1 \end{bmatrix} \begin{bmatrix} v_1 \\ v_2 \end{bmatrix}$$

$$\boldsymbol{y} = \begin{bmatrix} i_1 \\ i_2 \end{bmatrix} = \begin{bmatrix} k_1^{1,1} & k_1^{1,2} & k_2^{1,1} & k_2^{1,2} \\ k_1^{2,1} & k_1^{2,2} & k_2^{2,1} & k_2^{2,2} \end{bmatrix} \begin{bmatrix} x_1 \\ x_2 \\ x_3 \\ x_4 \end{bmatrix} + \begin{bmatrix} c^{1,1} & c^{1,2} \\ c^{2,1} & c^{2,2} \end{bmatrix} \begin{bmatrix} v_1 \\ v_2 \end{bmatrix}$$

If the matrix-transfer function $\boldsymbol{Y}_\pi(s)$ contains complex poles, then they need to be treated differently as they do not have a direct meaning in the time-domain. However, since all the coefficients of the denominator polynomials of $\boldsymbol{Y}_\pi(s)$ (which are obtained through Padé approximation) are real, if a complex number λ is a root of $\boldsymbol{Y}_\pi(s)$ then its complex conjugate λ^* is also a root of $\boldsymbol{Y}_\pi(s)$. Hence, a Jordan-form of state–space realization for a complex pole-pair would be [153]

$$\begin{bmatrix} \dot{\boldsymbol{x}}_1 \\ \dot{\boldsymbol{x}}_2 \end{bmatrix} = \begin{bmatrix} \boldsymbol{A}_1 & \boldsymbol{0} \\ \boldsymbol{0} & \boldsymbol{A}_1^* \end{bmatrix} + \begin{bmatrix} \boldsymbol{x}_1 \\ \boldsymbol{x}_2 \end{bmatrix} + \begin{bmatrix} \boldsymbol{b}_1 \\ \boldsymbol{0} \end{bmatrix} \boldsymbol{u}$$

$$\boldsymbol{y} = [\boldsymbol{C}_1 \quad \boldsymbol{C}_1^*] \begin{bmatrix} \boldsymbol{x}_1 \\ \boldsymbol{x}_2 \end{bmatrix} \tag{129}$$

where $\boldsymbol{A}_1$ is a diagonal matrix constructed using poles and $\boldsymbol{A}_1^*$ is complex conjugate of $\boldsymbol{A}_1$. Next, introducing an equivalence transformation defined by

$$[\hat{\boldsymbol{x}}] = [\boldsymbol{T}][\boldsymbol{x}], \qquad \boldsymbol{T} = \begin{bmatrix} \boldsymbol{I} & \boldsymbol{I} \\ i\boldsymbol{I} & -i\boldsymbol{I} \end{bmatrix} \tag{130}$$

(129) can now be easily transformed into

$$\begin{bmatrix} \dot{\hat{\boldsymbol{x}}}_1 \\ \dot{\hat{\boldsymbol{x}}}_2 \end{bmatrix} = \begin{bmatrix} \mathrm{Re}(\boldsymbol{A}_1) & \mathrm{Im}(\boldsymbol{A}_1) \\ -\mathrm{Im}(\boldsymbol{A}_1) & \mathrm{Re}(\boldsymbol{A}_1) \end{bmatrix} \begin{bmatrix} \hat{\boldsymbol{x}}_1 \\ \hat{\boldsymbol{x}}_2 \end{bmatrix} + \begin{bmatrix} 2\mathrm{Re}(\boldsymbol{b}_1) \\ \boldsymbol{0} \end{bmatrix} \boldsymbol{u}$$

$$\boldsymbol{y} = [\mathrm{Re}(\boldsymbol{C}_1) \quad \mathrm{Im}(\boldsymbol{C}_1)] \begin{bmatrix} \hat{\boldsymbol{x}}_1 \\ \hat{\boldsymbol{x}}_2 \end{bmatrix}. \tag{131}$$

An illustrative example of the above steps is given below. Consider a two-port network containing one pair of complex poles $\lambda_{1,2} = w \pm iz$. Let the corresponding residues at different ports be $c_{i,j} = (r \pm iv)_{i,j}$. The original Gilbert's realization will yield

$$\begin{bmatrix} \dot{x}_1 \\ \dot{x}_2 \\ \dot{x}_3 \\ \dot{x}_4 \end{bmatrix} = \begin{bmatrix} w+iz & 0 & 0 & 0 \\ 0 & w+iz & 0 & 0 \\ 0 & & w-iz & 0 \\ 0 & 0 & 0 & w-iz \end{bmatrix} \begin{bmatrix} x_1 \\ x_2 \\ x_3 \\ x_4 \end{bmatrix} + \begin{bmatrix} 1 & 0 \\ 0 & 1 \\ 1 & 0 \\ 0 & 1 \end{bmatrix} \begin{bmatrix} v_1 \\ v_2 \end{bmatrix}$$

$$\boldsymbol{y} = \begin{bmatrix} i_1 \\ i_2 \end{bmatrix} = \begin{bmatrix} (r+iv)_{11} & (r+iv)_{12} & (r-iv)_{11} & (r-iv)_{12} \\ (r+iv)_{21} & (r+iv)_{22} & (r-iv)_{21} & (r-iv)_{22} \end{bmatrix} \cdot \begin{bmatrix} x_1 \\ x_2 \\ x_3 \\ x_4 \end{bmatrix}$$

Define

$$\boldsymbol{T} \begin{bmatrix} 1 & 0 & 1 & 0 \\ 0 & 1 & 0 & 1 \\ i & 0 & -i & 0 \\ 0 & i & 0 & -i \end{bmatrix}.$$

Next, the realization represented by (131) can be obtained as

$$\begin{bmatrix} \dot{\hat{x}}_1 \\ \dot{\hat{x}}_2 \\ \dot{\hat{x}}_3 \\ \dot{\hat{x}}_4 \end{bmatrix} = \begin{bmatrix} w & 0 & z & 0 \\ 0 & w & 0 & z \\ -z & 0 & w & 0 \\ 0 & -z & 0 & w \end{bmatrix} \begin{bmatrix} \hat{x}_1 \\ \hat{x}_2 \\ \hat{x}_3 \\ \hat{x}_4 \end{bmatrix} + \begin{bmatrix} 2 & 0 \\ 0 & 2 \\ 0 & 0 \\ 0 & 0 \end{bmatrix} \begin{bmatrix} v_1 \\ v_2 \end{bmatrix}$$

$$\boldsymbol{y} = \begin{bmatrix} i_1 \\ i_2 \end{bmatrix} = \begin{bmatrix} r_{11} & r_{12} & v_{11} & v_{12} \\ r_{21} & r_{22} & v_{21} & v_{22} \end{bmatrix} \begin{bmatrix} \hat{x}_1 \\ \hat{x}_2 \\ \hat{x}_3 \\ \hat{x}_4 \end{bmatrix}.$$

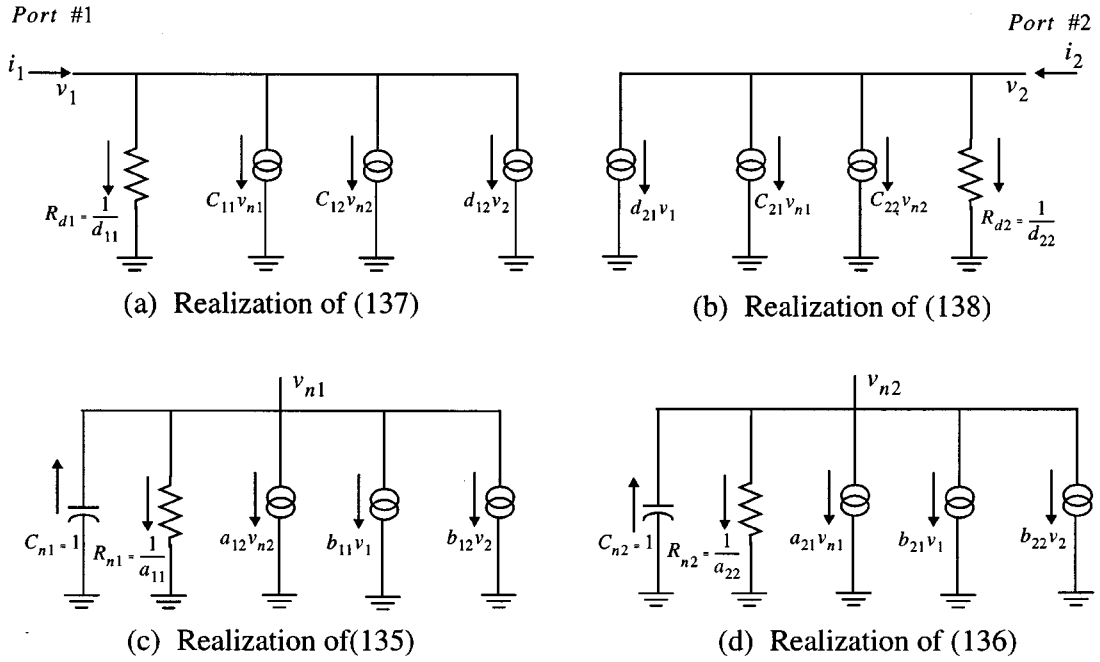

Fig. 25. Illustration of equivalent subcircuit generation from macromodels.

Unified Transient Simulation: Once a matrix-transfer function describing the multiport interconnect network is obtained, a time-domain realization in the form of state–space equations can be obtained as

$$\begin{aligned}\frac{d}{dt}[\boldsymbol{z}_\pi(t)] - [\boldsymbol{A}_\pi][\boldsymbol{z}_\pi(t)] - [\boldsymbol{B}_\pi][\boldsymbol{i}_\pi(t)] &= \boldsymbol{0}\\ [\boldsymbol{v}_\pi(t)] - [\boldsymbol{C}_\pi][\boldsymbol{z}_\pi(t)] + [\boldsymbol{D}_\pi][\boldsymbol{i}_\pi(t)] &= \boldsymbol{0}\end{aligned} \quad (132)$$

where $\boldsymbol{i}_\pi$ and $\boldsymbol{v}_\pi$ are the vector of terminal currents and voltages of the linear subnetwork π [described by (56)]. The differential equations represented by the macromodel (132) can be combined with (55) using the relation $\boldsymbol{v}_\pi = (\boldsymbol{L}_\pi)^t \boldsymbol{v}_\phi$ as

$$\begin{aligned}\frac{d}{dt}\boldsymbol{z}_\pi(t) - \boldsymbol{A}_\pi \boldsymbol{z}_\pi(t) - \boldsymbol{B}_\pi \boldsymbol{i}_\pi(t) &= \boldsymbol{0}\\ (\boldsymbol{L}_\pi)^t \boldsymbol{v}_\phi(t) - \boldsymbol{C}_\pi \boldsymbol{z}_\pi(t) - \boldsymbol{D}_\pi \boldsymbol{i}_\pi(t) &= \boldsymbol{0}\\ \boldsymbol{C}_\phi \frac{d}{dt}\boldsymbol{v}_\phi(t) + \boldsymbol{G}_\phi \boldsymbol{v}_\phi(t) + \boldsymbol{L}_\pi \boldsymbol{i}_\pi(t) + \boldsymbol{F}(\boldsymbol{v}_\phi(t)) - \boldsymbol{b}_\phi(t) &= \boldsymbol{0}.\end{aligned} \quad (133)$$

Using standard nonlinear solvers or any of the general-purpose circuit simulators, the unified set of differential equations represented by (133) can be solved to yield transient solution for the entire nonlinear circuit containing interconnect subnetworks. For those simulators (such as HSPICE) that do not directly accept the differential equations as input, the macromodel represented by (133) can be converted to an equivalent subcircuit and is described in the next section.

Conversion of Macromodels to Equivalent Subcircuits: Conversion of differential equations to equivalent subcircuits can be accomplished in several ways. For the purpose of illustration, consider a simple case of two-port network with two states represented in the form of (132)

$$\begin{bmatrix}\dot{x}_1\\ \dot{x}_2\end{bmatrix} = \begin{bmatrix}a_{11} & a_{12}\\ a_{21} & a_{22}\end{bmatrix}\begin{bmatrix}x_1\\ x_2\end{bmatrix} + \begin{bmatrix}b_{11} & b_{12}\\ b_{21} & b_{22}\end{bmatrix}\begin{bmatrix}v_1\\ v_2\end{bmatrix}$$
$$\begin{bmatrix}i_1\\ i_2\end{bmatrix} = \begin{bmatrix}c_{11} & c_{12}\\ c_{21} & c_{22}\end{bmatrix}\begin{bmatrix}x_1\\ x_2\end{bmatrix} + \begin{bmatrix}d_{11} & d_{12}\\ d_{21} & d_{22}\end{bmatrix}\begin{bmatrix}v_1\\ v_2\end{bmatrix}. \quad (134)$$

Next, (134) can be rearranged as

$$\dot{x}_1 = a_{11}x_1 + a_{12}x_2 + b_{11}v_1 + b_{12}v_2 \quad (135)$$
$$\dot{x}_2 = a_{21}x_1 + a_{22}x_2 + b_{21}v_1 + b_{22}v_2 \quad (136)$$
$$i_1 = c_{11}x_1 + c_{12}x_2 + d_{11}v_1 + d_{12}v_2 \quad (137)$$
$$i_2 = c_{21}x_1 + c_{22}x_2 + d_{21}v_1 + d_{22}v_2. \quad (138)$$

In the above equations, the port voltages and currents are represented by v_1, v_2 and i_1, i_2, respectively. An equivalent network representing (135)–(138) can be constructed as shown in Fig. 25. Each state in the macromodel requires a separate node in the equivalent circuit and are represented by nodes n_1, n_2. The state variables x_1, x_2 can be represented by the capacitor voltages. These capacitors are denoted by C_{n1}, C_{n2} and the corresponding voltages by v_{n1}, v_{n2}. Next, the terms such as $a_{11}x_1$ in (135)–(138) can be represented by voltage controlled current sources. Equations (135) and (136) are fully represented by Fig. 25(c) and (d). Output equations represented by (137) and (138) are realized through equivalent circuits shown in Fig. 25(a) and (b). Generalization of the above discussion in the presence of more number of states or ports is straightforward.

VIII. Model-Reduction Based on Krylov-Subspace Techniques

Direct MMTs such as AWE, discussed in Section VII, have some disadvantages associated with them. First one among them is the ill-conditioning associated with the moment-matrix. Due to this difficulty, the number of good poles that could be extracted from any expansion point is generally fewer than ten poles. The second major difficulty is that they do not guarantee the passivity of reduced models. In order to address these difficulties, a parallel class of algorithms, which can be classified as *indirect moment-matching techniques* were developed [77]–[90].

These algorithms are based on what is known as *Krylov-subspace formulation* and *Congruent transformation*. One of the main features of these algorithms is that they construct the reduced-model based on the extraction of *leading eigenvalues (those with the largest magnitude)* of a given system (on the contrary, the reduced models from the CFH technique discussed in Section VII-D is based on extracting the dominant poles of a given system). In the rest of this section, we will describe the concept and important features of these algorithms.

A. Preliminaries

Recall from Section IV, the time-domain MNA and the corresponding output equations can be represented in the form

$$\begin{aligned} \boldsymbol{C}\dot{\boldsymbol{x}}(t)+\boldsymbol{G}\boldsymbol{x}(t)=\boldsymbol{B}u(t), \qquad & \boldsymbol{C},\boldsymbol{G}\in\Re^{n\times n} \\ & \boldsymbol{B}\in\Re^{n\times 1} \quad \boldsymbol{x}\in\Re^{n\times 1} \\ w=\boldsymbol{L}^T\boldsymbol{x}(t), \qquad & \boldsymbol{L}\in\Re^{n\times 1} \end{aligned} \tag{139}$$

where n represents the total number of MNA variables. Premultiplying both sides of (139) by $\boldsymbol{G}^{-1}$, we can write

$$\begin{aligned} \boldsymbol{A}\dot{\boldsymbol{x}}(t)=\boldsymbol{x}(t)-\boldsymbol{R}u(t), \qquad & \boldsymbol{A}=-\boldsymbol{G}^{-1}\boldsymbol{C}, \quad \boldsymbol{R}=\boldsymbol{G}^{-1}\boldsymbol{B} \\ w=\boldsymbol{L}^T\boldsymbol{x}(t). & \end{aligned} \tag{140}$$

Taking the Laplace transform of (140), we can write

$$\begin{aligned} s\boldsymbol{A}\boldsymbol{X}(s)&=\boldsymbol{X}(s)-\boldsymbol{R}U(s) \\ W(s)&=\boldsymbol{L}^T\boldsymbol{X}(s). \end{aligned} \tag{141}$$

Rearranging (141), we can write the transfer function $Y(s)$ of the given system as

$$Y(s)=\frac{W(s)}{U(s)}=\boldsymbol{L}^T(\boldsymbol{I}-s\boldsymbol{A})^{-1}\boldsymbol{R} \tag{142}$$

where $\boldsymbol{I}$ is an identity matrix.

1) Why Direct Padé-Based Approximation (Moment-Matrix) is Ill-Conditioned: Consider the transfer-function of a system, as represented by (142). Expanding it in terms of Taylor series, we have

$$\begin{aligned} Y(s)&=\boldsymbol{L}^T(\boldsymbol{I}+s\boldsymbol{A}+s^2\boldsymbol{A}^2+s^3\boldsymbol{A}^3+\cdots+s^q\boldsymbol{A}^q)\boldsymbol{R} \\ &=\sum_{k=0}^{q}s^k(\boldsymbol{L}^T\boldsymbol{A}^k\boldsymbol{R}) \\ &=\sum_{k=0}^{q}s^k m_k \qquad \text{where } m_k=\boldsymbol{L}^T\boldsymbol{A}^k\boldsymbol{R}. \end{aligned} \tag{143}$$

Ideally, increasing the order of the Padé approximation (which is equivalent to matching more number of moments) should have given us better approximation results. However, in practice, this is true only up to very limited order, beyond which Padé approximation will not yield any better results [77], [160]. This can be explained by examining the nature of higher order moments, which are given by $m_k=\boldsymbol{L}^T\boldsymbol{A}^k\boldsymbol{R}$. As can be seen, when successive moments are explicitly calculated, they are obtained as powers of $\boldsymbol{A}$. With the increasing values of "k", this process *quickly converges to an eigenvector corresponding to an eigenvalue of $\boldsymbol{A}$ with the largest magnitude*. As a result, for relatively large values of "k", the explicitly calculated moments m_k, m_{k+1}, m_{k+2}, …, will not add any extra information to the moment-matrix, as all of them contain information only about the largest eigenvalue. In other words, the rows beyond "k" of moment-matrix are almost identical (or parallel to each other), making the matrix ill-conditioned.

2) Relationship Between Eigenvalues and Poles of the System: In this section we will show the correspondence between the leading eigenvalues and poles of the system. It is important to understand this concept as the Krylov-subspace-based techniques obtain the reduced-models by extracting the leading eigenvalues of a given system. Consider (140), and assume that the matrix $\boldsymbol{A}$ can be diagonalized in the form

$$\boldsymbol{A}=\boldsymbol{F}\lambda\boldsymbol{F}^{-1} \tag{144}$$

where $\lambda=\text{diag}[\lambda_1 \ \lambda_2\cdots\lambda_n]$ is a diagonal matrix whose diagonal elements represent the eigenvalues of matrix $\boldsymbol{A}$. The matrix $\boldsymbol{F}$ contains the eigenvectors of matrix $\boldsymbol{A}$. Using (144), the transfer-function represented by (142) can be rewritten as

$$\begin{aligned} Y(s)&=\boldsymbol{L}^T(\boldsymbol{I}-s\boldsymbol{F}\lambda\boldsymbol{F}^{-1})^{-1}\boldsymbol{R} \\ &=\boldsymbol{L}^T\boldsymbol{F}(\boldsymbol{I}-s\lambda)^{-1}\boldsymbol{F}^{-1}\boldsymbol{R} \\ &=\boldsymbol{L}^T\boldsymbol{F}\begin{bmatrix} \dfrac{1}{1-s\lambda_1} & & \\ & \cdots & \\ & & \dfrac{1}{1-s\lambda_n} \end{bmatrix}\boldsymbol{F}^{-1}\boldsymbol{R} \end{aligned} \tag{145}$$

which can be simplified as

$$Y(s)=\sum_i\frac{\eta_i}{1-s\lambda_i}=\sum_i\frac{-(\eta_i/\lambda_i)}{s-(1/\lambda_i)}=\sum_i\frac{k_i}{s-p_i} \tag{146}$$

where η_i is a function of the eigenvectors of matrix $\boldsymbol{A}$, and k_i represent the residues. From (146), we can draw following inferences. 1) Poles p_i are the reciprocal of eigenvalues of matrix $\boldsymbol{A}$; the leading eigenvalues (those with largest magnitudes) correspond to the poles closer to the origin. 2) The transfer function of $Y(s)$ can be easily obtained in terms of poles and residues, once the eigenvalues and eigenvectors of $\boldsymbol{A}$ are available.

However, for large interconnect circuits, it would be impractical to compute all the eigenvalues and eigenvectors. Hence, in the following sections, we will review some of the efficient techniques to extract leading eigenvalues.

Computation of Eigenvalues of Matrix "$\boldsymbol{A}$": In general, the numerical computation of all the eigenvalues and eigenvectors of a given matrix $\boldsymbol{A}$ becomes exceedingly expensive as its size gets above a few hundred. The general approach in such cases is to approximate $\boldsymbol{A}$ with a smaller matrix $\hat{\boldsymbol{A}}$, such that the eigenvalues of $\hat{\boldsymbol{A}}$ are reasonable approximation of the leading eigenvalues of $\boldsymbol{A}$. Due to the relatively small size of $\hat{\boldsymbol{A}}$, finding its eigenvalues will be a much simpler problem than finding the eigenvalues of $\boldsymbol{A}$. Next, we will review some of the basic matrix forms [160], which would be helpful in understanding the eigenvalue computation algorithms presented in this section.

Orthogonal Matrices: A real matrix $\boldsymbol{Q}$ is orthogonal if

$$\boldsymbol{Q}^T\boldsymbol{Q} = \boldsymbol{I}. \tag{147}$$

All columns, $\boldsymbol{q_i}$ of orthogonal matrices have unit two norms or $||\boldsymbol{q_i}||_2 = 1$ (which implies that $\boldsymbol{q_i^T q_i} = 1$) and are orthogonal to one another (which means that $\boldsymbol{q_i^T q}_j = 0$). For the special case where $\boldsymbol{Q}$ is a square matrix, the above definition implies $\boldsymbol{Q}^{-1} = \boldsymbol{Q}^T$.

QR Decomposition: Let $\boldsymbol{K}$ be a $m \times n$ matrix with $m > n$. Suppose that $\boldsymbol{K}$ has full column rank. Then there exists a unique $m \times n$ orthogonal matrix $\boldsymbol{Q}$ and a unique upper-triangular matrix $\boldsymbol{R_u}$ with positive diagonals ($r_{ii} > 0$) such that $\boldsymbol{K} = \boldsymbol{QR_u}$. There are several techniques (such as *modified Gram–Schmidt orthogonalization* process) available in the literature for performing this decomposition [160].

Upper-Hessenberg Matrix: A matrix $\boldsymbol{H}$ is called *Upper-Hessenberg* if $H_{ij} = 0$ for $(i > j+1)$. For example, consider an upper Hessenberg matrix of order n, having the following form (which is known as *companion form*):

$$\boldsymbol{H} = \begin{bmatrix} 0 & 0 & 0 & \cdots & 0 & -c_1 \\ 1 & 0 & 0 & \cdots & 0 & -c_2 \\ 0 & 1 & 0 & \cdots & \vdots & \vdots \\ \vdots & 0 & & \cdots & \vdots & \vdots \\ \vdots & \vdots & & \cdots & 0 & \vdots \\ \vdots & \vdots & & \cdots & 1 & -c_n \end{bmatrix}. \tag{148}$$

One of the important advantages of the above companion form is that its characteristic polynomial $\rho(x)$ can be analytically computed and is given by

$$\rho(x) = x^n + \sum_{i=1}^{n} c_i x^{i-1}. \tag{149}$$

The roots of $\rho(x)$ give the eigenvalues of $\boldsymbol{H}$.

Next, consider the circuit equations (140) and a simple similarity transformation as follows:

$$\boldsymbol{AK} = \boldsymbol{KH}_n \tag{150}$$

where the transformation matrix $\boldsymbol{K}$ is defined as

$$\boldsymbol{K} = [\boldsymbol{R}\ \boldsymbol{AR}\ \cdots\ \boldsymbol{A}^{n-1}\boldsymbol{R}] \tag{151}$$

and $\boldsymbol{H}_n$ has the *upper-Hessenberg companion form* discussed above. Obviously, since $\boldsymbol{H}_n$ is related to the matrix $\boldsymbol{A}$ through a similarity transformation, its eigenvalues are the same as that of $\boldsymbol{A}$. Although it looks straightforward, this approach has the following limitations.

Computation of $\boldsymbol{H}_n$ using the relation (150) ($\boldsymbol{H}_n = \boldsymbol{K^{-1}AK}$) requires the inverse of the matrix $\boldsymbol{K}$. However, $\boldsymbol{K}$ is a dense matrix and, hence, computation of its inverse will be expensive. Also, $\boldsymbol{K}$ is likely to be ill-conditioned since the columns of $\boldsymbol{K}$ are formed based on the sequence $\boldsymbol{A}^i\boldsymbol{R}$ which quickly converges to the eigenvector corresponding to the largest eigenvalue. In the next section, we will describe general techniques to overcome these problems. These algorithms belong to a class of methods known as *Krylov-subspace* techniques.

B. Krylov-Subspace Methods for Iterative Computation of Eigenvalues

We will start by replacing the matrix $\boldsymbol{K}$ in (150) with an orthogonal matrix $\boldsymbol{Q}$ such that for all n, the leading n columns of $\boldsymbol{K}$ and $\boldsymbol{Q}$ span the same space. This space is called Krylov-subspace and is denoted by $\kappa(\boldsymbol{A}, \boldsymbol{R}, n)$. In other words, any vector that is a linear combination of the leading n columns of $\boldsymbol{K}$ can be expressed also as a linear combination of the leading n columns of $\boldsymbol{Q}$. Mathematically, we will express this as

$$\begin{aligned} \kappa(\boldsymbol{A}, \boldsymbol{R}, n) &= ColumnSpace([\boldsymbol{R}\ \boldsymbol{AR}\ \cdots\ \boldsymbol{A}^{n-1}\boldsymbol{R}]) \\ &= ColumnSpace[\boldsymbol{Q}]. \end{aligned} \tag{152}$$

In contrast to matrix $\boldsymbol{K}$, the matrix $\boldsymbol{Q}$ has the following advantages.

- $\boldsymbol{Q}$ is well conditioned.
- It is easy to invert since $\boldsymbol{Q}^{-1} = \boldsymbol{Q}^T$.
- Most importantly, we can compute only as many leading columns of $\boldsymbol{Q}$ as needed to get accurate solution (more details about this are covered later in this section).

The next question is, how do we get the matrix $\boldsymbol{Q}$? We can achieve this as follows. Expressing the matrix $\boldsymbol{K}$ using QR decomposition as $\boldsymbol{K} = \boldsymbol{QR_u}$ (where $\boldsymbol{Q}$ is an orthogonal matrix and $\boldsymbol{R_u}$ is an upper-triangular matrix), we can modify (150) as

$$\begin{aligned} \boldsymbol{H}_n &= \boldsymbol{K^{-1}AK} \\ &= (\boldsymbol{QR_u})^{-1}\boldsymbol{A}(\boldsymbol{QR_u}) \\ &= (\boldsymbol{R_u^{-1}Q}^T)\boldsymbol{A}(\boldsymbol{QR_u}) \end{aligned} \tag{153}$$

or

$$\boldsymbol{Q}^T\boldsymbol{AQ} = \boldsymbol{R_u H}_n\boldsymbol{R_u^{-1}} = \boldsymbol{H}. \tag{154}$$

Since $\boldsymbol{R_u}$ and $\boldsymbol{R_u^{-1}}$ are both upper triangular and $\boldsymbol{H}_n$ is upper Hessenberg, it is easy to prove that the new matrix, $\boldsymbol{H} = \boldsymbol{R_u H}_n \boldsymbol{R_u^{-1}}$, is also upper Hessenberg.

Next, let us assume that we will use only the first leading q columns ($q < n$) of $\boldsymbol{Q}$. In this case, the matrices under consideration will have the following dimensions: $\boldsymbol{Q} \in \Re^{n\times q}$, and $\boldsymbol{H} \in \Re^{q\times q}$. The implications of (154) is that we can reduce the matrix $\boldsymbol{A}$ of dimension $n \times n$ to a smaller upper Hessenberg matrix $\boldsymbol{H}$ of dimension $q \times q$ using orthogonal transformation. In addition, the eigenvalues of the smaller system $\boldsymbol{H}$ are approximations of the first q leading eigenvalues of the larger system represented by $\boldsymbol{A}$.

Next, we will show that the columns of $\boldsymbol{Q}$ can be computed one at a time giving us the advantage of computing only as many leading columns of $\boldsymbol{Q}$ as needed. One of the popular approaches used for partial reduction of a large matrix to a smaller upper Hessenberg matrix using $\boldsymbol{Q}$, is known as *Arnoldi's algorithm* [80]–[87], [160]. More details about this are given in the next section.

C. Arnoldi Algorithm for (Partial) Reduction

Assume $\boldsymbol{Q} = [\boldsymbol{q}_1\ \boldsymbol{q}_2\ \cdots\ \boldsymbol{q}_k]$, where $\boldsymbol{q}_i$ represents the ith column of matrix $\boldsymbol{Q}$. From (154), we have $\boldsymbol{AQ} = \boldsymbol{QH}$, which can be written as

$$\boldsymbol{A}\left[\left[\boldsymbol{q}_1\right]\left[\boldsymbol{q}_2\right]\left[\boldsymbol{q}_3\right]\cdots\left[\boldsymbol{q}_k\right]\right] = \left[\left[\boldsymbol{q}_1\right]\left[\boldsymbol{q}_2\right]\left[\boldsymbol{q}_3\right]\cdots\left[\boldsymbol{q}_k\right]\right] \cdot \begin{bmatrix} h_{11} & h_{12} & h_{13} & \cdots & \cdots & \cdots \\ h_{21} & h_{22} & h_{23} & \cdots & \cdots & \cdots \\ 0 & h_{32} & h_{33} & \cdots & \cdots & \cdots \\ \vdots & \vdots & \vdots & \cdots & \vdots & \vdots \\ \vdots & \vdots & \vdots & \cdots & \vdots & \vdots \end{bmatrix}. \quad (155)$$

Recall that all columns $\boldsymbol{q_i}$ of orthogonal matrices have $\|\boldsymbol{q_i}\|_2 = 1$ (which implies that $\boldsymbol{q_i^T q_i} = 1$) and are orthogonal to one another (which means that $\boldsymbol{q_i^T q}_j = 0$). Using this information, the first few steps in obtaining the $\boldsymbol{Q}$ and $\boldsymbol{H}$ matrices are outlined below.

Since the $\|\boldsymbol{q}_1\|_2 = 1$, an easy way to compute it is to divide the vector $\boldsymbol{R}$ [from (139), assuming the single-input, single-output case, $\boldsymbol{R}$ will be a vector] by its magnitude $\|\boldsymbol{R}\|_2$ (we get a unit vector in the direction of $\boldsymbol{R}$). This step is illustrated in Fig. 26(a)

$$\boldsymbol{q}_1 = \boldsymbol{R}/\|\boldsymbol{R}\|_2. \quad (156)$$

To determine $\boldsymbol{q}_2$ and the first column of $\boldsymbol{H}$, we multiply $\boldsymbol{A}$ by the first column of $\boldsymbol{Q}$. This gives us $\boldsymbol{Aq}_1$, which is the first column on LHS of (155). Equating it with the first column of RHS, we have

$$\boldsymbol{Aq}_1 = h_{11}\boldsymbol{q}_1 + h_{21}\boldsymbol{q}_2. \quad (157)$$

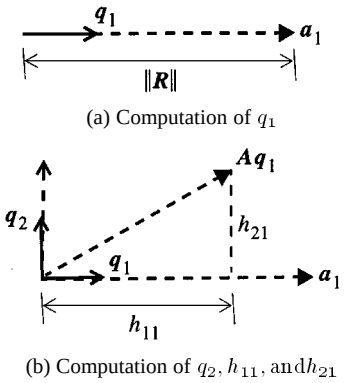

(a) Computation of q_1

(b) Computation of $q_2, h_{11}, \text{and} h_{21}$

Fig. 26. Illustration of steps in Arnoldi algorithm.

Premultiplying both sides by $\boldsymbol{q}_1^T$, we have

$$\begin{aligned} \boldsymbol{q}_1^T\boldsymbol{Aq}_1 &= h_{11}\boldsymbol{q}_1^T\boldsymbol{q}_1 + h_{21}\boldsymbol{q}_1^T\boldsymbol{q}_2 \\ \boldsymbol{q}_1^T\boldsymbol{Aq}_1 &= h_{11}. \end{aligned} \quad (158)$$

Knowing the value of h_{11} and using the fact that $\|\boldsymbol{q}_2\| = 1$, we can compute h_{21} from (157) as

$$h_{21} = \|\boldsymbol{Aq}_1 - h_{11}\boldsymbol{q}_1\|. \quad (159)$$

The direction for $\boldsymbol{q}_2$ can be obtained using (157) as [illustrated in Fig. 26(b)]

$$\boldsymbol{q}_2 = \frac{\boldsymbol{Aq}_1 - h_{11}\boldsymbol{q}_1}{h_{21}}. \quad (160)$$

Similarly, the rest of the columns of $\boldsymbol{Q}$ and $\boldsymbol{H}$ matrices can be obtained by generalizing the steps as shown in Fig. 27.

Note that we did not need to explicitly compute the product $\boldsymbol{A}^k\boldsymbol{R}$. As a result, we were able to avoid the ill-conditioning problem arising due to the quick convergence of the sequence $\lfloor \boldsymbol{R}\ \boldsymbol{AR}\ \boldsymbol{A}^2\boldsymbol{R}\ \boldsymbol{A}^3\boldsymbol{R}\ \cdots \rfloor$ to the eigenvector of the largest eigenvalue.

The columns $\boldsymbol{q}_j$ computed by Arnoldi algorithm are called Arnoldi vectors. The loop over i updating $\boldsymbol{z}$ corresponds to the *modified Gram–Schmidt algorithm* [160], which subtracts the components in the directions q_1 to q_j away from $\boldsymbol{z}$, leaving them orthogonal to $\boldsymbol{z}$. Computing a total of "k" Arnoldi vectors costs k matrix–vector multiplications involving $\boldsymbol{A}$, plus $O(k^2n)$ related cost.

There are several alternative methods available in the literature for finding the basis for Krylov-subspace [85]. For example, one can use multiple passes of orthogonalization to increase the robustness of the modified Gram–Schmidt orthogonalization process.

To recap, we started with the circuit equations $\boldsymbol{C\dot{x}}(t) + \boldsymbol{Gx}(t) = \boldsymbol{b}(t)$ and $w = \boldsymbol{L}^T\boldsymbol{x}(t)$. We formed the product $\boldsymbol{A} = \boldsymbol{G}^{-1}\boldsymbol{C}$. Using orthogonal transformation, we were able to determine the leading eigenvalues of $\boldsymbol{A}$ that correspond to the dominant poles of the transfer-function. In the following section, we will show how to use this information to perform circuit reduction.

```
/** Arnoldi algorithm for (partial) reduction to Hessenberg form) - simple implementation
Begin function_Arnoldi
    q_1 = R / ||R||_2   /* get the direction for q_1 */
    for j = 1 to k  /* k is the desired number of columns for Q & H matrices */
        z = A q_j
        for i = 1 to j
            h_ij = q_i^T z          ij
            z = z - h_ij q_i
        end for
        h_{j+1,j} = ||z|| ; if h_{j+1,j} = 0 , quit
        q_j = z / h_{j+1,j}
    end for
end function_Arnoldi
```

Fig. 27. Pseudocode for Arnoldi algorithm.

D. Circuit Reduction Using Arnoldi Algorithm

Finding the reduced-order circuit equations can be explained by a change of variables in (139) by mapping the vector $\boldsymbol{x}$ of dimension n into a smaller vector $\hat{\boldsymbol{x}}$ of dimension q ($q \ll n$) using the orthogonal matrix $\boldsymbol{Q}$ [80]–[92]

$$\boldsymbol{x} = \boldsymbol{Q}\hat{\boldsymbol{x}}. \tag{161}$$

Using (161), we can rewrite Laplace-domain circuit equations in (140) as

$$\begin{aligned} s\boldsymbol{A}\boldsymbol{Q}\hat{\boldsymbol{X}}(s) &= \boldsymbol{Q}\hat{\boldsymbol{X}}(s) - \boldsymbol{R}U(s) \\ W(s) &= \boldsymbol{L}^T\boldsymbol{Q}\hat{\boldsymbol{X}}(s). \end{aligned} \tag{162}$$

Premultiplying both sides of (162) by $\boldsymbol{Q}^T$ and using the relation $\boldsymbol{Q}^T\boldsymbol{Q} = \boldsymbol{I}$, we have

$$\begin{aligned} & s\boldsymbol{Q}^T\boldsymbol{A}\boldsymbol{Q}\hat{\boldsymbol{X}}(s) = \hat{\boldsymbol{X}}(s) - \boldsymbol{Q}^T\boldsymbol{R}U(s) \\ & \quad \Rightarrow \quad \hat{\boldsymbol{X}}(s) = (\boldsymbol{I} - s\boldsymbol{Q}^T\boldsymbol{A}\boldsymbol{Q})^{-1}\boldsymbol{Q}^T\boldsymbol{R}U(s) \\ & W(s) = \boldsymbol{L}^T\boldsymbol{Q}\hat{\boldsymbol{X}}(s) \\ & \quad \Rightarrow \quad W(s) = \boldsymbol{L}^T\boldsymbol{Q}(\boldsymbol{I} - s\boldsymbol{Q}^T\boldsymbol{A}\boldsymbol{Q})^{-1}\boldsymbol{Q}^T\boldsymbol{R}U(s). \end{aligned} \tag{163}$$

Hence, the transfer-function of the reduced system can be written as

$$\begin{aligned} \hat{Y}(s) = \frac{W(s)}{U(s)} &= \boldsymbol{L}^T\boldsymbol{Q}(\boldsymbol{I} - s\boldsymbol{Q}^T\boldsymbol{A}\boldsymbol{Q})^{-1}\boldsymbol{Q}^T\boldsymbol{R} \\ \hat{Y}(s) &= \boldsymbol{L}^T\boldsymbol{Q}(\boldsymbol{I} - s\boldsymbol{H})^{-1}\boldsymbol{Q}^T\boldsymbol{R}. \end{aligned} \tag{164}$$

Comparing the original transfer-function $Y(s)$ represented by (142) with the transfer-function $\hat{Y}(s)$ of the reduced system represented by (164), we can draw the following conclusions. The eigenvalues of $\hat{Y}(s)$ are given by the eigenvalues of $\boldsymbol{H}$. However, since the eigenvalues of $\boldsymbol{H}$ are good approximation of the leading eigenvalues of $\boldsymbol{A}$, we can conclude that the eigenvalues of the transfer function of the reduced system are good approximation of the poles of the original transfer function.

An important criterion during the above reduction is the accuracy of the response of the reduced system given by (164). The frequency response of the reduced system (164) is also a good approximation of the frequency-response of the original transfer function (142). An indicator for the accuracy of the response of the reduced system is the total number of moments it can preserve (match), for a given order of reduction (q). It can be proved that the reduced system (164) of order q preserves the first q moments of the original network [84].

In essence, we are able to implicitly match the moments and obtain a reduced-model without the need to directly use the moments as in the AWE algorithm. Hence, we will not suffer from the same numerical ill-conditioning that is associated with direct moment-matching algorithms. The accuracy of the Arnoldi approximation gradually increases as the order q is increased since more moments of the original transfer function will be matched.

A question that may possibly arise here: how are the accuracies of Arnoldi-based approximation and direct Padé-based approximation are compared? It was shown in Section VII that a Padé approximation of order q matches the first $2q$ moments. However, an Arnoldi-based reduction of order q matches only first q moments [84]. Essentially, this means that, for a comparable accuracy, the reduced-model from Arnoldi will have double the size of the reduced model from direct Padé-based approximation (in other words, direct Padé-based models are more optimal). On the other hand, due to the ill-conditioning, direct Padé-based approximation cannot achieve higher order approximation, whereas Arnoldi-based approximation can.

In an alternative approach, the reduction based on Lanczos algorithm can preserve the first $2q$ moments [77]–[79] (like direct Padé-based approximation). The difference between Arnoldi and Lanczos algorithms is that in Lanczos algorithm we transform the matrix $\boldsymbol{A}$ to a tridiagonal matrix $\boldsymbol{T}_q$. In addition, Lanczos algorithm uses two biorthogonal Krylov space, to recursively compute $\boldsymbol{T}_q$ [77]. However, the macromodels

using the above Lanczos-based reduction scheme does not guarantee the passivity of the macromodel.

E. Multiport Reduction using Arnoldi Algorithm

Consider an N-port characterization of a system based on the admittance parameters. The multiport circuit equations for this can be written as [80], [84]

$$\begin{aligned} \boldsymbol{C}\dot{\boldsymbol{x}}(t)+\boldsymbol{G}\boldsymbol{x}(t)&=\boldsymbol{B}\boldsymbol{u}(t), \quad \boldsymbol{C},\boldsymbol{G}\in\Re^{n\times n}, \quad \boldsymbol{B}\in\Re^{n\times N} \\ & \qquad \boldsymbol{x}\in\Re^{n\times 1} \\ \boldsymbol{w}&=\boldsymbol{L}^T\boldsymbol{x}(t), \quad \boldsymbol{L}\in\Re^{n\times N}, \quad \boldsymbol{u},\boldsymbol{w}\in\Re^{N\times 1} \end{aligned} \tag{165}$$

where the input $\boldsymbol{u} = [v_1 \cdots v_N]^T$ and the output $\boldsymbol{w} = [i_1 \cdots i_N]^T$ are vectors of port voltages and currents, respectively, instead of scalars. In this case, $\boldsymbol{R} \in \Re^{n\times N} = \boldsymbol{G}^{-1}\boldsymbol{B} = [\boldsymbol{r}_1\, \boldsymbol{r}_2 \cdots \boldsymbol{r}_N]$ becomes a matrix, instead of a vector. $\boldsymbol{r}_j$ represents the jth column of $\boldsymbol{R}$ (an example of multiport formulation is given in Section VIII-F).

In the case of multiport characterization, *block moments* are used, instead of moments of a particular output. Block moments are defined as

$$\begin{aligned} \boldsymbol{Y}(s)&=\boldsymbol{M}_0+\boldsymbol{M}_1 s+\boldsymbol{M}_2 s^2+\cdots \\ \boldsymbol{M}_i&\in\Re^{N\times N}=\boldsymbol{L}^T\boldsymbol{A}^i\boldsymbol{R} \end{aligned} \tag{166}$$

where an entry in the jth row and kth column of $\boldsymbol{M}_i$ represents the ith moment of the current (output) that flows into port j due to a voltage source (only nonzero source) at port k.

Block Krylov-subspace spanning q columns can be constructed using the block moments (166) as

$$\begin{aligned} &K(\boldsymbol{A},\boldsymbol{R},q) \\ &\quad = ColumnSpace[\boldsymbol{R}\ \boldsymbol{A}\boldsymbol{R}\ \boldsymbol{A}^2\boldsymbol{R}\ \cdots\ \boldsymbol{A}^{k-1}\boldsymbol{R}\ \boldsymbol{A}^k\tilde{\boldsymbol{R}}] \\ &\quad = ColumnSpace[\boldsymbol{Q}] \\ &\quad \tilde{\boldsymbol{R}} = [\boldsymbol{r}_1\ \boldsymbol{r}2\ \cdots\ \boldsymbol{r}_l], \quad k=\lfloor q/N\rfloor 20, \quad l=q-kN \end{aligned} \tag{167}$$

where the operator $\lfloor\cdot\rfloor$ represents the truncation to the nearest integer, toward zero.

For example, assume a three-port characterization involving $\boldsymbol{A}\in\Re^{50\times 50}$, and let $q=14$. In this case, we have $k=\lfloor 14/3\rfloor = 4$; $l = 14-4\times 3 = 2$ and (167) can be written as

$$\begin{aligned} &K(\boldsymbol{A},\boldsymbol{R},q) \\ &\quad = ColumnSpace[\boldsymbol{R}\ \boldsymbol{A}\boldsymbol{R}\ \boldsymbol{A}^2\boldsymbol{R}\ \boldsymbol{A}^3\boldsymbol{R}\ \boldsymbol{A}^4\boldsymbol{r}_1\ \boldsymbol{A}^4\boldsymbol{r}_2]. \end{aligned}$$

Using the block Arnoldi algorithm [80], matrix $\boldsymbol{A}$ can be reduced to a small *block upper Hessenberg matrix*, $\boldsymbol{H}\in q\times q$. The multiport admittance matrix of the reduced-system is given by

$$\begin{bmatrix} i_1 \\ \vdots \\ i_N \end{bmatrix} = \boldsymbol{L}^T\boldsymbol{Q}(\boldsymbol{I}-s\boldsymbol{H})^{-1}\boldsymbol{Q}^T\boldsymbol{R}\begin{bmatrix} v_1 \\ \vdots \\ v_N \end{bmatrix} \tag{168}$$

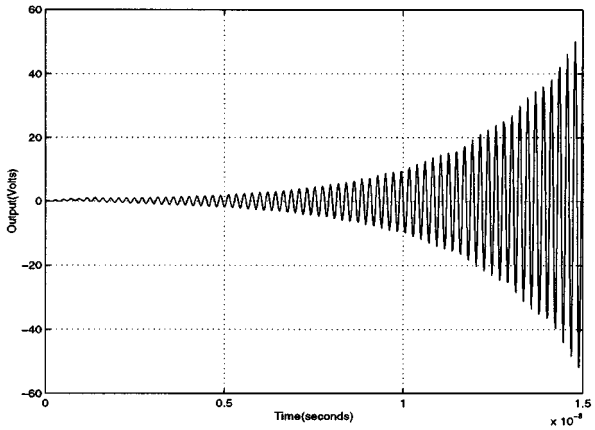

Fig. 28. Transient response of a nonpassive macromodel with passive terminations.

where $\hat{\boldsymbol{Y}} = \boldsymbol{L}^T\boldsymbol{Q}(\boldsymbol{I}-s\boldsymbol{H})^{-1}\boldsymbol{Q}^T\boldsymbol{R}$. In this case, it can be proved that the reduced system (168) of order q preserves the first $\lfloor q/N\rfloor$ block moments of the original network [84]. This implies that for a desired predefined accuracy, the order of the reduced system should be increased with the increase in the number of ports.

In the next section, the review of an important property of macromodels, passivity, and extension of Krylov-subspace techniques for passivity preservation are provided.

F. Passivity Preservation

Passivity implies that a network cannot generate more energy than it absorbs, and no passive termination of the network will make the system unstable. Passivity is an important property, because stable but not passive macromodels can lead to unstable systems when connected to other passive systems. The loss of passivity can be a serious problem because transient simulations of nonpassive networks may encounter artificial oscillations. This is illustrated in Fig. 28, which represents the transient response of a reduced-order macromodel of a large linear RLC circuit, when connected to an external load of 50 kΩ. In this section, we will review important algorithms that are available in the literature, for preservation of passivity during the reduction of interconnect networks [83]–[92].

1) Review of Passivity Properties: A passive network cannot generate power on its own. It is essential that the reduced-order model must be passive. A network with admittance matrix represented by $\boldsymbol{Y}(s)$ is passive iff [83], [84], [154]–[157]:

a) $\boldsymbol{Y}(s^*) = \boldsymbol{Y}^*(s)$ where "$*$" is the complex conjugate operator;

b) $\boldsymbol{Y}(s)$ is a positive real (PR) matrix, that is the product $\boldsymbol{z}^{*t}[\boldsymbol{Y}^t(s^*)+\boldsymbol{Y}(s)]\boldsymbol{z}\geq 0$ for all complex values of s with $\mathrm{Re}(s)>0$ and any arbitrary vector $\boldsymbol{z}$.

2) Passive Reduction: The algorithm discussed here is based on the PRIMA technique [84]. Recall from Section VIII-D, where circuit reduction was achieved by applying Arnoldi on the set of equations represented by (162) (we refer this approach as classical Arnoldi). However, this approach does not preserve the passivity of the reduced

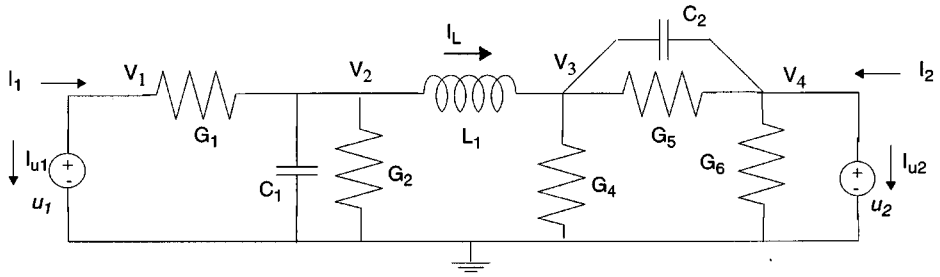

Fig. 29. Example circuit for MNA formulation compatible with passive reduction algorithms.

system. Instead, if the Arnoldi is applied on the original set of circuit equations represented by (165), reducing the $\boldsymbol{C}$ and $\boldsymbol{G}$ directly, passivity can be preserved (with certain conditions, which is discussed later in this section). A brief description of this process is given below.

Using (161), we can rewrite (165) in the Laplace-domain as

$$\begin{aligned} s\boldsymbol{CQ}\hat{\boldsymbol{X}}(s) + \boldsymbol{GQ}\hat{\boldsymbol{X}}(s) &= \boldsymbol{BU}(s) \\ \boldsymbol{W}(s) &= \boldsymbol{L}^T\boldsymbol{Q}\hat{\boldsymbol{X}}(s). \end{aligned} \tag{169}$$

Premultiplying both sides MNA equations of (169) by $\boldsymbol{Q}^t$, we have

$$\begin{aligned} s\boldsymbol{Q}^T\boldsymbol{CQ}\hat{\boldsymbol{X}}(s) + \boldsymbol{Q}^T\boldsymbol{GQ}\hat{\boldsymbol{X}}(s) &= \boldsymbol{Q}^T\boldsymbol{BU}(s) \\ \hat{\boldsymbol{X}}(s) &= (\hat{\boldsymbol{G}} + s\hat{\boldsymbol{C}})^{-1}\hat{\boldsymbol{B}}\boldsymbol{U}(s) \\ \boldsymbol{W}(s) &= \hat{\boldsymbol{L}}^T(\hat{\boldsymbol{X}}(s)) \end{aligned} \tag{170}$$

where

$$\begin{aligned} \hat{\boldsymbol{C}} &= \boldsymbol{Q}^T\boldsymbol{CQ}, \qquad \hat{\boldsymbol{G}} = \boldsymbol{Q}^T\boldsymbol{GQ} \\ \hat{\boldsymbol{B}} &= \boldsymbol{Q}^T\boldsymbol{B}, \qquad \hat{\boldsymbol{L}} = \boldsymbol{Q}^T\boldsymbol{L}. \end{aligned} \tag{171}$$

The above type of transformations are known as congruence transformations. Using (170) and (171), the output equation in (169) can be rewritten as

$$\boldsymbol{W}(s) = [\hat{\boldsymbol{L}}^T(\hat{\boldsymbol{G}} + s\hat{\boldsymbol{C}})^{-1}\hat{\boldsymbol{B}}]\boldsymbol{U}(s). \tag{172}$$

From (172), it can be easily noted that the admittance matrix of the reduced system is given by

$$\hat{\boldsymbol{Y}}(\boldsymbol{s}) = [\hat{\boldsymbol{L}}^T(\hat{\boldsymbol{G}} + s\hat{\boldsymbol{C}})^{-1}\hat{\boldsymbol{B}}]. \tag{173}$$

It can be proved that the reduced model, given by (173) is passive [84]. In addition, like the block Arnoldi algorithm also preserves the first $\lfloor q/N \rfloor$ block moments of the original network). One of the conditions required to prove the passivity of the reduced model is that the original $\boldsymbol{C}$ matrix must be a symmetric and nonnegative definite matrix. This condition can be satisfied with a slight change during the MNA formulation step, as follows.

3) MNA Formulation Compatible with Passive Reduction Algorithms: Consider the lumped circuit equations (162). The matrices $\boldsymbol{C}, \boldsymbol{G} \in \Re^{n\times n}$ can be formulated, such that

$$\begin{aligned} \boldsymbol{C} &= \begin{bmatrix} \boldsymbol{C_a} & 0 \\ 0 & \boldsymbol{C_b} \end{bmatrix}, \qquad \boldsymbol{G} = \begin{bmatrix} \boldsymbol{F} & \boldsymbol{E} \\ -\boldsymbol{E}^T & 0 \end{bmatrix} \\ \boldsymbol{x} &= \begin{bmatrix} \boldsymbol{v} \\ \boldsymbol{i} \end{bmatrix} \end{aligned} \tag{174}$$

where $\boldsymbol{v}$, $\boldsymbol{i}$ represent the MNA variables, $\boldsymbol{G}$, $\boldsymbol{C}$ represent the conductance and susceptance matrices, with an important note that the rows corresponding to current variables are negated (such that the diagonal entries of $\boldsymbol{C}$ matrix contributed by inductor elements remain positive). $\boldsymbol{C_a}$, $\boldsymbol{C_b}$, $\boldsymbol{F}$ are the matrices containing the stamps of resistors, capacitors and inductors, respectively. Matrix $\boldsymbol{E} \in (1, -1, 0)$ corresponds to the current variables in a KCL formulation. Provided that the original network is composed of passive elements only, $\boldsymbol{C_a}$, $\boldsymbol{C_b}$, $\boldsymbol{F}$ lead to symmetric nonnegative definite matrices. With this MNA formulation, it can be proved that the resulting $\boldsymbol{C}$ is also symmetric nonnegative definite [84]. An illustration of the above formulation is given at the bottom of the next page in (175) for the circuit in Fig. 29.

IX. Related Topics and Further Reading

In addition to the interconnection simulation algorithms discussed in the previous sections, there are several related topics that may be of interest to the readers of this paper.

Full-Wave Models: At further subnanosecond rise times, the line cross section dimensions become a significant fraction of the wavelength and field components in the direction of propagation can no longer be neglected. Consequently, full-wave models that take into account all possible field components and satisfy all boundary conditions are required to accurately estimate high-frequency effects. However, circuit simulation of full-wave models is highly involved. The information that is obtained through a full-wave analysis is in terms of electromagnetic field parameters such as propagation constant, characteristic impedance, etc. However, a circuit simulator requires the information in terms of currents, voltages, and circuit impedances. This demands a generalized method to combine modal results into circuit simulators in terms of a full-wave stamps. References [26]–[29], [56], [74] provide solution techniques and moment generation schemes for such cases.

Measured Data: In practice, it may not be possible to obtain accurate analytical models for interconnects because of the geometric inhomogeneity and associated discontinuities. To handle such situations, modeling techniques based on measured data have been proposed in the literature [102]–[113]. In general, the behavior of high-speed interconnects can easily be represented by measured frequency-dependent scattering parameters or time-domain terminal measurements. However, handling measured data in circuit simulation is a tedious and a computationally expensive process. References [102]–[113] address such cases.

EMI Subnetworks: Electrically long interconnects function as spurious antennas to pick up emissions from other nearby electronic systems. This makes susceptibility to emissions a major concern to current system designers of high-frequency product. Hence, the availability of interconnect simulation tools including the effect of incident fields is becoming an important design requirement. References [119]–[139] provide analysis techniques for interconnects subjected to external EM interferences and also for radiation analysis of interconnects.

Sensitivity Analysis: Sensitivity analysis involving large interconnect subnetworks can be highly CPU intensive. Model-reduction-based approaches provide an efficient means for this purpose [114]–[118].

Minimum Realization of Reduced-Order Models: It is evident from the discussions in Sections VII and VIII that the size of the reduced-order model increases with the increase in the number of ports. In such cases, it may become essential to realize the macromodels with a minimum possible number of states, so as to achieve fast transient simulations [93]. Also, it is observed that Krylov-subspace-based reduced models require high order to capture high-frequency effects such as skin effect. This can make the transient simulation expensive as the reduced model becomes expensive to evaluate and post-processing of macromodels to further reduce the order may become necessary [94], [95].

ACKNOWLEDGMENT

The authors wish to thank and acknowledge the help and contributions provided by the current and past graduate students of the Computer-Aided Engineering Group at Carleton University. Relevant information regarding this Proceedings paper can be accessed at http://www.doe.carleton.ca/~achar/ieee.html.

REFERENCES

[1] H. B. Bakoglu, *Circuits, Interconnections and Packaging for VLSI.* Reading, MA: Addison-Wesley, 1990.

[2] H. W. Jhonson and M. Grahaml, *High-Speed Digital Design*. Englewood Cliffs, NJ: Prentice-Hall, 1993.

[3] M. Nakhla and R. Achar, *High-Speed Circuit and Interconnect Analysis*. Multimedia Learning Course, OT: Omniz Global Knowledge Corporation (www.omniz.com), 2001.

[4] R. K. Poon, *Computer Circuits Electrical Design*. Englewood Cliffs, NJ: Prentice-Hall, 1995.

[5] W. W. M. Dai, Guest Editor, "Special issue on simulation, modeling, and electrical design of high-speed and high-density interconnects," *IEEE Trans. Circuits Syst.*, vol. 39, pp. 857–982, Nov. 1992.

[6] M. Nakhla and A. Ushida, Guest Editors, "Special issue on modeling and simulation of high-speed interconnects," *IEEE Trans. Circuits Syst.*, vol. 47, pp. 239–305, Apr. 2000.

[7] M. Nakhla and R. Achar, "Interconnect modeling and simulation," in *The VLSI Handbook*. Boca Raton, FL: CRC Press, 2000, ch. XVII, pp. 17.1–17.29.

[8] E. Chiprout and M. Nakhla, *Asymptotic Waveform Evaluation and Moment Matching for Interconnect Analysis.* Boston, MA: Kluwer, 1993.

[9] A. Deustsch, "Electrical characteristics of interconnections for high-performance systems," *Proc. IEEE*, vol. 86, pp. 315–355, Feb. 1998.

$$\underbrace{\left[\begin{array}{cccc|ccc} 0 & 0 & 0 & 0 & & & \\ 0 & C_1 & 0 & 0 & & & \\ 0 & 0 & C_2 & -C_2 & & \mathbf{0} & \\ 0 & 0 & -C_2 & C_2 & & & \\ \hline & & & & L_1 & 0 & 0 \\ & \mathbf{0} & & & 0 & 0 & 0 \\ & & & & 0 & 0 & 0 \end{array}\right]}_{\boldsymbol{C}} \begin{bmatrix} \dot{v}_1 \\ \dot{v}_2 \\ \dot{v}_3 \\ \dot{v}_4 \\ \dot{i}_L \\ \dot{i}_{u1} \\ \dot{i}_{u2} \end{bmatrix} + \underbrace{\left[\begin{array}{cccc|ccc} G_1 & -G_1 & 0 & 0 & 0 & 1 & 0 \\ -G_1 & G_1+G_2 & 0 & 0 & 1 & 0 & 0 \\ 0 & 0 & G_4+G_5 & -G_5 & -1 & 0 & 0 \\ 1 & 0 & -G_5 & G_5+G_6 & 0 & 0 & 1 \\ \hline 0 & -1 & 1 & 0 & & \mathbf{0} & \\ -1 & 0 & 0 & 0 & & & \\ 0 & 0 & 0 & -1 & & & \end{array}\right]}_{\boldsymbol{G}} \underbrace{\begin{bmatrix} v_1 \\ v_2 \\ v_3 \\ v_4 \\ i_L \\ i_{u1} \\ i_{u2} \end{bmatrix}}_{\boldsymbol{x}}$$

$$= \underbrace{\begin{bmatrix} 0 & 0 \\ 0 & 0 \\ 0 & 0 \\ 0 & 0 \\ 0 & 0 \\ -1 & 0 \\ 0 & -1 \end{bmatrix}}_{\boldsymbol{B}} \underbrace{\begin{bmatrix} u_1 \\ u_2 \end{bmatrix}}_{\text{Port Voltages}}$$

$$\text{Port Currents} \nearrow \begin{bmatrix} i_1 \\ i_2 \end{bmatrix} = \underbrace{\begin{bmatrix} 0 & 0 & 0 & 0 & 0 & -1 & 0 \\ 0 & 0 & 0 & 0 & 0 & 0 & -1 \end{bmatrix}}_{\boldsymbol{L}^T} \boldsymbol{x} \tag{175}$$

[10] R. Goyal, "Managing signal integrity," *IEEE Spectr.*, pp. 54–62, Mar. 1994.
[11] J. B. Faria, *Multiconductor Transmission Line Structures*. New York: Wiley, 1993.
[12] C. Paul, *Analysis of Multiconductor Transmission Lines*. New York: Wiley, 1994.
[13] ——, *Introduction to Electromagnetic Compatibility*. New York: Wiley, 1992.
[14] K. C. Gupta and R. Grag, *Microstrip Lines and Slotlines*. Boston, MA: Artech House, 1996.
[15] A. E. Ruehli, "Equivalent circuit models for three dimensional multiconductor systems," *IEEE Trans. Microwave Theory Tech.*, vol. 22, pp. 216–224, Mar. 1974.
[16] ——, "Inductance calculations in a complex integrated circuit environment," *IBM J. Res. Develop.*, pp. 470–481, Sept. 1972.
[17] P. K. Wolff and A. E. Ruehli, "Inductance computations for complex three dimensional geometries," *IEEE Trans. Circuits Syst.*, pp. 16–19, 1981.
[18] A. E. Ruehli and P. A. Brennan, "Efficient capacitance calculations for three dimensional multiconductor systems," *IEEE Trans. Microwave Theory Tech.*, pp. 76–82, Feb. 1973.
[19] A. E. Ruehli, "Survey of computer-aided analysis of integrated circuit interconnections," *IBM J. Res. Develop.*, pp. 626–639, Nov. 1979.
[20] A. E. Ruehli and H. Heeb, "Circuit models for three dimensional geometries including dielectrics," *IEEE Trans. Microwave Theory Tech.*, pp. 1507–1516, Mar. 1992.
[21] D. D. Ling and A. E. Ruehli, "Interconnection modeling," in *Advances in CAD for VLSI, 3—Part II, Circuit Analysis, Simulation and Design*. Amsterdam: Noth-Holland, 1987, pp. 211–291.
[22] J. Cullum, A. Ruehli, and T. Zhang, "A method of reduced-order modeling and simulation of large interconnect circuits and its application to PEEC models with retardation," *IEEE Trans. Circuits Syst.*, pp. 261–273, Apr. 2000.
[23] T. L. Quarles, "The SPICE3 implementation guide," Univ. California, Berkeley, Tech. Rep., ERL-M89/44, 1989.
[24] D. Gao, A. Yang, and S. Kang, "Modeling and simulation of interconnection delays and cross talks in high-speed integrated circuits," *IEEE Trans. Circuits Syst.*, pp. 1–9, Jan. 1990.
[25] H. Hasegawa and S. Seki, "Analysis of interconnection delay on very high-speed LSI/VLSI chips using a microstrip line model," *IEEE Trans. Electron Devices*, pp. 1954–1960, Dec. 1984.
[26] T. Itoh and R. Mittra, "Spectral domain approach for calculating the dispersion characteristics of microstrip lines," *IEEE Trans. Microwave Theory Tech.*, pp. 496–499, Feb. 1973.
[27] D. Mirshekar-Syahkal, *Spectral Domain Method for Microwave Integrated Circuits*: Joinery, 1990.
[28] R. H. Jansen, "Spectral domain approach for microwave integrated circuits," *IEEE Trans. Microwave Theory Tech.*, vol. MTT-33, pp. 1043–1056, Feb. 1985.
[29] R. Wang and O. Wing, "A circuit model of a system of VLSI interconnects for time response computation," *IEEE Trans. Microwave Theory Tech.*, vol. 39, pp. 688–693, April 1991.
[30] A. R. Djordjević and T. K. Sarkar, "Closed-form formulas for frequency-dependent resistance and inductance per unit length of microstrip and strip transmission lines," *IEEE Trans. Microwave Theory Tech.*, vol. 42, pp. 241–248, Feb. 1994.
[31] A. R. Djordjević, R. F. Harrington, T. K. Sarkar, and M. Bazdar, *Matrix Parameters for Multiconductor Transmission Lines: Software and Users Manual*. Boston, MA: Reteach House, 1989.
[32] A. Deutch *et al.*, "Modeling and characterization of long on-chip interconnections for high performance microprocessors," *IBM J. Res. Develop.*, vol. 39, pp. 547–567, Sept. 1995.
[33] A. Deutch *et al.*, "High-speed signal propagation on lossy transmission lines," *IBM J. Res. Develop.*, vol. 39, pp. 601–615, July 1990.
[34] A. Deutch *et al.*, "When are transmission-line effects important for on-chip interconnections," *IEEE Trans. Microwave Theory Tech.*, Oct. 1997.
[35] J. Poltz, "Optimizing VLSI interconnect model for SPICE simulation," *J. Analog Integr. Circuits Signal Process.*, vol. 5, Jan. 1994.
[36] T. Dhane and D. D. Zutter, "Selection of lumped element models for coupled lossy transmission lines," *IEEE Trans. Computer-Aided Design*, vol. 11, pp. 959–967, July 1992.
[37] M. Celik, A. C. Cangellaris, and A. Yaghmour, "An all purpose transmission line model for interconnect simulation in SPICE," *IEEE Trans. Microwave Theory Tech.*, pp. 127–138, Oct. 1997.
[38] C. Moler and C. Van Loan, "Nineteen dubious ways to compute the exponential of a matrix," *SIAM Rev.*, pp. 801–836, Oct. 1978.
[39] A. Dounavis, X. Li, M. Nakhla, and R. Achar, "Passive closed-loop transmission line model for general purpose circuit simulators," *IEEE Trans. Microwave Theory Tech.*, vol. 47, pp. 2450–2459, Dec. 1999.
[40] A. Dounavis, R. Achar, and M. Nakhla, "Efficient passive circuit models for distributed networks with frequency-dependent parameters," *IEEE Trans. Adv. Packag.*, vol. 23, pp. 382–392, Aug. 2000.
[41] F. H. Branin Jr., "Transient analysis of lossless transmission lines," *Proc. IEEE*, vol. 55, pp. 2012–2013, 1967.
[42] M. Cases and D. M. Quinn, "Transient response of uniform distributed RLC transmission lines," *IEEE Trans. Circuits Syst.*, vol. 27, pp. 200–980, 1980.
[43] F. Y. Chang, "Transient analysis of lossless coupled transmission lines in a nonhomogeneous medium," *IEEE Trans. Microwave Theory Tech.*, vol. MTT–18, pp. 616–626, Sept. 1970.
[44] ——, "The generalized method of characteristics for waveform relaxation analysis of lossy coupled transmission lines," *IEEE Trans. Microwave Theory Tech.*, vol. 37, pp. 2028–2038, Dec. 1989.
[45] ——, "Waveform relaxation analysis of nonuniform lossy transmission lines characterized with frequency-dependent parameters," *IEEE Trans. Circuits Syst.*, vol. 38, pp. 1484–1500, Dec. 1991.
[46] Q. Chu, Y. Lau, and F. Y. Chang, "Transient analysis of microwave active circuits based on time-domain characteristic models," *IEEE Trans. Microwave Theory Tech.*, pp. 1097–1104, Aug. 1998.
[47] A. R. Djordjević, T. K. Sarkar, and R. F. Harrington, "Analysis of lossy transmission lines with arbitrary nonlinear terminal networks," *IEEE Trans. Microwave Theory Tech.*, vol. 34, pp. 660–666, June 1986.
[48] ——, "Time-domain response of multiconductor transmission lines," *Proc. IEEE*, vol. 75, pp. 743–764, June 1987.
[49] H. Grabinski, "An algorithm for computing the signal propagation on lossy VLSI interconnect systems in the time-domain," *Integr. VLSI J.*, pp. 35–48, Oct. 1989.
[50] M. Nakhla, "Analysis of pulse propagation on high-speed VLSI chips," *IEEE J. Solid-State Circuits*, vol. 25, pp. 490–494, Apr. 1990.
[51] R. Griffith and M. Nakhla, "Time-domain analysis of lossy multiconductor transmission lines," *IEEE Trans. Microwave Theory Tech.*, vol. 38, Oct. 1990.
[52] ——, "Mixed frequency/time domain analysis on nonlinear circuits," *IEEE Trans. Computer-Aided Design*, vol. 10, pp. 1032–1043, Aug. 1992.
[53] E. C. Chang and S. M. Kang, "Computationally efficient simulation of a lossy transmission line with skin effect by using numerical inversion of Laplace transform," *IEEE Trans. Circuits Syst.*, vol. 39, pp. 861–868, July 1992.
[54] D. Kuznetsov and J. E. Schutt-Aine, "Optimal transient simulation of transmission lines," *IEEE Trans. Circuits Syst.*, vol. 43, pp. 110–121, Feb. 1996.
[55] W. T. Beyene and J. E. Schutt-Aine, "Accurate frequency-domain modeling and efficient simulation of high-speed packaging interconnects," *IEEE Trans. Microwave Theory Tech.*, pp. 1941–1947, Oct. 1997.
[56] R. Wang and O. Wing, "Transient analysis of dispersive VLSI interconnects terminated in nonlinear loads," *IEEE Trans. Computer-Aided Design*, vol. 11, pp. 1258–1277, Oct. 1992.
[57] W. C. Elmore, "The transient response of damped linear networks with particular regard to wide-band amplifiers," *J. Appl. Phys.*, pp. 55–63, Jan. 1948.
[58] J. Rubinstein, P. Penfield, and M. Horowitz, "Signal delay in RC trees," *IEEE Trans. Computer-Aided Design*, pp. 202–211, July 1983.
[59] L. T. Pillage and R. A. Rohrer, "Asymptotic waveform evaluation for timing analysis," *IEEE Trans. Computer-Aided Design*, vol. 9, pp. 352–366, Apr. 1990.
[60] G. A. Baker Jr., *Essential of Padé Approximants*. New York: Academic, 1975.
[61] J. H. McCabe, "A formal extension of the Padé table to include two point Padé quotients," *J. Inst. Math. Applicat.*, vol. 15, pp. 363–372, 1975.
[62] S. Kumashiro, R. A. Rohrer, and A. J. Strojwas, "Asymptotic waveform evaluation for transient analysis of 3-D interconnect structures," *IEEE Trans. Computer-Aided Design*, vol. 12, no. 7, pp. 988–996, 1993.

[63] T. Tang and M. Nakhla, "Analysis of high-speed VLSI interconnect using asymptotic waveform evaluation technique," *IEEE Trans. Computer-Aided Design*, pp. 2107–2116, Mar. 1992.
[64] D. Xie and M. Nakhla, "Delay and crosstalk simulation of high speed VLSI interconnects with nonlinear terminations," *IEEE Trans. Computer-Aided Design*, pp. 1798–1811, Nov. 1993.
[65] S. Lin and E. S. Kuh, "Transient simulation of lossy interconnects based on the recursive convolution formulation," *IEEE Trans. Circuits Syst.*, vol. 39, pp. 879–892, Nov. 1992.
[66] S. Y. Kim, N. Gopal, and L. T. Pillage, "Time-domain macromodels for VLSI interconnect analysis," *IEEE Trans. Computer-Aided Design*, vol. 13, pp. 1257–1270, Oct. 1994.
[67] Q. Yu and E. S. Kuh, "Exact moment-matching model of transmission lines and application to interconnect delay estimation," *IEEE Trans. VLSI Syst.*, pp. 311–322, Jun. 1995.
[68] V. Raghavan, J. E. Bracken, and R. A. Rohrer, "AWESpice: A general tool for accurate and efficient simulation of interconnect problems," in *Proc. ACM/IEEE Design Automation Conf.*, June 1992, pp. 87–92.
[69] J. E. Bracken, V. Raghavan, and R. A. Rohrer, "Interconnect simulation with asymptotic waveform evaluation (AWE)," *IEEE Trans. Circuits Syst.*, pp. 869–878, Nov. 1992.
[70] R. Griffith, E. Chiprout, Q. J. Zhang, and M. Nakhla, "A CAD framework for simulation and optimization of high-speed VLSI interconnections," *IEEE Trans. Circuits Syst.*, vol. 39, pp. 893–906, Nov. 1992.
[71] T. Tang, M. Nakhla, and R. Griffith, "Analysis of lossy multiconductor transmission lines using the asymptotic waveform evaluation technique," *IEEE Trans. Microwave Theory Tech.*, vol. 39, Dec. 1991.
[72] E. Chiprout and M. Nakhla, "Analysis of interconnect networks using complex frequency hopping," *IEEE Trans. Computer-Aided Design*, vol. 14, pp. 186–199, Feb. 1995.
[73] R. Sanaie, E. Chiprout, M. Nakhla, and Q. J. Zhang, "A fast method for frequency and time domain simulation of high-speed VLSI interconnects," *IEEE Trans. Microwave Theory Tech.*, vol. 42, pp. 2562–2571, Dec. 1994.
[74] R. Achar, M. Nakhla, and Q. J. Zhang, "Full-wave analysis of high-speed interconnects using complex frequency hopping," *IEEE Trans. Computer-Aided Design*, pp. 997–1016, Oct. 1998.
[75] M. A. Kolbehdari, M. Srinivasan, M. Nakhla, Q. J. Zhang, and R. Achar, "Simultaneous time and frequency domain solution of EM problems using finite element and CFH techniques," *IEEE Trans. Microwave Theory Tech.*, vol. 44, pp. 1526–1534, Sept. 1996.
[76] R. Achar, M. Nakhla, P. Gunupudi, and E. Chiprout, "Passive interconnect reduction algorithm for distributed/measured networks," *IEEE Trans. Circuits Syst. II*, pp. 287–301, Apr. 2000.
[77] P. Feldmann and R. W. Freund, "Efficient linear circuit analysis by Padé via Lanczos process," *IEEE Trans. Computer-Aided Design*, vol. 14, pp. 639–649, May 1995.
[78] R. W. Freund, "Reduced-order modeling techniques based on Krylov subspace and their use in circuit simulation," in *Tech. Memo.*: Lucent Technologies, 1998.
[79] P. Feldmann and R. W. Freund, "Reduced order modeling of large linear subcircuits via a block Lanczos algorithm," in *Proc. Design Automation Conf.*, June 1995, pp. 474–479.
[80] I. M. Elfadel and D. D. Ling, "A block rational Arnoldi algorithm for multiport passive model-order reduction of multiport RLC networks," in *Proc. ICCAD-97*, Nov. 1997, pp. 66–71.
[81] L. M. Silviera, M. Kamen, I. Elfadel, and J. White, "A coordinate transformed Arnoldi algorithm for generating guaranteed stable reduced-order models for RLC circuits," in *Tech. Dig. ICCAD*, Nov. 1996, pp. 2288–2294.
[82] L. M. Silviera, M. Kamen, and J. White, "Efficient reduced-order modeling of frequency-dependent coupling inductances associated with 3-D interconnect structures," *IEEE Trans. Comp., Packag., Manufact. Technol. A*, pp. 283–288, May 1996.
[83] K. J. Kerns and A. T. Yang, "Preservation of passivity during RLC network reduction via split congruence transformations," *IEEE Trans. Computer-Aided Design*, pp. 582–591, July 1998.
[84] A. Odabasioglu, M. Celik, and L. T. Pillage, "PRIMA: Passive reduced-order interconnect macromodeling algorithm," *IEEE Trans. Computer-Aided Design*, pp. 645–654, Aug. 1998.
[85] A. Odabasioglu, M. Celik, and L. T. Pillage, "Practical considerations for passive reduction of RLC circuits," in *Proc. DAC*, June 1999, pp. 214–219.
[86] Q. Yu, J. M. L. Wang, and E. S. Kuh, "Passive multipoint moment-matching model order reduction algorithm on multiport distributed interconnect networks," *IEEE Trans. Circuits Syst. I*, pp. 140–160, Jan. 1999.
[87] A. Dounavis, E. Gad, R. Achar, and M. Nakhla, "Passive model-reduction of multiport distributed networks including frequency-dependent parameters," *IEEE Trans. Microwave Theory Tech.*, pp. 2325–2334, Dec. 2000.
[88] M. Raugi, "Wavelet transform solution of MTL transients," *IEEE Trans. Magn.*, pt. I, pp. 1554–1557, May 1999.
[89] S. Barmada and M. Raugi, "Transient numerical Solutions of nonuniform MTL equations with nonlinear loads with wavelet expansion in time or space-domain," *IEEE Trans. Circuits Syst. I*, pp. 1178–1190, Aug. 2000.
[90] A. C. Cangellaris, S. Pasha, J. L. Prince, and M. Celik, "A new discrete time-domain model for passive model order reduction and macromodeling of high-speed interconnections," *IEEE Trans. Comp., Packag., Manufact. Technol.*, pp. 356–364, Aug. 1999.
[91] M. Celik and A. C. Cangellaris, "Simulation of dispersive multiconductor transmission lines by Padé approximation via Lanczos process," *IEEE Trans. Microwave Theory Tech.*, pp. 2525–2535, Dec. 1996.
[92] P. Gunupudi, M. Nakhla, and R. Achar, "Simulation of high-speed distributed interconnects using Krylov-subspace techniques," *IEEE Trans. Computer-Aided Design*, vol. 19, pp. 799–808, July 2000.
[93] R. Achar and M. Nakhla, *Minimum Realization of Reduced-Order Models of High-Speed Interconnect Macromodels*. Boston, MA: Kluwer, 1998, ch. Signal Propagation on Interconnects, pp. 23–44.
[94] M. Kamon, F. Wang, and J. White, "Generating nearly optimally compact models from Krylov-subspace based reduced-order models," *IEEE Trans. Circuits Syst.*, pp. 239–248, Apr. 2000.
[95] R. Khazaka and M. Nakhla, "Multilevel passive order reduction of interconnects," in *IMS Dig.*, May 2001, to be published.
[96] O. Palusinski and A. Lee, "Analysis of transients in nonuniform and uniform multiconductor transmission lines," *IEEE Trans. Microwave Theory Tech.*, pp. 127–138, Jan. 1989.
[97] S. Manney, M. S. Nakhla, and Q. J. Zhang, "Time domain analysis of nonuniform frequency dependent high-speed interconnects," in *Proc. IEEE Int. Conf. Computer-Aided Design*, 1992, pp. 449–453.
[98] N. Boulejfen, A. Kouki, and F. Ghannouchi, "Frequency and time-domain analysis nonuniform lossy coupled transmission lines with linear and nonlinear terminations," *IEEE Trans. Microwave Theory Tech.*, pp. 367–379, Mar. 2000.
[99] C. Yen, Z. Fazarinc, and R. L. Wheeler, "Time-domain skin-effect model for transient analysis of lossy transmission lines," *Proc. IEEE*, pp. 750–757, 1982.
[100] R. Khazaka, E. Chiprout, M. Nakhla, and Q. J. Zhang, "Analysis of high-speed interconnects with frequency dependent parameters," in *Proc. Int. Symp. EMC*, Zurich, Switzerland, Mar. 1995, pp. 203–208.
[101] W. Sui, D. A. Christensen, and C. H. Durney, "Extending the two-dimensional FDTD method to hybrid electromagnetic systems with active and passive lumped elements," *IEEE Trans. Microwave Theory Tech.*, vol. 40, pp. 724–730, Apr. 1992.
[102] Y. Tsuei, A. C. Cangellaris, and J. L. Prince, "Rigorous electromagnetic modeling of chip-to-package (first-level) interconnections," *IEEE Trans. Comp. Hybrids Manufact. Technol.*, vol. 16, pp. 876–883, Aug. 1993.
[103] M. Picket-May, A. Taflove, and J. Baron, "FD-TD modeling of digital signal propagation in 3-D circuits with passive and active loads," *IEEE Trans. Microwave Theory Tech.*, vol. 42, pp. 1514–1523, Aug. 1994.
[104] P. C. Cherry and M. F. Iskander, "FDTD analysis of high frequency electronic interconnection effects," *IEEE Trans. Microwave Theory Tech.*, vol. 43, pp. 2445–2451, Oct. 1995.
[105] S. D. Corey and A. T. Yang, "Interconnect characterization using time-domain reflectometry," *IEEE Trans. Microwave Theory Tech.*, vol. 43, pp. 2151–2156, Sept. 1995.
[106] B. J. Cooke, J. L. Prince, and A. C. Cangellaris, "S-parameter analysis of multiconductor integrated circuit interconnect systems," *IEEE Trans. Computer-Aided Design*, pp. 353–360, Mar. 1992.
[107] L. Vakanas, A. C. Cangellaris, and O. Palusinski, "Scattering parameter based simulation of transients in lossy, nonlinearly terminated packaging interconnects," *IEEE Trans. Comp., Packag., Manufact. Technol. B*, pp. 472–479, Feb. 1994.
[108] M. Celik, A. C. Cangellaris, and A. Deutsch, "A new moment generation technique for interconnects characterized by measured or calculated S-parameters," in *IEEE Int. Microwave Symp. Dig.*, June 1996, pp. 196–201.
[109] J. E. Schutt-Aine and R. Mittra, "Scattering parameter transient analysis of transmission lines loaded with nonlinear terminations," *IEEE Trans. Microwave Theory Tech.*, pp. 529–536, 1988.

[110] ——, "Nonlinear analysis of coupled transmission lines," *IEEE Trans. Circuits Syst.*, vol. 36, pp. 959–967, 1989.
[111] W. T. Beyene and J. E. Schutt-Aine, "Efficient transient simulation of high-speed interconnects characterized by sampled data," *IEEE Trans. Comp., Packag., Manufact. Technol. B*, vol. 21, pp. 105–113, Feb. 1998.
[112] G. Zheng, Q. J. Zhang, M. Nakhla, and R. Achar, "An efficient approach for simulation of measured subnetworks with complex frequency hopping," in *Proc. IEEE/ACM Int. Conf. Computer Aided Design*, San Jose, CA, Nov. 1996, pp. 23–26.
[113] R. Achar and M. Nakhla, "Efficient transient simulation of embedded subnetworks characterized by S-parameters in the presence of nonlinear elements," *IEEE Trans. Microwave Theory Tech.*, vol. 46, pp. 2356–2363, Dec. 1998.
[114] N. Liu, M. Nakhla, and Q. J. Zhang, "Time domain sensitivity of high-speed VLSI interconnects," *Int. J. Circuit Theory Applicat.*, vol. 22, pp. 479–511, Nov. 1994.
[115] Q. J. Zhang, S. Lum, and M. Nakhla, "Minimization of delay and crosstalk in high-speed VLSI interconnects," *IEEE Trans. Microwave Theory Tech.*, vol. 42, pp. 1555–1563, July 1992.
[116] S. Lum, M. Nakhla, and Q. J. Zhang, "Sensitivity analysis of lossy coupled transmission lines with nonlinear terminations," *IEEE Trans. Microwave Theory Tech.*, vol. 42, 1994.
[117] R. W. Freund and P. Feldmann, "Small signal circuit analysis and sensitivity computations with PVL algorithm," *IEEE Trans. Circuits Syst. II*, pp. 577–585, 1996.
[118] C. Jiao, A. C. Cangellaris, A. Yaghmour, and J. L. Prince, "Sensitivity analysis of multiconductor transmission lines and optimization for high-speed interconnect design," *IEEE Trans. Comp., Packag., Manufact. Technol.*, pp. 132–141, May 2000.
[119] R. Khazaka and M. Nakhla, "Analysis of high-speed interconnects in the presence of electromagnetic interference," *IEEE Trans. Microwave Theory Tech.*, vol. 46, pp. 940–947, July 1998.
[120] I. Erdin, R. Khazaka, and M. Nakhla, "Simulation of high-speed interconnects in the presence of incident field," *IEEE Trans. Microwave Theory Tech.*, vol. 46, pp. 2251–2257, Dec. 1998.
[121] I. Ierdin, M. Nakhla, and R. Achar, "Circuit analysis of electromagnetic radiations and field coupling effects for networks with embedded full-wave modules," *IEEE Trans. Electromagn. Compat.*, vol. 42, pp. 449–460, Nov. 2000.
[122] F. Olyslager, D. D. Zutter, and A. T. de Hoop, "New reciprocal circuit model for lossy waveguide structures based on the orthogonality of the eigenmodes," *IEEE Trans. Microwave Theory Tech.*, vol. 42, no. 12, pp. 2261–2269, Dec. 1994.
[123] F. Olyslager, D. D. Zutter, and K. Blomme, "Rigorous analysis of the propagation characteristics of general lossless and lossy multiconductor transmission lines in multi-layered media," *IEEE Trans. Microwave Theory Tech.*, vol. 41, pp. 79–88, Jan. 1993.
[124] C. D. Taylor, R. S. Satterwhite, and C. W. Harrison, "The response of a terminated two-wire transmission line excited by a nonuniform electromagnetic field," *IEEE Trans. Antennas Propagat.*, vol. 13, pp. 987–989, Nov. 1965.
[125] A. A. Smith, "A more convenient form of the equations for the response of a transmission line excited by nonuniform fields," *IEEE Trans. Electromagn. Compat.*, vol. 15, pp. 151–152, Aug. 1973.
[126] C. R. Paul, "Frequency response of multiconductor transmission lines illuminated by an incident electromagnetic field," *IEEE Trans. Microwave Theory Tech.*, vol. 22, pp. 454–457, Apr. 1976.
[127] ——, "A comparison of the contributions of common-mode and differential-mode currents in radiated emissions," *IEEE Trans. Electromagn. Compat.*, pp. 189–193, May 1989.
[128] ——, "A SPICE model for multiconductor transmission lines excited by an incident electromagnetic field," *IEEE Trans. Electromagn. Compat.*, pp. 342–354, Nov. 1994.
[129] I. Wuyts and D. De Zutter, "Circuit model for plane-wave incidence on multiconductor transmission lines," *IEEE Trans. Electromagn. Compat.*, vol. 36, pp. 206–212, Aug. 1994.
[130] E. S. M. Mok and G. I. Costache, "Skin-effect considerations on transient response of a transmission line excited by an electromagnetic wave," *IEEE Trans. Electromagn. Compat.*, vol. 34, pp. 320–329, Aug. 1992.
[131] Y. Kami and R. Sato, "Circuit-concept approach to externally excited transmission lines," *IEEE Trans. Electromagn. Compat.*, vol. 27, pp. 177–183, Nov. 1985.
[132] N. Ari and W. Blumer, "Analytic formulation of the response of a two-wire transmission line excited by a plane wave," *IEEE Trans. Electromagn. Compat.*, vol. 30, pp. 437–448, Nov. 1988.
[133] C. R. Paul, "Literal solutions for the time-domain response of a two-conductor transmission line excited by an incident electromagnetic field," *IEEE Trans. Electromagn. Compat.*, vol. 37, May 1995.
[134] P. Bernardi, R. Cicchetti, and C. Pirone, "Transient response of a microstrip line circuit excited by an external electromagnetic source," *IEEE Trans. Electromagn. Compat.*, vol. 34, pp. 100–108, May 1992.
[135] G. J. Burke, E. K. Miller, and S. Chakrabarti, "Using model based parameter estimation to increase the efficiency of computing electromagnetic transfer functions," *IEEE Trans. Magn.*, vol. 25, pp. 2087–2089, July 1989.
[136] F. M. Tesche, M. V. Ianoz, and T. Karlsson, *EMC Analysis Methods and Computational Models*. New York: Wiley, 1997.
[137] A. K. Agrawal, H. J. Price, and S. H. Gurbaxani, "Transient response of multiconductor transmission lines excited by a nonuniform electromagnetic field," *IEEE Trans. Electromagn. Compat.*, vol. 22, pp. 119–129, May 1980.
[138] Y. Kami and R. Sato, "Circuit-concept approach to externally excited transmission lines," *IEEE Trans. Electromagn. Compat.*, vol. 27, pp. 177–183, Nov. 1985.
[139] R. Raut, W. J. Steenart, and G. Costache, "A note on the optimum layout of electronic circuits to minimize electromagnetic field strength," *IEEE Trans. Electromagn. Compat.*, pp. 88–89, Feb. 1988.
[140] C. W. Ho, A. E. Ruehli, and P. A. Brennan, "The modified nodal approach to network analysis," *IEEE Trans. Circuits Syst.*, vol. CAS-22, pp. 504–509, June 1975.
[141] A. E. Ruehli, *Circuit Analysis, Simulation and Design*. New York: Noth-Holland, 1988.
[142] J. K. White and A. S. Vincentelli, *Relaxation Techniques for the Simulation of VLSI Circuits*. Boston, MA: Kluwer, 1990.
[143] D. O. Pederson, "A historical review of circuit simulation," *IEEE Trans. Circuits Syst.*, vol. CAS-31, no. 1, Jan. 1984.
[144] A. S. Vincentelli, "Circuit Simulation," in *Computer Design Aids for VLSI Circuits*, P. Antognetti, D. O. Pederson, and H. De Man, Eds: Martinus Nijhoff, 1986, pp. 19–122.
[145] J. K. Ousterhout, "CRYSTAL: A timing analyzer for NMOS VLSI circuits," in *Proc. 3rd Caltech. Conf. VLSI*, Mar. 1983, pp. 57–69.
[146] N. P. Jouppi, "Timing analysis and performance improvement of MOS VLSI design," *IEEE Trans. Computer-Aided Design*, vol. 6, pp. 650–665, July 1987.
[147] S. Lin, M. M. Sadowska, and E. S. Kuh, "SWEC: A step wise equivalent conductance timing simulator for CMOS VLSI circuits," in *Proc. Electron. Design Automation Conf.*, 1991, pp. 142–148.
[148] A. S. Vincetelli, E. Lelarasmee, and A. Ruehli, "The waveform relaxation method for the time-domain analysis of large scale integrated circuits," *IEEE Trans. Computer-Aided Design*, vol. 1, pp. 131–145, Aug. 1982.
[149] A. Devgan and R. A. Roher, "Adaptively controlled explicit simulation," *IEEE Trans. Computer-Aided Design*, vol. 13, Jun. 1994.
[150] S. Lele, "Compact finite difference schemes with spectral-like resolution," *J. Comput. Phys.*, vol. 103, pp. 16–42, 1992.
[151] J. Vlach and K. Singhal, *Computer Methods for Circuit Analysis and Design*. New York: Van Nostrand, 1983.
[152] T. Kailath, *Linear Systems*. Toronto: Prentice-Hall, 1980.
[153] C. T. Chen, *Linear System Theory and Design*. New York: Holt, Rinehart and Winston, 1984.
[154] L. Weinberg, *Network Analysis and Synthesis*. New York: McGraw-Hill, 1962.
[155] W. Louis, *Network Analysis and Synthesis*. New York: McGraw-Hill, 1962.
[156] E. Kuh and R. Rohrer, *Theory of Active Linear Networks*. San Francisco, CA: Holden-Day, 1967.
[157] E. A. Guillemin, *Synthesis of Passive Networks*. New York: Wiley, 1957.
[158] M. E. V. Valkenburg, *Introduction to Modern Network Synthesis*. New York: Wiley, 1960.
[159] U. S. Pillai, *Spectrum Estimation and System Identification*. New York: Springer-Verlag, 1993.
[160] J. W. Demmel, *Applied Numerical Linear Algebra*. Philadelphia, PA: SIAM, 1997.

Ramachandra Achar (Member, IEEE) received the B.Eng. degree in electronics engineering from Bangalore University, India, in 1990, the M.Eng. degree in microelectronics from Birla Institute of Technology and Science, Pilani, India, in 1992, and the Ph.D. degree from Carleton University, Ottawa, ON, Canada, in 1998, where he received the University Medal for his doctoral work on high-speed VLSI interconnect analysis.

He currently serves as an Assistant Professor in the Department of Electronics, Carleton University. He spent the summer of 1995 working on high-speed interconnect analysis at T. J. Watson Research Center, IBM, New York. He was a Graduate Trainee at Central Electronics Engineering Research Institute, Pilani, India, during 1992 and was also previously employed at Larsen and Toubro Engineers Ltd., Mysore, India, and at Indian Institute of Science, Bangalore, India, as an R&D Engineer. During 1998–2000, he served as a Research Engineer in the CAE Group at Carleton University. His research interests include modeling and simulation of high-speed interconnects, numerical algorithms, and development of computer-aided design tools for high-frequency circuit analysis.

Dr. Achar received several prestigious awards, including NSERC (Natural Science and Engineering Research Council) Doctoral Award (2000), Strategic Microelectronics Corporation (SMC) Award (1997), Canadian Microelectronics Corporation (CMC) Award (1996), and the Best Student Paper Award in the 1998 Micronet (a Canadian network of centers of excellence on Microelectronics) annual workshop.

Michel S. Nakhla (Fellow, IEEE) received the M.A.Sc. and Ph.D. degrees in electrical engineering from University of Waterloo, Ontario, Canada in 1973 and 1975, respectively.

He is Professor of Electrical Engineering at Carleton University, Ottawa, ON, Canada. From 1976 to 1988, he was with Bell-Northern Research, Ottawa, as the Senior Manager of the Computer-Aided Engineering Group. In 1988, he joined Carleton University as a Professor and the holder of the Computer-Aided Engineering Senior Industrial Chair established by Nortel Networks and the Natural Sciences and Engineering Research Council of Canada. He is the founder of the High-Speed CAD Research Group at Carleton University and is a frequent invited speaker on the topic of high-speed interconnects. His research interests include CAD of VLSI and microwave circuits, modeling and simulation of high-speed interconnects, nonlinear circuits, multidisciplinary optimization, thermal and electromagnetic (EM) emission analysis, MEMS, and neural networks. He serves as Technical Consultant for several industrial organizations and is the principal investigator for several major sponsored research projects.